TOWARDS CONTROL OF PHASE SEGREGATION IN DONOR-ACCEPTOR BLENDS BY POST-FUNCTIONALIZATION OF CONJUGATED POLYMER

by

Zhongyuan Zhou
M.Sc., Delft University of Technology, 2004
B.Sc., Nanjing University of Chemical Technology, 2000

THESIS SUBMITTED IN PARTIAL FULFILLMENT OF
THE REQUIREMENTS FOR THE DEGREE OF

DOCTOR OF PHILOSOPHY

In the
Department of Chemistry

SIMON FRASER UNIVERSITY

Summer 2010

APPROVAL

Name: **Zhongyuan Zhou**

Degree: **Doctor of Philosophy**

Title of Thesis: **Towards Control of Phase Segregation in Donor-Acceptor Blends by Post-Functionalization of Conjugated Polymer**

Examining Committee:

Chair: **Dr. Erika Plettner (Associated Professor)**

_____

Dr. Steven Holdcroft (Professor)
Senior Supervisor

_____

Dr. Byron Gates (Assistant Professor)
Supervisor

_____

Dr. Hua-Zhong Yu (Professor)
Supervisor

_____

Dr. Robert Britton (Assistant Professor)
Internal Examiner

_____

Dr. Alex Jen (Professor)

External Examiner
University of Washington

_____

Date Defended/Approved: August 12, 2010

Declaration of Partial Copyright Licence

ABSTRACT

π-Conjugated polymers are promising active materials on account of their special properties, which include electronic conductivity, electroluminescence and light-harvesting. Post-functionalization of conjugated polymers is a facile approach towards tailed structures and properties of polymers. This thesis reports on the synthesis and characterization of post-functionalized conjugated polymers and control phase segregation in donor-acceptor blends by post-functionalization of conjugated polymers for photovoltaic applications. Structure - property relationships were investigated using a variety of techniques including NMR, GPC, UV-vis absorption, photoluminescence spectroscopy, cyclic voltammetry, X-ray diffraction, TEM and photovoltaic devices.

A graft copolymer, poly(3-hexlthiophene) bearing poly(vinyltriazole) (P3HT-g-PVTAZ), was used as the primary model material to demonstrate a novel strategy for controlling the size, contiguous nature, and extent of phase segregation of donor and acceptor domains. The graft copolymer was obtained by nitroxide-mediated radical polymerization of a vinyl triazole onto a postfunctionalized poly(3-hexylthiophene) (P3HT) backbone. The graft copolymer was blended with a fullerene modified with a similar motif - a pendant triazole functionality ($TAZC_{60}$). For a given ratio of polymer:$TAZC_{60}$, graft copolymer (P3HT-g-PVTAZ:$TAZC_{60}$) blends exhibit substantially reduced photoluminescence compared to P3HT:$TAZC_{60}$ blends, while TEM analysis

revealed that the graft polymer undergoes extensive mixing with the fullerene to form bicontinuous 10 nm phase domains. Graft polymer blends annealed for 1 h at 140 °C retain their nanometer phase separation as evidenced by TEM, UV-vis, XRD, and photoluminescence analysis, and domain purity was enhanced. In contrast, P3HT:TAZC_{60} blends exhibit micron-sized phase-segregated morphologies before and after annealing. The chemical similarity of the triazole functionality attached to P3HT and the fullerene leads to the formation of films with uniform, stable, nanophase morphologies. This strategy may prove a useful strategy for controlling the extent of phase segregation in electron donor and acceptor blends of π-conjugated polymers (πCPs) and fullerenes.

Synthesis of a perylene-functionalized conjugated polymer was used to demonstrate the templated growth of 1-D assemblies of perylene diimides (PDI) formed within a conjugated polymer. The strategy is demonstrated with poly(3-hexylthiophene) (P3HT), partially functionalized at the 4-position with N-(1-hexylheptyl)-N'-(12-carboxylicdodecyl)perylene-3,4,9,10-tetracarboxylbisimide (PP3HT). The 1-D assemblies of PDI embedded in the optoelectronically active polymer are hundreds of nanometers wide, 10 – 20 nm thick, several microns in length, and run parallel to the surface of the substrate. Surrounding the 1-D structures is a heterogeneous PP3HT-PDI blend, comprised of PP3HT domains less than 10 nm in size. The excitation energy in thin film blends of PP3HT:PDI is quenched to a much greater extent than in simple molecular blends of P3HT and PDI. These systems represent structures of multiple hierarchy, wherein nano-sized domains of a π-conjugated polymer and an n-type material are in intimate

contact and which encapsulate 1-D assemblies of nanocrystallites that run parallel to the films surface. They offer an alternative route for the fabrication of innovative supramolecular structures for optoelectronic applications.

Keywords: π-conjugated polymer; post-functionalization; graft copolymer; polythiophene; fullerene; perylene; donor-acceptor blend; phase segregation; 1-D assembly

DEDICATION

To my wife, Liya Xue,

my parents and my families

ACKNOWLEDGEMENTS

I would like to thank:

My senior supervisor Dr. Steven Holdcroft for providing me the opportunity to study and work in his laboratory; for his guidance, endless patience and research assistantships throughout my thesis research.

My supervisory committee Dr. Byron Gates and Dr. Hua-Zhong (Hogan) Yu for giving me feedback and suggestions to improve my thesis and presentation during committee meetings.

My examining committee for taking the time to read my thesis.

Members of the Holdcroft group for their help and hard work.

All of the collaborators I have worked with over past years, especially

Dr. Xiwen Chen for providing fullerene modified with a triazole ($TAZC_{60}$), sharing his knowledge and experience as well as for interesting discussions.

Dr. Jaclyn Brusso for providing part of the XRD data in my thesis and helping to organize the published manuscript.

Former group members Drs. Gisela Schulz, Zhaobin Zhang and Yunsong Yang, who taught me many synthesis techniques.

Bobak Gholamkhass who helped with instrumentation and for scientific discussion. Dr. Yang Li for her assistance with TEM training.

Mr. Tzy Horng Sai for proof reading this thesis.

Simon Fraser University and the National Sciences and Engineering Research Council of Canada for financial support.

TABLE OF CONTENTS

LIST OF FIGURES

LIST OF SCHEMES

LIST OF TABLES

GLOSSARY

1-D	1-dimensional
A	absorbance
ACN	acetonitrile
ATRP	atom-transfer radical polymerization
C	molar concentration
CV	cyclic voltammetry
D/A	donor/acceptor
dppp	diphenylphosphinopropane
E	energy
$\mathbf{E_g}$	energy of band gap
ε	molar extinction coefficient
F	integrated emission area
FET	field effect transistor
FF	fill factor
GPC	gel permeation chromatography
GRIM	Grignard metathesis
HOMO	highest occupied molecular orbital
$\mathbf{I_{sc}}$	short circuit current
ITO	indium tin oxide

λ	wavelength
L	pathlength
LUMO	lowest unoccupied molecular orbital
MEH-PPV	poly[2-methoxy-5-(2'-ethylhexoxy)-1,4-phenylenevinylene]
M_n	number average molecular weight
n	refractive index
NBS	N-bromosuccinimide
NMR	nuclear magnetic resonance
NMRP	nitroxide-mediated living radical polymerization
πCP	π-conjugated polymer
P_{in}	incident light power density
P3HT	poly(3-hexylthiophene)
P3AT	poly(3-alkylthiophene)
PA	polyacetylene
PCBM	[6,6]-phenyl-C61-butyric acid methyl ester
PDI	perylene diimide
PEDOT:PSS	poly(styrene sulfonic acid) doped poly(3, 4-ethylenedioxythiophene)
PF	polyfluorene
Φ_{PL}	quantum yield of photoluminescence
PL	photoluminescence
PLED	polymer light-emitting diodes
PCE	power conversion efficiency

PP3HT	post-functionalized P3HT bearing PDI moieties
PPP	poly(p-phenylene)
PPV	poly(p-phenylene vinylene)
PPy	polypyrrole
PS	polystyrene
PT	polythiophene
PV	photovoltaic
RR-P3HT	regioregular poly(3-hexylthiophene)
τ_r	rates of radiative decay
T	temperature
T_g	glass transition temperature
TAZ	triazole
TAZC$_{60}$	C_{60} modified with a triazole group
TEM	transmission electron microscopy
TEMPO	2,2,6,6-tetramethylpiperidine-1-oxyl
THF	tetrahydrofuran
UV-vis	ultraviolet-visible
V_{oc}	open circuit voltage
XRD	X-ray diffractometry

1: INTRODUCTION

1.1 Overview of π-conjugated Polymers

Polymers have been traditionally used as electrically insulating materials. Since the discovery of conducting polyacetylene in 1977 by Shirakawa, MacDiarmid, and Heeger et al, conjugated polymers have attracted great attention, due to their novel properties and many potential applications.[1, 2] Conjugated polymers can be oxidized to their p-doped state or be reduced to their n-doped state. They become electronically conducting after doping. In the case of trans-polyacetylene, I_2 was used to oxidize the polymer to introduce charged defects, which served as charge carriers. The mechanism of conductivity in these polymers is based on the motion of charge defects within the conjugated framework. Conductive or conducting polymers, are electrically conductive in their “doped” state, and are already used in industry in applications such as anti-static materials, electromagnetic radiation shields for computer screens, capacitors, artificial micromuscles and electrochromic windows.[3-5] In their neutral state, conjugated polymers are semiconducting and are attracting interest in electronic applications such as light-emitting devices (PLED), field-effect transistors (FET), photovoltaic (PV) cells.[6-9] In recognition of their discovery and with maturation of the field of conducting polymers, Shirakawa, MacDiarmid, and Heeger were awarded the Nobel Prize for Chemistry in 2000.

Common conjugated polymers are polyacetylene (PA), Polypyrrole (PPy), Polythiophene (PT), Poly(p-phenylene) (PPP), Poly(phenylene-vinylene) (PPV), Polyfluorene (PF), and their structures are illustrated in **Figure 1.1.**

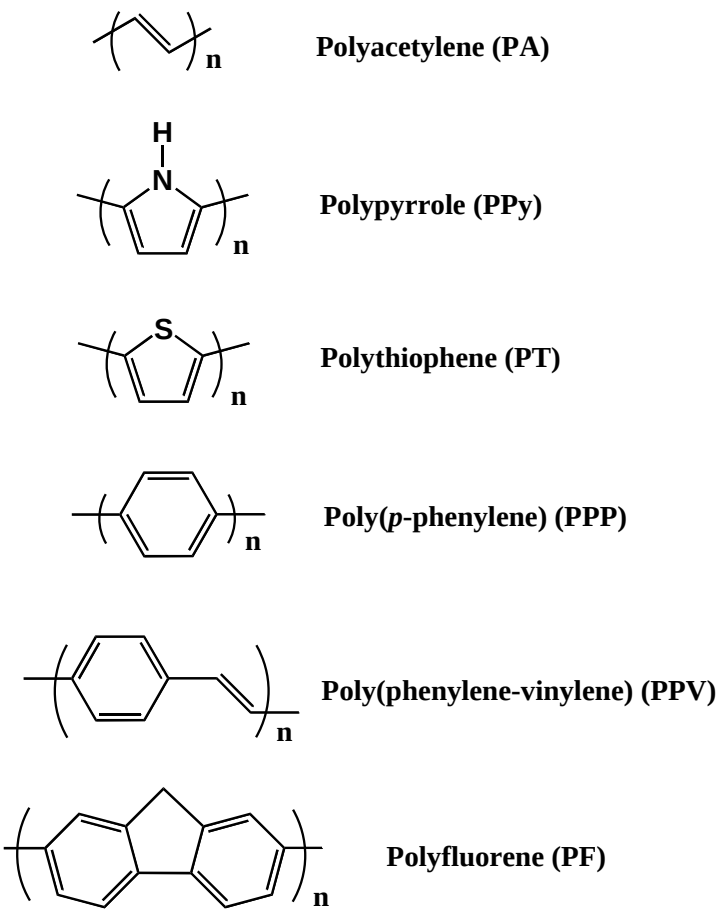

Figure 1.1: The major classes of conjugated polymers

Conjugated polymers like polythiophene (PT), without flexible side chains are insoluble and infusible, which makes their processing difficult. Substituting hydrogen atoms with flexible alkyl side chains can improve the solubility.[9] For PT, alkyl chains can be added to the 3-position, forming soluble poly(3-alkylthiophene) (P3AT).[10] The ability to deposit organic films by solution processing on glass, plastic or metal foil substrates provides potential low cost

fabrication methods of electronic devices, including roll-to-roll processing for large area electronics.

1.2 Properties of Conjugated Polymers

π-conjugated polymers are polymers consisting of alternating single covalent bonds (σ-bonds) and double bonds (π-bonds). This chemical structure results in a general delocalization of the electrons across the adjacent parallel-aligned p-orbitals of contiguous atoms. The delocalized electrons and the overlap of the p-orbitals increase the stability and thereby decreases the overall energy of the molecules.

The electro-optical properties of conjugated polymers depend on the energy difference between the highest occupied molecular orbital (HOMO) or valence band and the lowest unoccupied molecular orbital (LUMO) or conduction band, and is defined as energy of band gap (E_g), as shown in **Figure 1.2**. Electrons have the tendency to associate with the lower energy valence band. As temperature rises or light is introduced, electrons are promoted to the conduction band. Metals have a narrow or nonexistent band gap and exhibit a high conductivity due to the free movement of electrons. An insulator has a large band gap. Its valence band is completely filled, while the conduction band is empty. The band gap is higher than 3 eV (e.g. NaCl: 7 eV, Diamond: 5.5 eV). An excitation of electrons to the conducting band is difficult or not possible. In the undoped states, the conjugated polymers are semiconductors with the energy gap determined by the structure of the polymer and the typical band gap is 1~3

eV. The band gap between the empty conduction band and the full valence band is so small that electrons can populate the empty upper band by thermal or optical excitation. They represent an intermediary class of material between a metal and an insulator. For conjugated polymers, the valence band represents the π band and the conducting band represents the π* band. Interchain interactions between the conjugated main chains decrease the band gap.[11] As the number of repeat units in the molecule increases, the band gap narrows and the conjugated length extends so that light in the visible region of the spectrum can be absorbed by conjugated polymer.

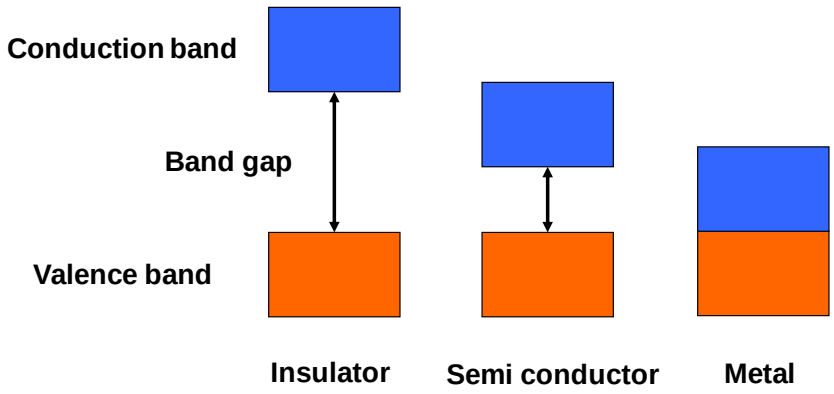

Figure 1.2: Electronic properties of solid state materials

UV-vis absorption and photoluminescence (PL) spectra are important characteristics of conjugated polymers. Detailed characterization of conjugated polymers by UV-vis absorption and PL will be discussed later in the section on Characterization of Conjugated Polymers. Here, poly(3-hexylthiophene) (P3HT) is used as an example to illustrate general optical properties and interchain interactions of conjugated polymers. UV-vis absorption and PL spectra of P3HT

in solution and in solid state are shown in **Figure 1.3** and **Figure 1.4**, respectively.

In comparison with the absorption spectra of both P3HT in solution and in solid state, the PL spectra are red shifted. This red shift is called the Stokes shift and a large red shift is a general phenomenon for conjugated polymers. The Stokes shift occurs when PL emission from the lowest vibrational excited state relaxes to various vibrational levels of the electronic ground state. Other events, such as solvent orientation effects, excited-state reactions, complex formation, and resonance energy transfer can also contribute to longer emission wavelengths.

Interchain interactions of the conjugated polymers also influence the absorption and the PL spectra. In the solid state, stacked polymer chains experience much more interchain interactions than in solution and the absorption and PL wavelength maxima are red shifted with respect to their corresponding solution values. Fluorescence quantum yields (Φ_{PL}) are also smaller in the solid state. For instance, the absorption maximum for P3HT in solution is at 440 nm, while the maxima is at 550 nm for the film. The PL maximum is at 550 nm in solution with a quantum yield of 0.40 while PL maximum is 740 nm with a quantum yield of ~0.02. These differences are due to strong π-π interchain interactions due to aggregate of polymer chains.[12] The aggregate states can be identified as occurring when the distance between the conjugated polymer chains is short enough that the electronic wavefunction of both ground and excited

states overlap. This results in a red shift for both absorption and PL of spectra with respect to isolated polymer chains in solution.

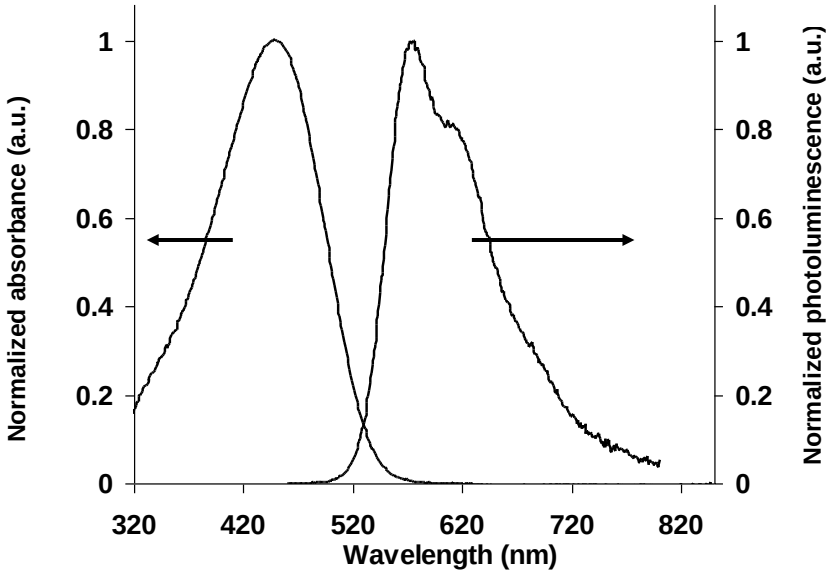

Figure 1.3: Absorption and PL spectra of P3HT in THF solution.

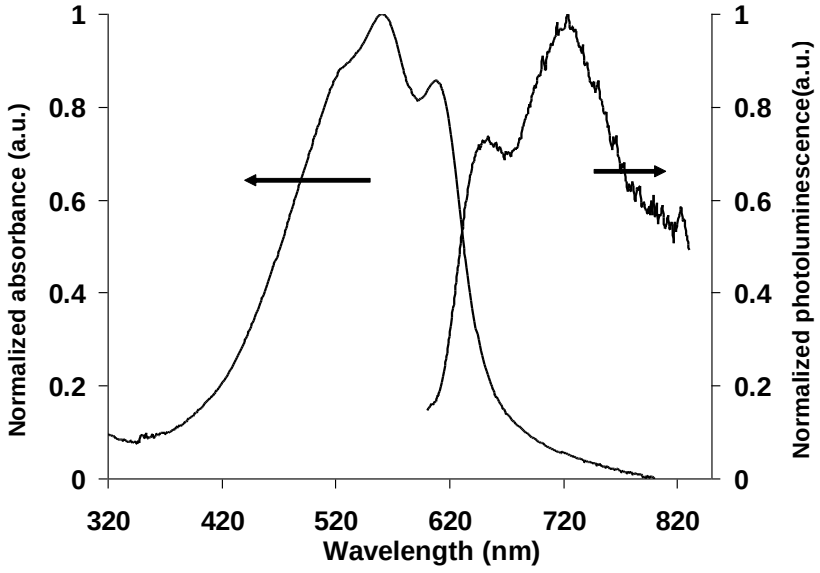

Figure 1.4: Absorption and PL spectra of P3HT film.

1.3 Synthesis of Conjugated Polymers

The chemical structure of conjugated polymers determines their properties and device applications. Among the various conjugated polymers, polythiophene is relatively stable, solution processable and shows synthetically versatile.[13] A large fraction of work described in this thesis is based on polythiophene and its post-functionalized derivative.

For poly(3-alkylthiophene)s (P3AT), three configurational isomers can be formed when two alkylthiophenes combine, as shown in **Figure 1.5**.

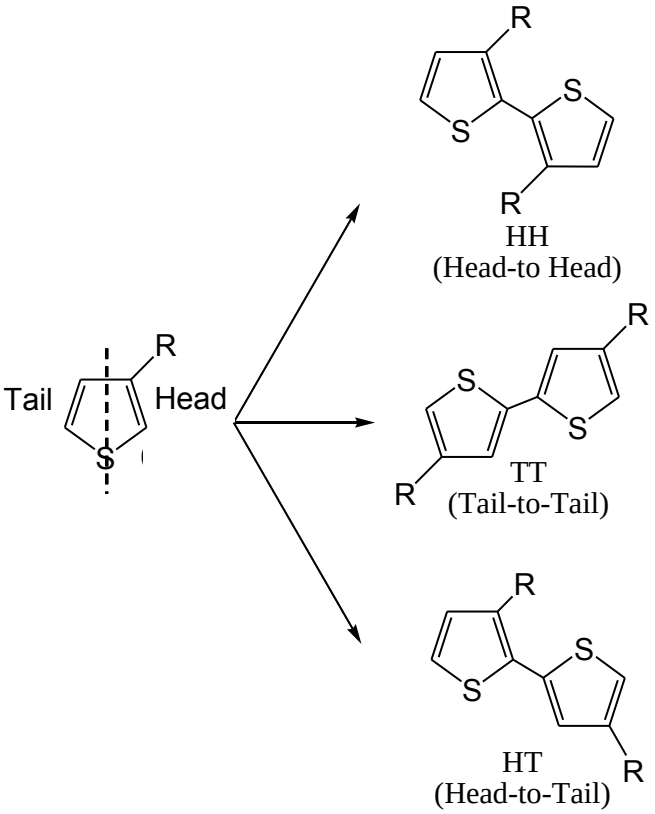

Figure 1.5: Possible configurational isomers of 3-alkylthiophene dyads.

Regiorandom poly(3-alkylthiophene) contains all three isomers, while regioregular poly(3-alkylthiophene) contains only the head (H) to tail (T) isomer. Structure-property relationships of poly(3-alkylthiophene) have been studied intensively.[14] It has previously been proposed that regioregular polythiophene has electrical and electro-optical properties superior to the regiorandom polythiophene as regiorandom polymers cannot readily adopt planar conformations, and irregular placement of the solubilizing alkyl substituents prevents efficient solid-state packing.[15] Conversely, regioregular, head-to-tail coupled poly(3-alkylthiophenes) can undergo self-assembly, both in solution and the solid state, resulting in highly ordered two- and three-dimensional polymer architectures.

Various synthetic methods have been developed that either yield regioregular or regiorandom P3AT. The examples of synthesis are discussed below.

1.3.1 Oxidation Method

The polymerization of 3-alkylthiophene by oxidative coupling of the monomer with $FeCl_3$ is illustrated in **Scheme 1.1**.[16, 17] In the reaction, the 3-alkyl thiophene monomer is dissolved in a suspension of $FeCl_3$ in $CHCl_3$. The polymerization is carried out for several hours under an inert gas. $FeCl_3$ oxidizes the monomer to produce radical centres which propagate to form P3AT. The

advantage for this reaction is its potential large-scale. The molecular weights of P3ATs obtained are relatively high (30 to 300 K), but vary from batch to batch and possess a wide polydispersity. The regioregularity achieved is 70% to 80%. The reaction has its drawbacks in the formation of structural defects beyond the desirable 2,5-coupling.[18] These defects disrupt conjugation and greatly influence crystallinity and electrical conductivity.

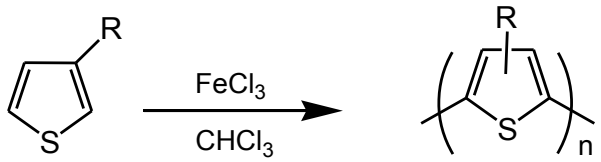

Scheme 1.1: Synthesis of P3ATs by oxidative coupling.

1.3.2 McCullough and GRIM Method

In 1992, McCullough reported a synthetic method for head-to-tail coupled P3AT with ~100% regioregularity.[19, 20] This route is illustrated in **Scheme 1.2**. 2-bromo-5-(bromomagnesio)-3-alkylthiophene was obtained from 2-bromo-3-alkylthiophene at cryogenic temperature. Polymerization in a head-to-tail fashion is achieved by Kumada coupling using catalytic amounts of $Ni(dppp)Cl_2$ (dppp=diphenylphosphinopropane).

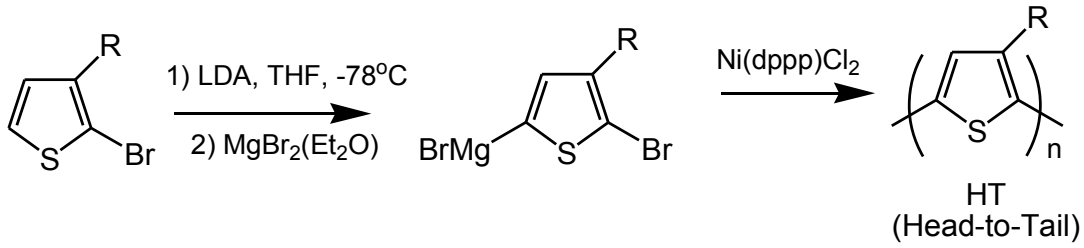

Scheme 1.2: Synthesis of HT-HT P3ATs by the McCullough method.

The Kumada coupling route was the first Ni or Pd-catalyzed cross-coupling reaction. The advantage of this route is the direct coupling of Grignard reagents with organohalides.[21] The coupling of Grignard reagents with alkyl, vinyl or aryl halides provide an economical transformation. The main steps in the reaction mechanism for Ni(0) or Pd(0) catalysts are oxidative addition of organohalide, transmetallation of the Grignard reagent, and reductive elimination, as illustrated in **Scheme 1.3.**

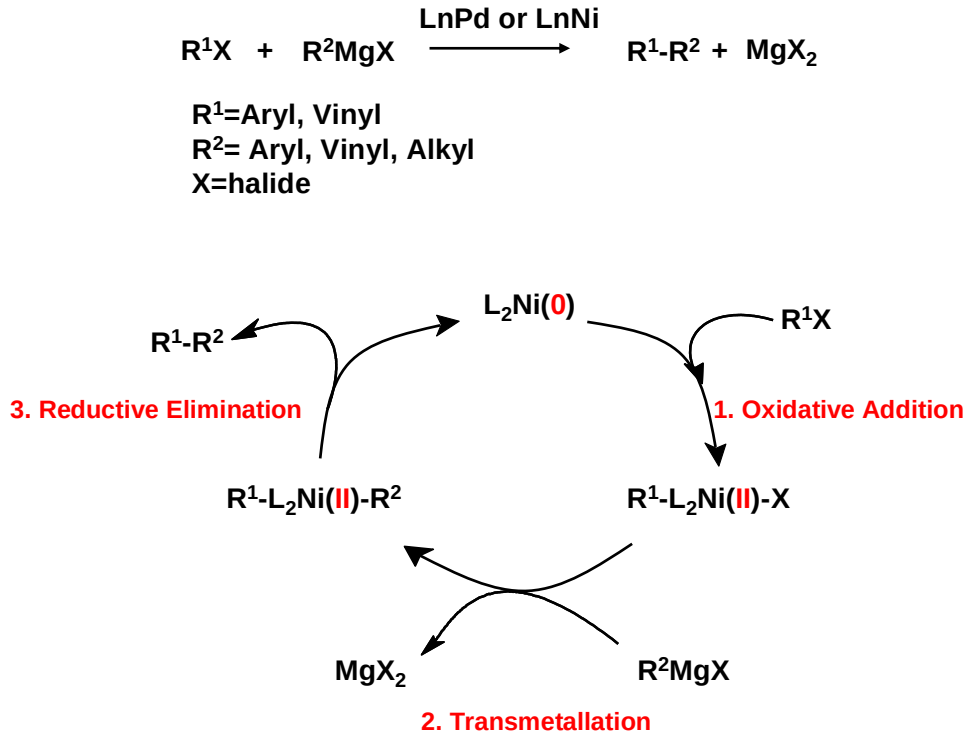

Scheme 1.3: Mechanism of the Kumada coupling reaction.

Recently a new method to synthesize regioregular head-to-tail poly(3-alkylthiophenes) was developed, as illustrated in **Scheme 1.4**. Treatment of 2,5-

dibromo-3-alkylthiophene monomer with 1 equiv of an alkyl Grignard reagent results in a magnesium bromine exchange reaction, the method is referred to as Grignard metathesis (GRIM).[22] This reaction proceeds with a moderate degree of regioselectivity leading two isomers **1**:**2** with a molar ratio of 85:15. Treatment of this **1**:**2** mixture with a catalytic amount of $Ni(dppp)Cl_2$ affords analytically pure, highly regioregular P3ATs.

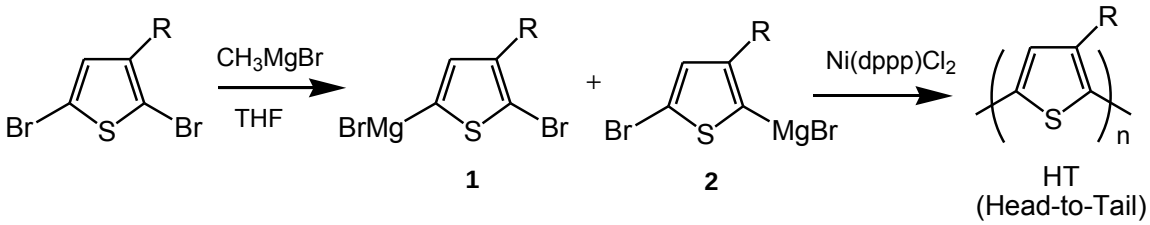

Scheme 1.4: Synthesis of HT-HT P3ATs by the GRIM method.

The regioselective control was rationalized on the basis of steric congestion at the reductive elimination step in the catalytic cycle.[23] It was shown that catalysts with sterically demanding ligands (like dppe and dppp) and small metal centers like Ni afford poly(3-alkylthiophenes) with a high degree of regioselectivity (>98.5% HT coupling). As shown in **Figure 1.6**, the steric congestion on the catalyst may prevent the formation of the catalyst intermediate leading to HH coupling, while the lack of steric interactions upon forming the catalyst intermediately leading to TT and HT couplings is favourable. Once a TT coupling forms, the polymer can only grow in an HT fashion. This leads to a polymer with only one TT defect. This reaction is an improvement over previous methods due to its simplicity and cost-effectiveness.

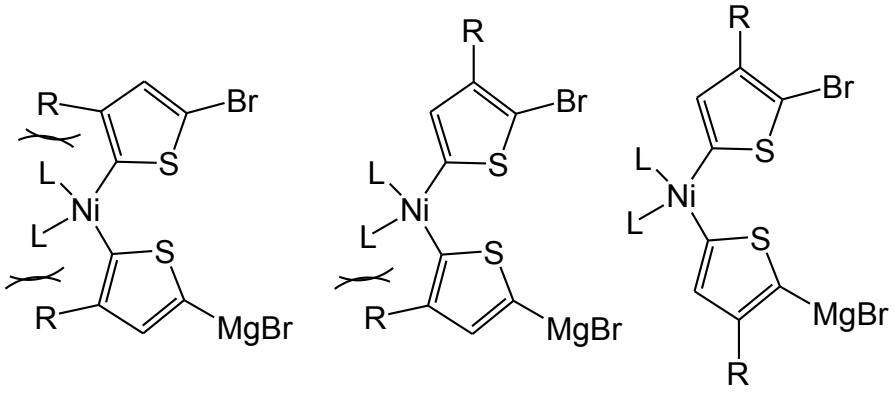

Figure 1.6: Varying degrees of steric congestion after formation of the catalyst intermediate.

1.3.3 Rieke Method

Another synthetic approach to synthesize HT-PATs is the Rieke method. In this method, 2,5-dibromo-3-alkylthiophene is added to a solution of Rieke zinc, noted as Zn*.[24, 25] The reaction undergoes selective oxidative addition to 2,5-dibromo-3-alkylthiophenes at cryogenic temperatures to afford a mixture of **3** and **4** as shown in **Scheme 1.5**. This metalated intermediate undergoes regioselective polymerization in a Negishi cross-coupling reaction.[26] With a similar mechanism as the Kumada coupling reaction, the generalized Negishi coupling reaction is shown in the **Scheme 1.6**. As with Kumada coupling in the GRIM method, regioselective control is rationalized on the basis of steric congestion during the reductive elimination step of the catalytic cycle. Although the ratio of **3** to **4** is ~ 90:10, HT-HT couplings are favored 98.5%. The molecular weight and PDI of P3ATs obtained via the Rieke method are similar to that from

the GRIM method. However, organic zinc reagents are tolerant of more functional groups, including nitrile, cyano, and carbonyl groups.

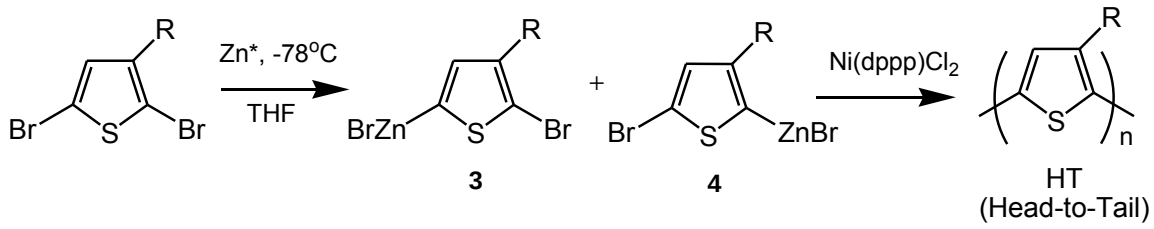

Scheme 1.5: Synthesis of HT-HT P3ATs by the Reike method.

$$R^1X + R^2ZnX \xrightarrow{\text{LnPd or LnNi}} R^1\text{-}R^2 + ZnX_2$$

R^1=alkenyl, aryl, allyl, benzyl, propargyl
R^2=alkenyl, aryl, alkynyl, alkyl, benzyl, allyl
X=halide

Scheme 1.6: The generalized Negishi coupling reaction.

1.3.4 Suzuki Coupling Polymerization

The Suzuki cross coupling reaction is an extremely versatile methodology for making carbon-carbon bonds. This usually involves a reaction of an aryl- or vinyl-boronic acid or ester with an aryl-, vinyl- or an alkyl-halide catalyzed by a palladium(0) complex. The reaction was first reported by Suzuki in 1979.[27, 28] As a typical metal-catalyzed cross coupling, the reaction mechanism is essentially the same as Kumada coupling and follows three basic steps: 1) Oxidative addition, 2) Transmetallation and 3) Reductive elimination. This thesis describes the use of Suzuki coupling to post-functionalize conjugated polymers. For Suzuki coupling polymerization, this method is very suitable for the preparation of

alternating copolymers and it was also applied to prepare regioregular P3AT as illustrated in **Scheme 1.7**.[29, 30]

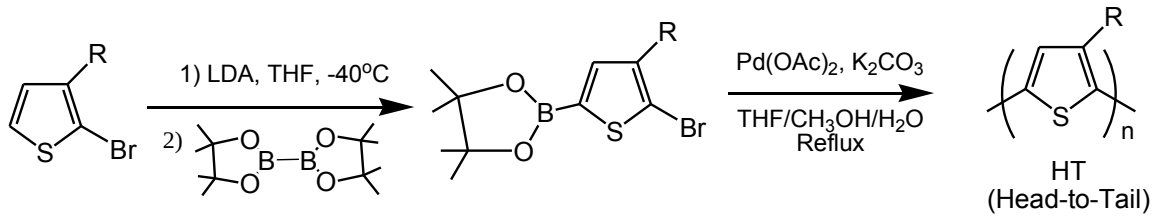

Scheme 1.7: Synthesis of HT-HT P3ATs by Suzuki Coupling polymerisation.

1.3.5 Yamamoto Coupling Polymerization

Yamamoto coupling polymerization is another common and effective method to synthesize conjugated polymers.[31] The Ni-promoted reaction uses the polycondensation of dihaloaromatic compounds such as 2,7-dibromofluorene, as shown in **Scheme 1.8**. As the Ni(0) complex reagent is oxidized and reduced, but does not return to the Ni(0) state, Yamamoto coupling employs a large (stoichiometric) amount of Ni(0) complex.

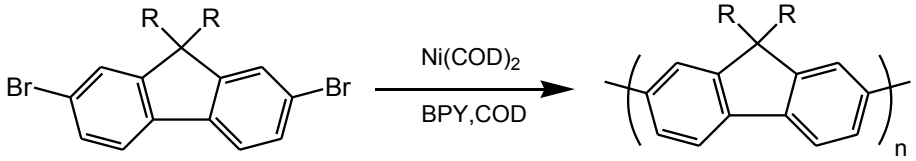

Scheme 1.8: Synthesis of poly(9,9-dialkylfluorene) by Yamamoto coupling.

1.3.6 Post-functionalization of Conjugated Polymers

A facile approach towards tailored conjugated polymers is post-functionalization.[32-35] The advantage of post-functionalization is that the reactions are performed on pre-formed polymers, rather than monomers, as

many monomers cannot survive the harsh conditions of polymerization. Furthermore, a functional group on a monomer can inhibit its polymerization. Post-functionalization of polythiophenes has been researched and developed previously.[36-38] A synthetic route is halogenation of a poly(thiophene) and further introduction of aromatic units through cross-coupling reactions as shown in **Scheme 1.9**. The 4-position of thiophene rings in poly(3-alkylthiophene)s (P3ATs) is susceptible to electrophilic substitution. A comprehensive number of functional groups have been attached to the P3AT through Pd catalyzed cross coupling and it is shown that they can be used to modify the polymers' electro-optical properties through electronic and steric interactions.

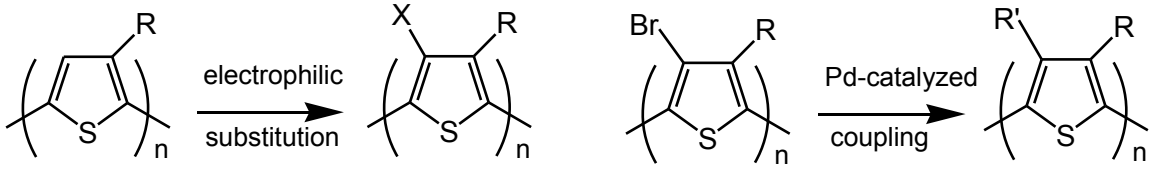

X=Br, Cl, NO_2
R=alkyl
R'=phenyl, thienyl, etc.

Scheme 1.9: General synthetic route of post-functionalization of P3AT.

Substitution with phenyl, p-tolyl, 2- and 4-methoxyphenyl, biphenyl, 1-naphthyl, 2-thienyl, and phenylethylenyl groups causes a red shift in the absorption and emission λ_{max} values and a slight increase in the solid-state quantum yields compared to brominated P3HT. Polymers containing o-tolyl, o-hexylphenyl, 2-(3-methyl)thienyl, and 2-(3-hexyl)thienyl groups exhibit a significantly higher quantum yield in the solid state (9-22%) compared to P3HT (1.6%) and Br-PHT (1.8%). The substituents serve to limit rotation of the

backbone and force the phenyl or thienyl group perpendicular to the main-chain π system. Such a conformation not only increases the planarity and rigidity of the polymer backbone but also enlarges the interplanar distance to the point that highly substituted films are amorphous. The suppression of π stacking, together with rigidification of the main chain, leads to a significant enhancement of luminescence yield.

Molecular order/disorder and optical/photophysical properties of polymers were controlled by partial postfunctionalization of P3HT with o-tolyl groups. For degrees of substitution ranging from 50 to 100%, the solid-state quantum yield is enhanced to 13-22%, and the emission wavelength can be readily tuned from 556 to 640 nm. The postfunctionalization approach allows for a series of highly luminescent poly(thiophene)s to be prepared from a weakly luminescent parent poly(3-hexylthiophene).

1.4 Characterization of Conjugated Polymers

Conjugated polymers and small molecule blocks synthesized and described in this thesis were characterized using ^{1}H Muclear Magnetic Resonance (NMR) spectroscopy, ^{13}C NMR spectroscopy, gel permeation chromatography (GPC), elemental analyses, ultra-violet-visible (UV-vis) absorption spectroscopy, photoluminescence (PL) spectroscopy and quantum efficiency measurement, cyclic voltammetry (CV), transmission electron microscope (TEM), X-ray diffractometry (XRD), surface profilometry, as well as photovoltaic devices. The characterization techniques including UV-vis, PL, CV,

TEM and XRD are important for understanding polymer structure-morphology-property relationships and will be discussed in the following sections.

1.4.1 UV-vis Absorption Spectropscopy

Ultraviolet-visible (UV-vis) absorption spectroscopy (ultraviolet = 200-400 nm, visible = 400-800 nm) corresponds to electronic excitations between energy levels. For organic compounds, especially those with a high degree of conjugation, ultraviolet and visible light promote electrons to higher energy levels. Electron promotion is from the highest occupied molecular orbital (HOMO) to the lowest unoccupied molecular orbital (LUMO), and resulting in an excited state. Generally, UV-vis absorption transitions in conjugated polymers is due to an electronic π to π* transition, as illustrated in **Figure 1.7**. The higher the extent of conjugation in the system, the smaller the HOMO-LUMO gap (ΔE), the lower the frequency, and the longer the wavelength, λ.

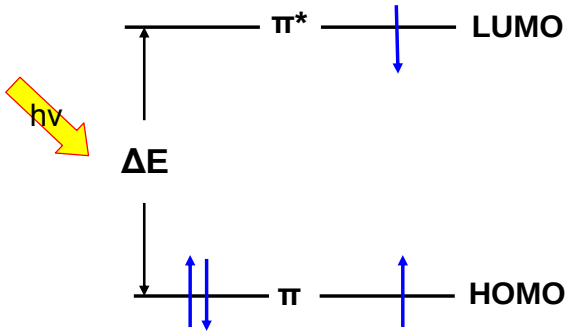

Figure 1.7: Band diagram illustrating electronic excitation of conjugated polymer.

The Beer-Lambert law, represented by **Equation 1.1,** is used quantitatively to determine concentrations of an absorbing species in solution.[39]

Equation 1.1: $A = \varepsilon . c . L$

where *A* is the absorbance, *L* the path length, *c* the concentration, and ε the molar absorptivity or extinction coefficient of the absorbing species.

The dual-beam design of the spectrometer, as shown in **Figure 1.8**, measures the light intensity impinging the sample and reference cells. Many spectrometers use a mirrored rotating chopper wheel to alternately direct the light beam through the sample and reference cells. The detection electronics and software can process the light intensity values from both beams as the wavelength scans to produce an absorbance spectrum or transmittance as a function of wavelength.

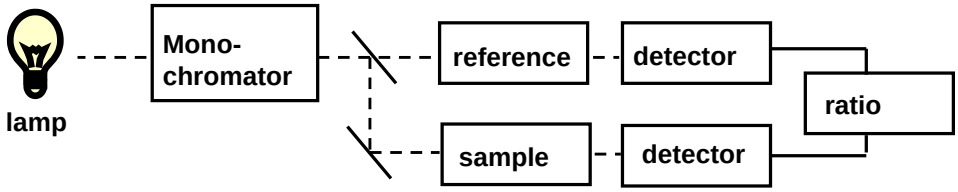

Figure 1.8: Schematic of a dual-beam UV-vis spectrophotometer.

1.4.2 Photoluminescence and Quantum Yield

Photoluminescence (PL) is a process in which a substance absorbs photons (electromagnetic radiation) and then re-radiates photons. For emission of conjugated polymers, it is attributed to a π* - π transition. Photo-physical processes include fluorescence, phosphorescence, and internal conversion. These are summarized in the Jablonski diagram shown in **Figure 1.9**.[40]

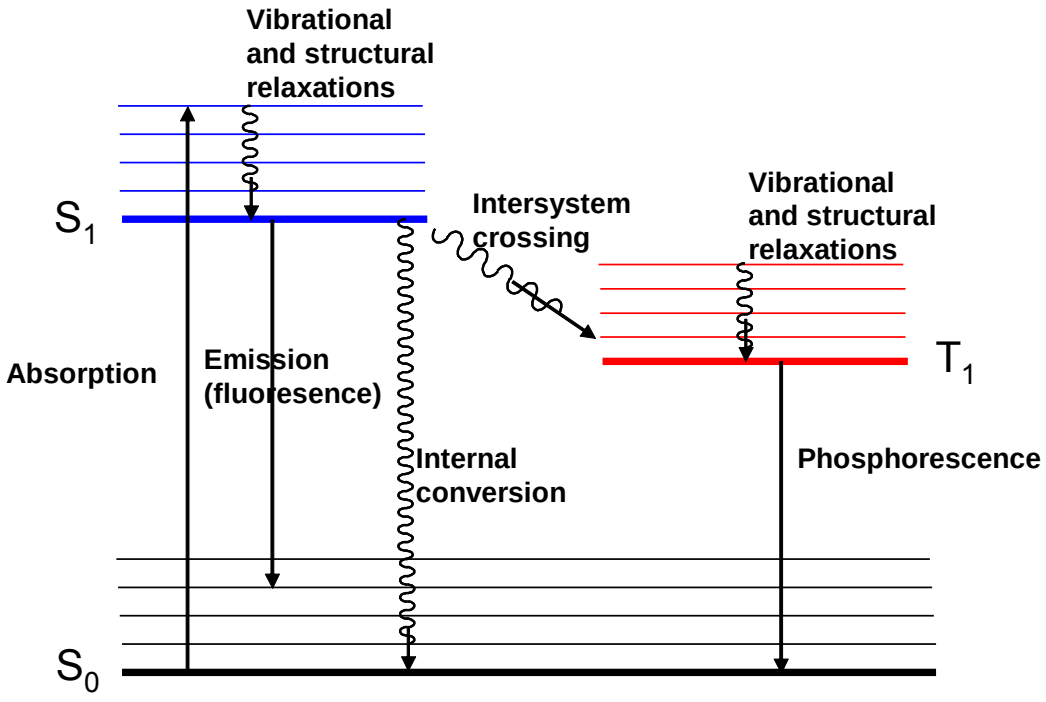

Figure 1.9: Jablonski diagram.

S_0 represents the system ground state, S_1 represents first excited state, and T_1 represents the first triplet state. Fluorescence emission is observed when singlet relaxes from the first excited state. If intersystem crossing from S_1 to T_1 occurs, e.g., via an electron spin flip, a singlet exciton becomes a triplet exciton. Relaxation from a triplet state T_1 to the singlet ground state S_0 results in phosphorescence emission. Phosphorescence is a much slower process compared to fluorescence. The S_1 exciton can also relax to the ground state via radiationless decay and the excitation is converted into rotational and vibrational motion. In such a process, heat, instead of light, is released.

The fluorescence quantum yield (Φ_{PL}) is used to quantitatively analyze the efficiency of singlet emission. Φ_{PL} is the ratio of the number of photons emitted to the number absorbed, as shown in **Equation 1.2**.

Equation 1.2: $$\Phi_{PL} = \frac{Photons(EM)}{Photons(ABS)}$$

Φ_{PL} can reach a maximal value of 1 (100%), however, 100% conversion efficiency is very rarely reached. The value of Φ_{PL} is related to the rates of radiative (τ_r) and non-radiative (τ_{nr}) decay, as shown in **Equation 1.3**. Energy losses through vibrational motion or other intra- and intermolecular effects (non-radiating processes) cause a reduction of both fluorescence lifetime and the quantum yield.

Equation 1.3: $$\Phi_{PL} = \frac{\tau_r}{\tau_r + \tau_{nr}}$$

Quantum yields can be measured by either primary or secondary methods.[41] The primary method is an absolute method based on an integrating sphere sample chamber. An integrating sphere is hollow and coated on the inside with a high reflecting substance, allowing for isotropic light distribution. It accurately measures the fluorescence quantum yield by collecting light in all directions and is not influenced by the emission angle from the sample.

An example of a Φ_{PL} experiment using an integrating sphere spectrofluorometer is shown in **Figure 1.10**. Two spectra are needed to obtain

the Φ_{PL} of an unknown sample. The first spectrum records the light reflected over a range of wavelengths, including the excitation wavelength (450 nm, in this case) in the absence of the sample (blank spectrum). The second measurement uses the same parameters and records the reflected and emitted light in the presence of a sample. The number of photons absorbed and emitted is measured by the difference in intensity as a function of wavelength. The number of photons emitted is related to the area under the emission peak.

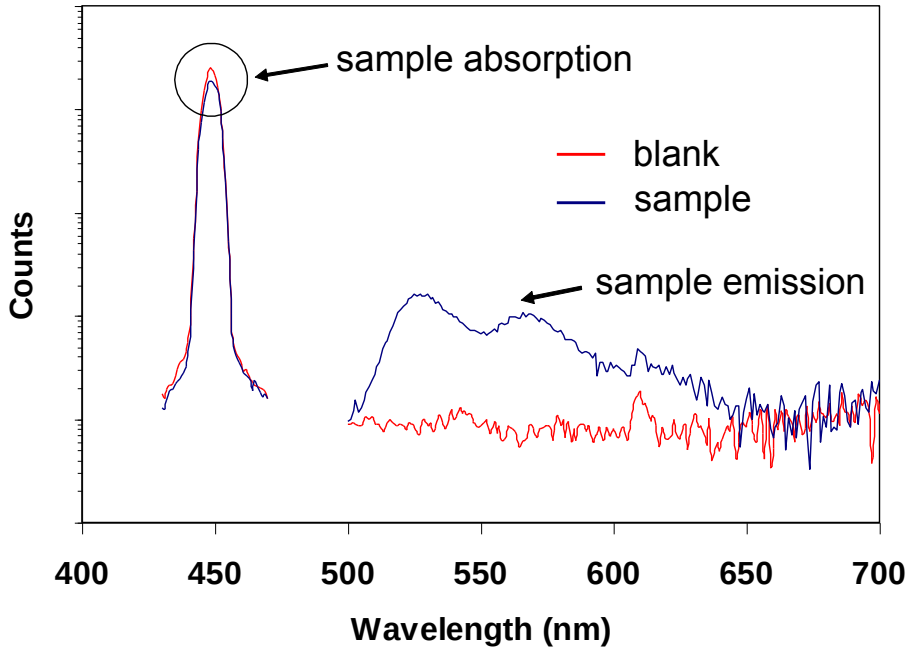

Figure 1.10: An example of a quantum yield measurement using an integrating sphere spectrofluorimeter.

In the secondary method, the quantum yield is related to that of a known standard as shown in **Equation 1.4**.

Equation 1.4: $$\Phi_u = \left[\frac{n_u^2 \times A_s \times F_u}{n_s^2 \times A_u \times F_s}\right]\Phi_s$$

In this equation, Φ represents the quantum yield of luminescence, A is integrated absorbance area at excitation wavelength, F is the integrated emission area under the peak, and n is the refractive index of the solvent. The u subscript represents an unknown and s subscript represents a standard. This method assumes that the emission from the sample is isotropic.

1.4.3 X-Ray Diffractometry

Polymer crystallinity is typically probed using X-ray diffractometry (XRD). The atomic planes of a crystal cause an incident beam of X-rays to interfere with one another as they leave the crystal, as illustrated in **Figure 1.11a**.[42] This phenomenon is called X-ray diffraction and can be expressed by Bragg's law: $n\lambda = 2d\sin\theta$, where n is an integer determined by the order given, λ is the wavelength of the X-rays, d is the spacing between the planes in the atomic lattice, and θ is the angle between the incident ray and the scattering planes. In XRD, a polymer film containing a crystalline phase is irradiated with a monochromatic beam of X-rays with the assumption that the orientation of the crystallite is random. The beam is diffracted at angles determined by the spacing of the planes in the crystals and the signals are collected by the detector as illustrated in **Figure 1.11b**.

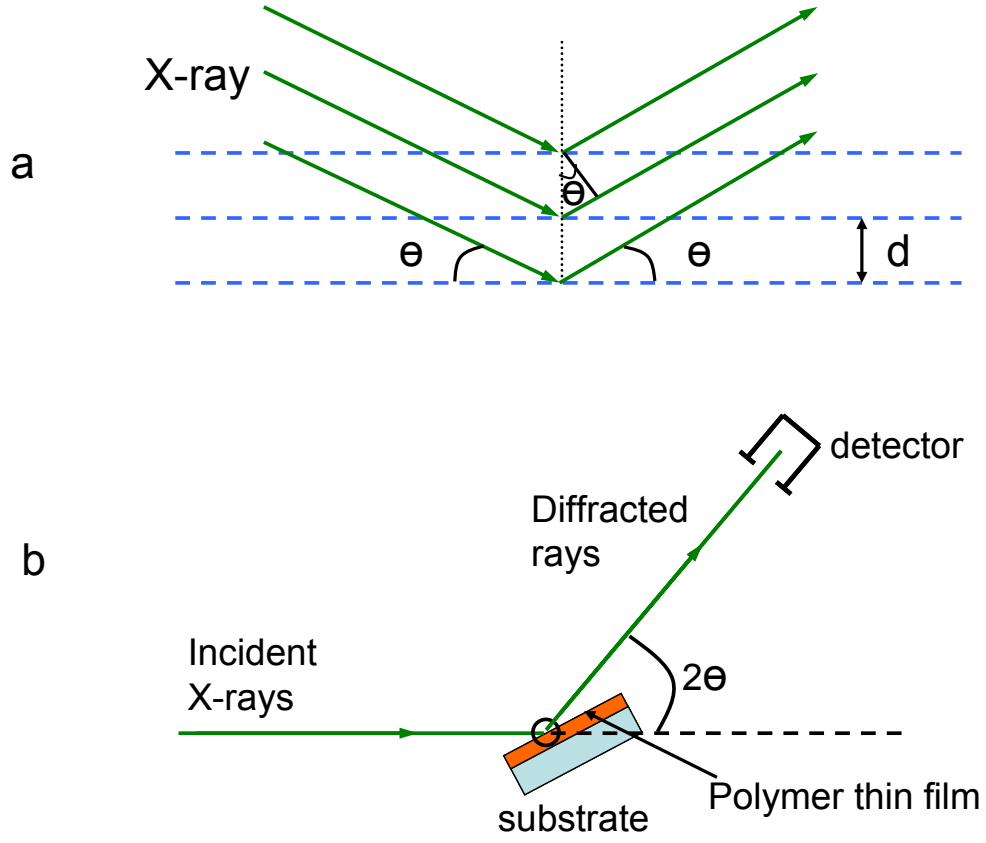

Figure 1.11: Structure characterization of thin film by X-ray Diffraction (XRD)

A morphological model for poly(3-alkylthiophene) (P3HT) has been proposed according to the XRD observation (see **Figure 1.12**).[15, 43] In this model, thiophene chains, with the thienylene moieties linked in a planar anti-conformation, co-facially stack to form a lamellar structure. In each layer of the lamellar structure, the alkyl side chains, adopting mainly all-trans conformation, stretch between the fully extended thiophene main chains.

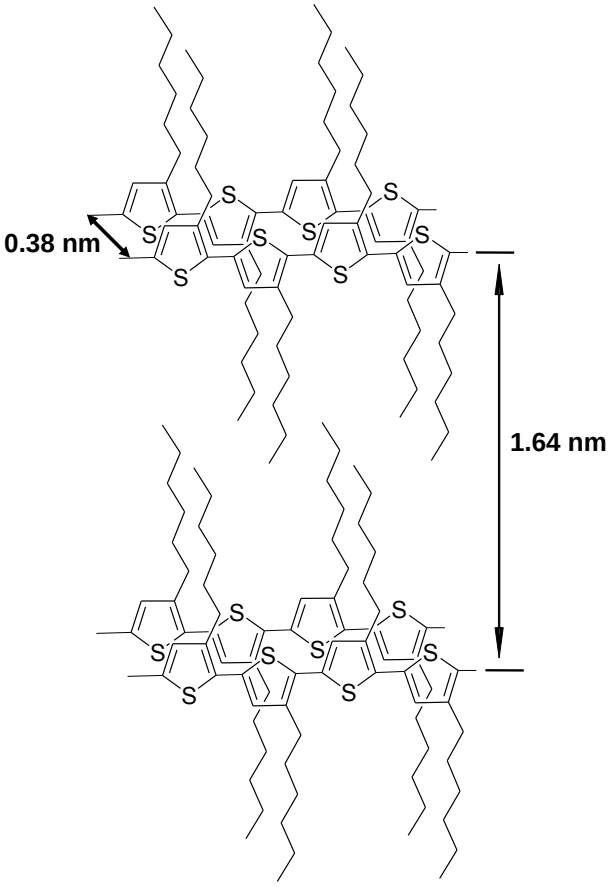

Figure 1.12: A model for the crystal structure of P3HT.

An example of thermally annealing of regioregular poly(3-alkylthiophene) is shown in **Figure 1.13**. It has been shown that thermal annealing of poly(3-alkylthiophene) (P3HT) increases packing of polymer chains and hence the crystallinity of the film. A film of regio-regular (93%) P3HT before and after annealing shows a different diffraction pattern. Comparing the two films, the increased crystallinity is evidenced by an increased peak intensity at ~5° 2θ, which is represents d = 1.64 nm. The ~23° 2θ peak corresponds to interchain spacing associated with face-to-face packing of thiophene rings, but it is often

difficult to distinguished it from background scattering, as glass substrates also shows a broad signal in this area.

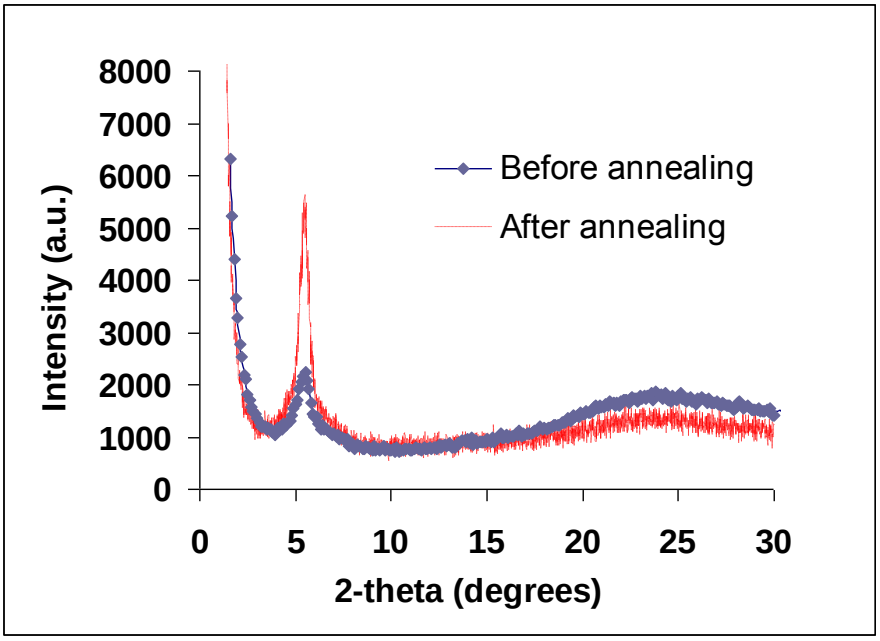

Figure 1.13: X-ray diffractiion profile of P3HT thin film before and after annealing at 140 °C for 1 hour.

1.4.4 Transmission Electron Microscopy

Transmission electron microscopy (TEM) uses a beam of electrons to provide information on a thin film of a material. Most of the electrons pass straight through the film but some are diffracted or scattered as they interact with specimen. The maximum resolution, d, is limited by the wavelength of the electrons that are being used to probe the sample, λ and the numerical aperture of the system, NA as shown in the **Equation 1.5**.[44] TEMs have significantly higher resolution than light microscopes, due to the small wavelength of

electrons. This enables TEM to examine very fine details, tens of thousands times smaller than the smallest resolvable object in a light microscope.

Equation 1.5: $d = \frac{\lambda}{2n\sin\alpha} \approx \frac{\lambda}{2NA}$

A TEM is composed of several components, including a vacuum system, an electron emission source, a series of electromagnetic lenses, and electrostatic plates. The latter two components allow the operator to guide and manipulate the beam. Also required is a device to allow the insertion into, motion within, and removal of specimens from the beam path.

The most common mode of operation of a TEM is the bright field imaging mode. In this contrast and image formation is formed directly by the electron beam interacting with the sample (e.g. by absorption, diffraction, elastic scattering and/or inelastic scattering). In the bright field mode, an aperture is placed in the back focal plane of the objective lens to allow only the direct beam to pass. In this case, the image results from a weakening of the direct beam by its interaction with the sample. Therefore, areas that scatter few electrons appear as bright areas in the image whilst areas that scatter more electrons or absorb electrons (electron-dense areas) appear as dark areas. Adding heavy metal stains increases electron scattering/contrast. Interactions which occur between the primary-beam electrons and atoms of the specimen that contribute to the formation of the TEM image include: unscattered electrons, elastically scattered electrons and inelastically scattered electrons, as shown in the

Figure 1.14.[45]

Unscattered electrons pass through the specimen unchanged. Elastically scattered electrons interact with the nuclei of the atoms in the sample and are scattered through wide angles with no energy loss. The degree of scattering is related to the atom Z number (size of nucleus). A higher Z number translates to a wider scattered angle and higher contrast of the image. Inelastically scattered electrons interact with the orbital electrons of the atoms in the sample and are scattered at low angles, but suffer energy loss (because the beam and orbital electrons have the same mass). This energy loss results in a change in wavelength and is the primary source for a phase contrast image. This differential scattering between transmitted and scattered electrons gives contrast to the specimen.

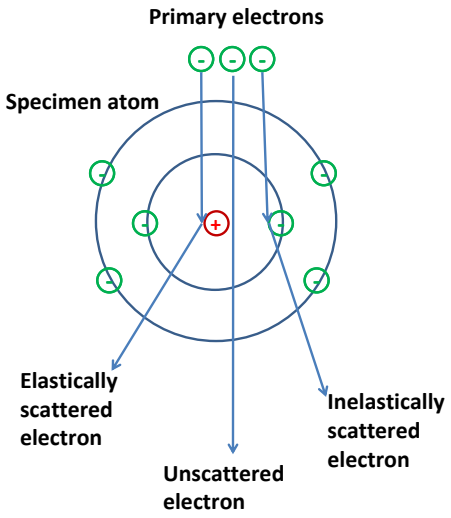

Figure 1.14: Interactions between the primary-beam electrons and atoms of the specimen.

1.4.5 Cyclic Voltammetry

Cyclic Voltammetry (CV) is an electrochemical technique that measures the current that develops in an electrochemical cell, which consists of a working electrode, counter electrode, reference electrode, and electrolytic solution as illustrated in **Figure 1.15**. In a cyclic voltammetry experiment, the working electrode potential is ramped linearly versus time, while the reference electrode maintains a constant potential. The purpose of the electrolytic solution is to provide ions to the electrodes during oxidation and reduction. CV is performed by cycling the potential of a working electrode in a linear fashion and measuring the resulting current.[46, 47]

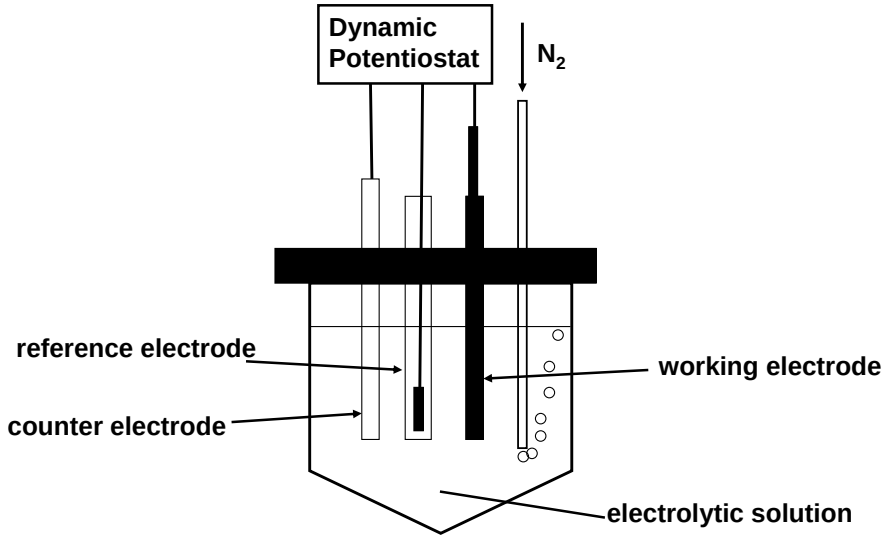

Figure 1.15: A typical electrochemical cell

CV can be used to estimate the HOMO and LUMO energy levels of conjugated polymers by measuring the onset oxidation (p-doping) potential and onset reduction (n-doping) potential. **Figure 1.16** shows a typical cyclic voltammogram of P3HT film in acetonitrile solution of 0.1 M n-Bu_4NClO_4 at scan

rates of 50 mVs^{-1}. In the positive and negative potential region, there are reversible redox peaks that correspond to the p-doping/dedoping and n-doping/dedoping processes, respectively. The onset potential of oxidation and reduction are shown at 0.08 V and -2.24 V, respectively. The oxidation process corresponds to the removal of electrons from the π-band (HOMO) of the polymer; the reduction process corresponds to the transfer of electrons to the π*-band (LUMO).

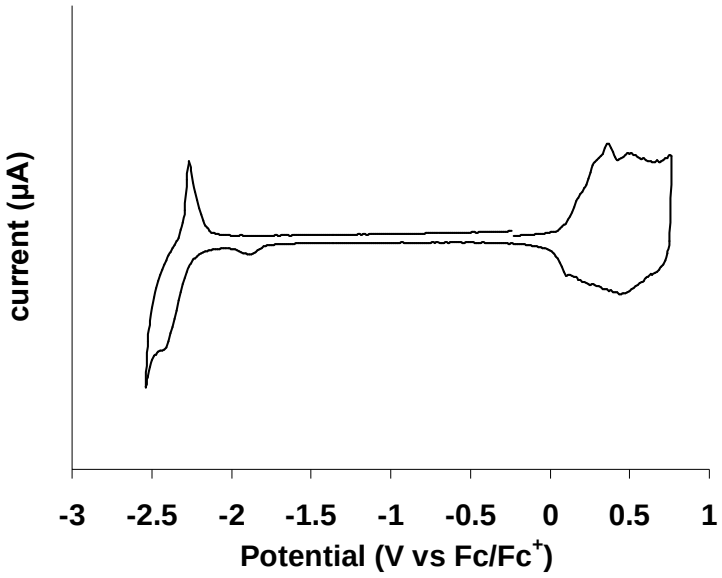

Figure 1.16: Cyclic voltammogram of a P3HT film in acetonitrile solution of 0.1 M n-Bu_4NClO_4 at scan rates of 50 mVs^{-1}.

The ionization potential (HOMO) and electron affinity (LUMO) can be estimated by using **Equation 1.6**.

Equation 1.6: HOMO = φ_{ox} + 4.8 (eV); LUMO = φ_{red} + 4.8 (eV)

where φ_{ox} and φ_{red} represent the onset oxidation and reduction potentials. Potentials are often measured against the ferrocene/ferrocenium redox couple. The energy required to remove one electron from ferrocene relative to the vacuum level is 4.8 eV.[48] In the case of P3HT, the HOMO and LUMO levels are ~ 4.9 and 2.6 eV, respectively. The energy band gap (E_g) can be calculated from the difference between the LUMO and HOMO or from the difference in the onset oxidation and reduction potentials as described in **Equation 1.7**. In case of P3HT, E_g is ~2.3 eV

Equation 1.7: E_g = HOMO –LUMO = e(φ_{ox} - φ_{red}) (eV)

1.5 Polymer Photovoltaic Devices

Photovoltaic devices generate electric power by converting energy from the sun into electricity. The first practical application of “photovoltaics” was to power orbiting satellites and other spacecraft, but today the majority of photovoltaic modules are used for grid connected power generation. Organic, polymer-based photovoltaic devices have introduced the potential of obtaining cheap and easy processes to produce energy from light. The versatility of chemical synthesis and tunable electronic/optical properties of organic and polymer materials, combined with a variety of easy and cheap processing techniques, leads to many potential applications. They also possess advantages such as mechanical flexibility, compatibility with plastic substrates, and are lightweight.[49]

The conversion of light into electricity by organic/polymer solar cells involves several steps as illustrated in **Figure 1.17**.[50] First, a photon is absorbed to create an exciton (electron-hole pair), which is an excited state species. However, the electron and hole remain strongly bound by electrostatic forces and must split to provide free carriers. In organic polymers, excitons typically have binding energies on the order of several tenths of an eV, and the charges do not typically separate. Effective charge separation however can occur in a strong electric field. In organic materials, this field can be designed into the material, in the form of a donor-acceptor interface. Across this interface, a large HOMO-LUMO energy level offset (~0.3 eV) is necessary to produce a large enough internal electric field gradient. For dissociation to occur the exciton must be able to diffuse to the donor-acceptor junction. In the final step, the charge carriers are transported to the respective electrodes.

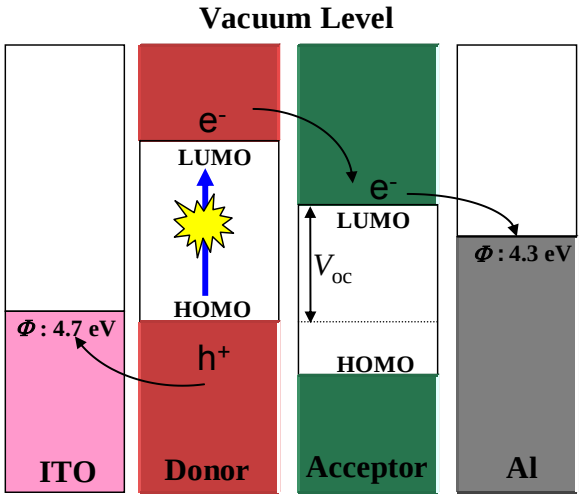

Figure 1.17: Schematic diagram of molecular frontier orbital in solid state illustrating operation of a solid state polymer solar cell.

In 1986 Tang et al. made a breakthrough in the creation of donor-acceptor junctions by forming an interface between bilayers of two organic materials of different electronegativity.[51] In between of the anode and the cathode, a p-type (electron donor) and n-type (electron acceptor) semiconductor are sequentially stacked on top of each other. Organic solar cells behave very differently from their inorganic counterparts, since organic molecules do not show extensive regular 3-D lattices and they possess small exciton diffusion lengths, <20 nm.[52, 53] This leads to the loss of absorbed photons further away from the interface (donor-acceptor junction) and lower quantum efficiencies.

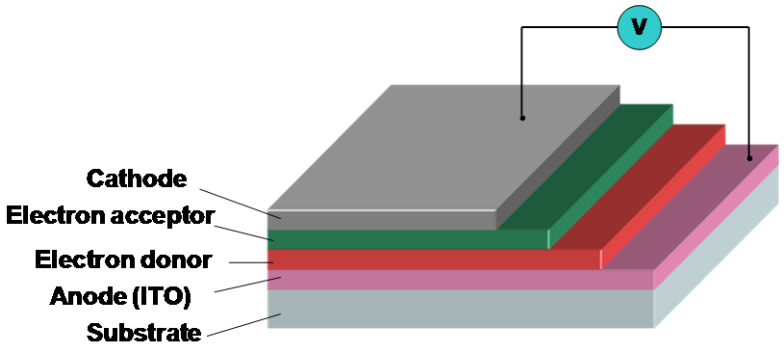

Figure 1.18: Typical structure of a bilayer organic solar cell.

An advance in organic solar cell design came with the introduction of a bulk heterojunction device, where the donor and acceptor materials are blended together to form a giant bulk donor – acceptor heterojunction, as illustrated in **Figure 1.19**.[54, 55] The ideal bulk heterojunction system is an interpenetrating, bicontinuous network of donors and acceptors. Because the length scale of network is less than 20 nm,[52, 53] the problem of the short diffusion distance for the exciton is solvable. Bulk heterojunction systems also possess relatively pure

and continuous phase domains and large interfacial areas that improve charge-carrier conduction through the film to the appropriate electrode and allow maximum exciton separation. PT, PPV, PF and their derivatives blended with PCBM have all been used to prepare bulk heterojunction polymer photovoltaics devices.

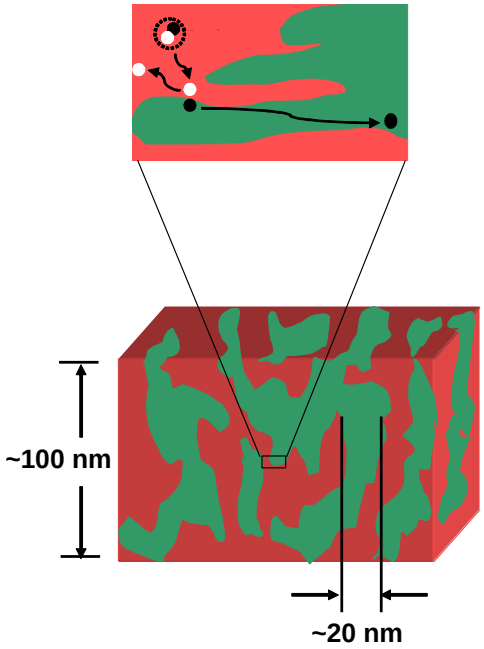

Figure 1.19: Illustration showing the phase separated morphology of a bulk heterojunction system.

Typical current-voltage characteristics of a solar cell device under illumination are shown in **Figure 1.20**.

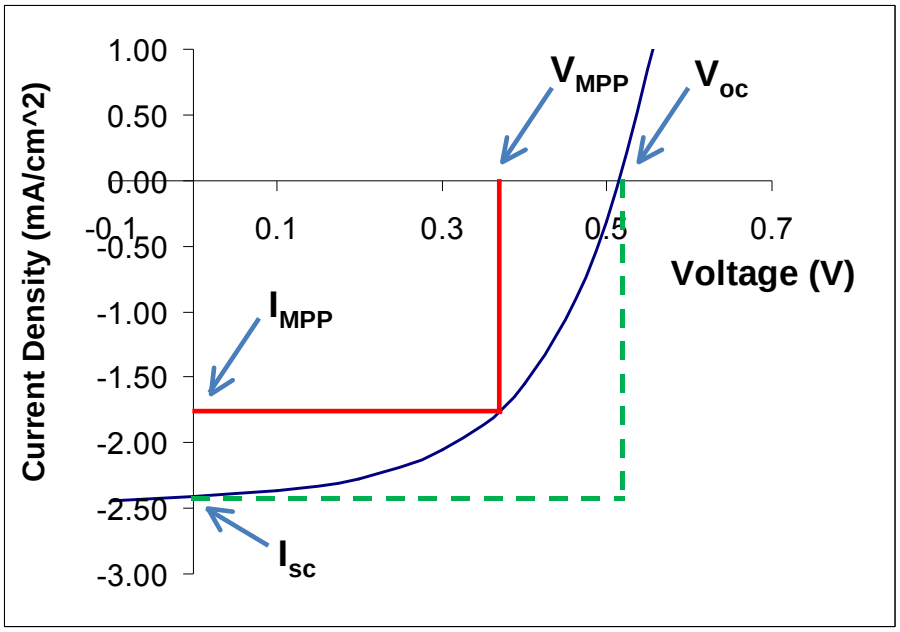

Figure 1.20: Typical current-voltage (I-V) curves of an organic solar cell.

The device generates power under light. The maximum power point (MPP) is where the product of current and voltage is the largest. The photovoltaic power conversion efficiency of a solar cell device is described by **Equation 1.8**.[56]

Equation 1.8: $$\eta_e = \frac{V_{oc} * I_{sc} * FF}{P_{in}}$$

where *V*oc is the open circuit voltage, I_{sc} is the short circuit current. *FF* is the fill factor, and P_{in} is the incident light power density. This light intensity is normally standardized at 100 mW/cm^2 or 80 mW/cm^2 with a spectral intensity distribution matching that of the sun on the earth's surface at an incident angle of 48.2°C, i.e., the AM 1.5 spectrum. I_{mpp} and V_{mpp} are the current and voltage at the maximum power point, respectively.

The largest power output (P_{max}) is determined by the point where the product of voltage and current is maximized. Division of P_{max} by the product of I_{sc} and Voc yields the fill factor FF as shown in **Equation 1.9**.

Equation 1.9: $$FF = \frac{I_{mpp} * V_{mpp}}{I_{sc} * V_{oc}}$$

Common conjugated polymers used for photovoltaic devices are P3HT and poly[2-methoxy-5-(2'-ethylhexoxy)-1,4-phenylenevinylene] (MEH-PPV). Their chemical structures are shown in **Figure 1.21**. Power conversion efficiencies (PCE) of ~5% have been achieved based on P3HT/[6,6]-phenyl-C_{61}-butyric acid methyl ester (PCBM) derivatives.[43] [2,6-(4,4-bis(2-ethylhexyl)-4H-cyclopenta[2,1-b;3,4-b']-dithiophene)-alt-4,7-(2,1,3-benzothiadiazole)] (PCPDTBT) and C_{71}-PCBM devices yield even higher PCEs, up to 5.5%, which is attributed to the interconnected regions of the low band gap polymer donor material.[57] A bicontinuous network can be formed by the incorporation of additives. Recently a poly[4,8-bis-substituted-benzo[1,2-b:4,5-b']dithiophene-2,6-diyl-alt-4-substituted-thieno[3, 4-b]thiophene-2,6-diyl] (PBDTTT) polymer derivative system, provided PCEs > 7%, by combining the advantages of a low HOMO level in the polymer and long wavelength absorption.[58, 59]

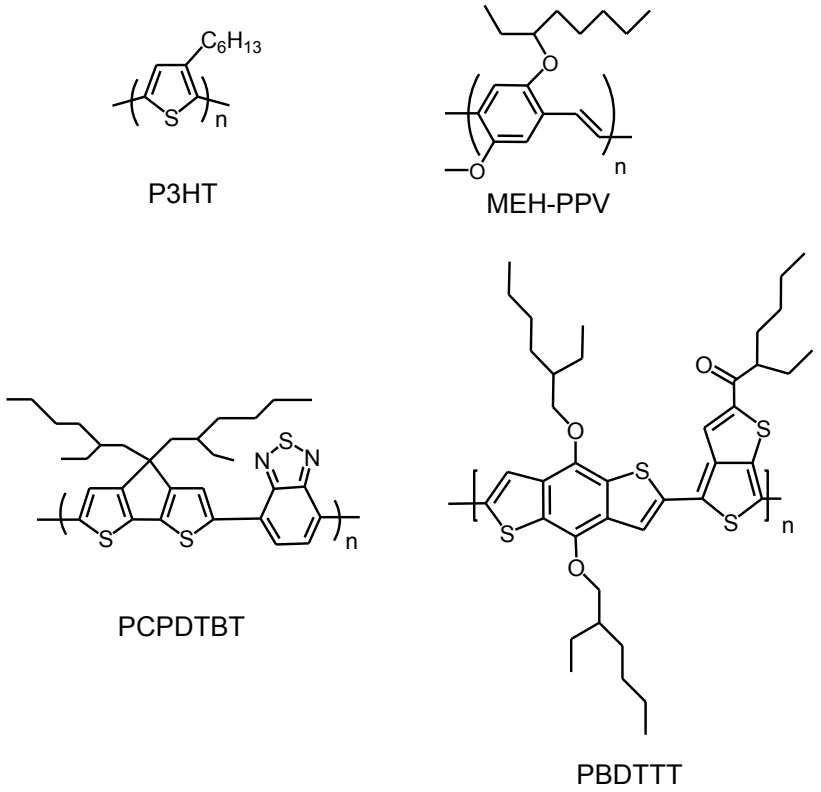

Figure 1.21: Representative electron donor polymers for photovoltaic devices. P3HT; MEH-PPV; PCPDTBT and PBDTTT

1.6 Electron acceptor (n-type) materials

Conjugated polymers are p-type, hole conducting materials that serve as electron donors, whereas materials like PCBM and perylene diimide and their derivatives show an n-type, electron conducting behaviour and serve as electron-acceptor material (see **Figure 1.22**). Fullerenes (C_{60}) are known as excellent electron acceptors and can be chemically modified to improve solubility in organic solvents. Soluble fullerene derivatives, such as PCBM, is considered to be one of the best n-type organic materials. The high affinity of PCBM results facilitates photo-induced electron transfer from p-type polymers.[60] However, C_{60} and its

derivatives have relatively weak molar absorption coefficients at the visible region.

Perylene diimide (PDI) is a common n-type material, which possesses high electron mobility and strong absorption in visible region as well as high optical and thermal stability. In recent years, perylene diimide and its derivatives have been applied to organic photovoltaic cells, largely in the form of layered structures obtained through vapor deposition of insoluble PDIs.[61, 62] Applications of PDIs to bulk heterojunction photovoltaic devices are limited. Perylene diimide is synthesized by sequential imidization of perylene dianhydride with alkylamine in order to aid solublility . Perylene diimide exhibits is a rigid, flat π-systems and can be regarded as being composed of two naphthalene half units (shown in **Figure 1.22**), each of which is attached to an imide unit and connected to the other naphthalene unit by two C sp^2–C sp^2 single bonds. The flat framework allows them to π stacking. [63] PDIs stack in a parallel orientation with a distance of 3.34 -3.55 Å.[63] This π stacking leads to supramolecular organization of which significantly affects properties such as absorption and fluorescence. This π-stacking may also improve exciton and charge transport, which may be relevant to organic solar cells if it is possible to obtain conduction along the p–p stacking axis.[64, 65] As in the case of polymer-based electronics and photovoltaics limitations in charge carrier mobilities and exciton diffusion length are directly related to the structural disorder in PDI. Therefore, it remains to be established that rational organization of perylene bisimides on the nano- and meso-scopic scale may lead to an improvement of the PV device performance.

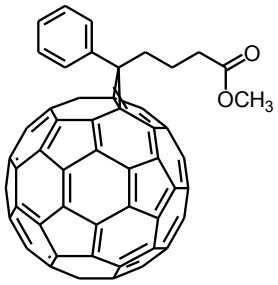

PCBM

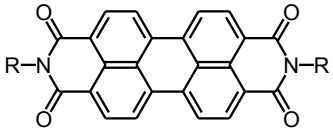

PDI

Figure 1.22: Electron acceptor materials for polymer photovoltaic devices. [6,6]-phenyl-C61-butyric acid methyl ester (PCBM) and perylene diimide (PDI).

1.7 Controlling Nanophase Segregation in Donor/Acceptor Conjugated Polymers

As mentioned in the last section, after photoexcitation, excitons must reach a donor/acceptor interface in order to split into free electrons and holes. If the excitons are > 20 nm from an interface, they will recombine and their potential to develop electricity is lost. This process places strict geometrical requirements on the design of donor-acceptor interfaces: domain sizes must be < 20 nm and the donor and acceptor phases must form continuous pathways to the electrodes. Phase segregation of polymer blends has been investigated to achieve this.[66]

1.7.1 Self-assembly of Block and Graft Copolymers

Copolymers consist of two or more segments of a polymer chain. If the segments are immiscible the domains phase separate into macroscopically distinct regions. Area minimization at the interface of two blocks takes place to lower the interfacial energy. As a result, of competing effects, self-organized

periodic microstructures are formed on the nanoscopic length scale, typically in the range of 10 to 100 nm. Various microdomain structures are achieved, depending on relative volume ratio between blocks and chain architecture.[67]

Various synthetic strategies for preparing block copolymers are available. The most prominent of these is living anionic polymerization.[68] This method yields products with very low polydispersities, but it has its drawbacks. One drawback is that the experimental conditions are very strict, as water and oxygen must be rigorously excluded. Moreover, the highly reactive carbanion prohibits the use of many functional groups. This has been overcome to some extent by the development of the controlled living radical polymerization techniques using either stable nitroxide radicals[69, 70] (nitroxide-mediated living radical polymerization, NMRP) or atom-transfer radical polymerization (ATRP).[71]

Several groups have studied π-conjugated block copolymers in the context of forming bulk heterojunction PV devices. An early example is that reported by the Hadziioannou group of a diblock copolymer consisting of poly(p-phenylene vinylene) (PPV) and a non-conjugated block bearing C_{60} moieties obtained by means of nitroxide-mediated living radical polymerization.[72] The structure of the block copolymer is shown in **Figure 1.23**. The flexible part of the block copolymer consists of a random copolymer of styrene and 4-chloromethylstyrene. Atom-transfer radical addition to a chloromethyl group was used to graft C_{60} onto the flexible part of the block copolymer. Efficient electron transfer at the donor-acceptor interface was confirmed by the quenching of the

luminescence from the PPV block. Films exhibit a honeycomb structuring on the micrometer level.

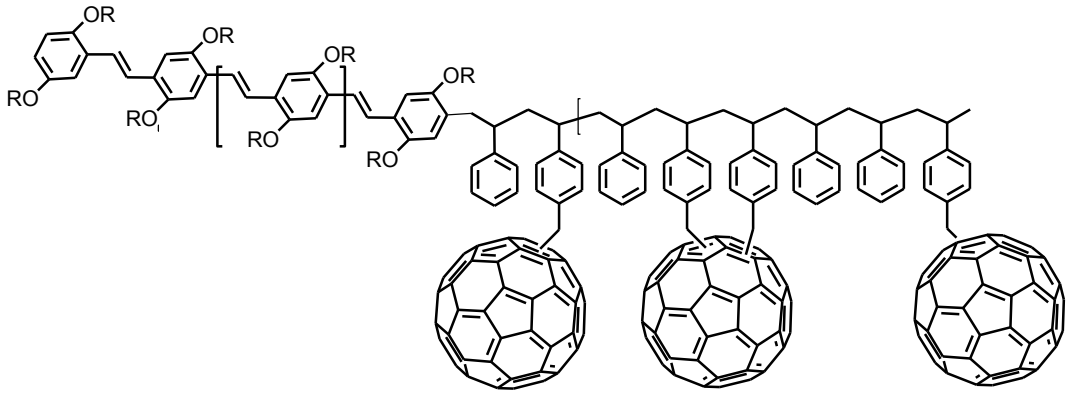

Figure 1.23: Structure of PPV block copolymer.

In research directed to understand the relationship between polymeric structure, materials morphology and the mobility of ionic charges in proton conducting polymer systems, it has been shown that bi-continuous, nano-phase segregated domains of charge carriers can be consistently obtained by placing the charge carrier on grafted side chains of polymer backbone, and that the morphology, and subsequently, charge mobility can be controlled by the number and length of the charge carrying grafts.[73-75] This strategy, of separating charge carriers from the backbone in the form of grafts, would appear applicable to the study of structure-property relationships in the design of conjugated polymer systems where a bi-continuous architectures, consisting of electron and hole transporting domains is a fundamental requirement.

Graft copolymers for photovoltaic applications have been reported.[76] Here, poly(3-hexylthiophene) was post-functionalized to form a macroinitiator

bearing a 2,2,6,6-tetramethylpiperidine-1-oxyl (TEMPO) group on each thienyl ring. This macroinitiator initiated the nitroxide-mediated radical polymerization of styrene and 4-chloromethylstyrene, and subsequently reacted with C_{60} to yield soluble graft, rod-coil polymers as shown in **Figure 1.24**. Electronic excitation of the π-conjugated main chain was completely quenched by the C_{60} whereas comparable solution blends of P3HT and C_{60} were only partially quenched. The 100% substituted P3HT is characterized by a considerably blue-shift in absorption compared to pristine P3HT, the partially-substituted (10%) polymers exhibits an absorption spectrum similar to pristine P3HT. Films of the polymers display a bi-continuous and tens of nanometers phase structure. The research opens up new possibilities for photonic applications.

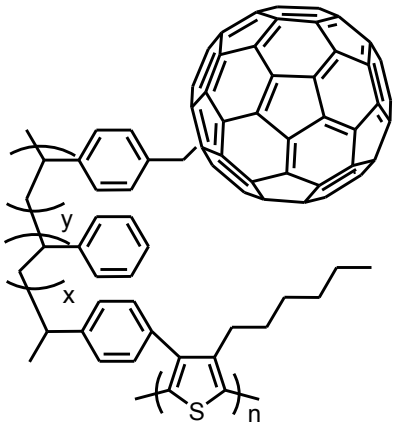

Figure 1.24: Structure of P3HT graft copolymer.

Block copolymers with polyacrylate segment bearing perylene bisimide side groups have been synthesized and the structures are shown in **Figure 1.26**.[77, 78] Single-active-layer photovoltaic device was obtained by the self-assembly of the diblock copolymer (**a**). The block copolymer self-assembles into

a nanostructure, which provides charge separating interfaces on the nanometer scale. The performance of the block-copolymer device is improved with respect to devices made from a blend of the two individual segment polymers. Copolymers of P3HT as donor block and poly(perylene bisimide acrylate) as acceptor block (**b**) provide stable microphase separated domains.

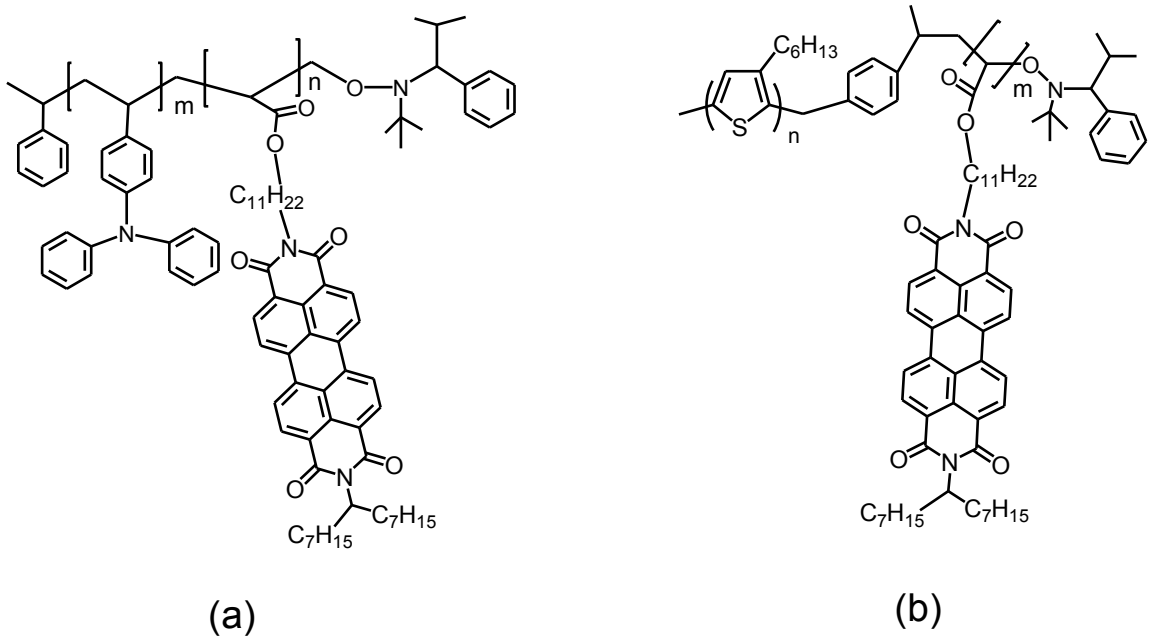

Figure 1.25: Structure of block copolymers with polyacrylate segment bearing perylene bisimide side groups.

1.7.2 Controlling Phase Segregation using a Copolymer Compatiblizer

For PV devices based on P3HT donor and PCBM acceptor blends, a thermal-annealing step above the P3HT's glass-transition temperature (T_g), ~ 120 °C, is required to improve device performance.[79] However, the phase segregation of the bulk blend can change drastically upon heating owing to the diffusion and aggregation of PCBM.[80] Frechet's group thus reported a side chain diblock polymer possessing an oligothiophene donor block and C_{60} as the

acceptor block as shown in **Figure 1.26**.[81] This polymer is shown to function as a compatibilizer. It was demonstrated that lowering the interfacial energy between the polymer and fullerene by adding small amounts of the diblock copolymer altered the morphology of blended thin film and stabilized nano-phase segregation, which ultimately preserved device performance.

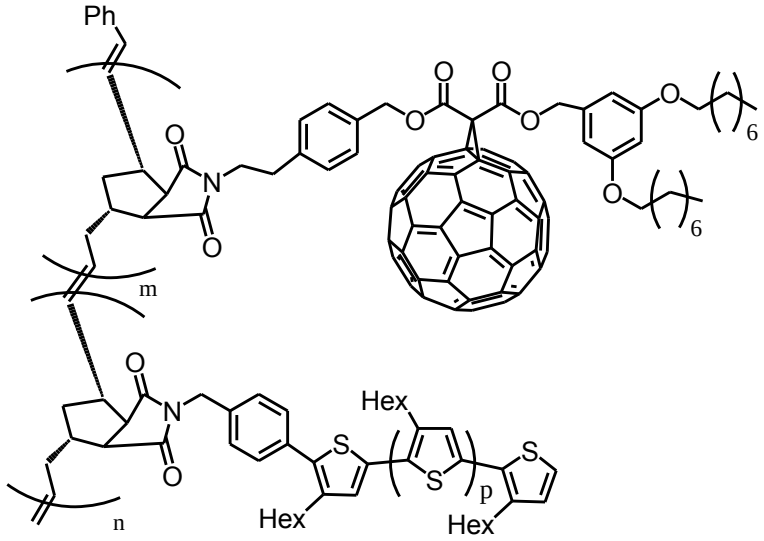

Figure 1.26: Structure of diblock copolymers incorporating fullerene and P3HT.

Kallitsis et al. described the synthesis of copolymers based on a polythiophene backbone and a poly(vinyl quinoline) graft chain as shown in **Figure 1.27**.[82] The brushtype copolymers were obtained by atom transfer radical polymerization of a vinyl quinoline monomer. This copolymer has been used to study the compatibilizing efficiency in a P3HT/polyquinoline system. Morphological studies reveal a vast improvement of the morphology with the use of the compatibilizing copolymers. Phase separation is greatly reduced, along with the roughness of the thin films. Without the graft copolymer compatibilizer,

blends of P3HT and polyquinoline are immiscible and phase segregate with domains reaching 400 nm. By introduction of the copolymer, a uniform morphology throughout the active layer was achieved. The morphology provides phase separation in a scale of ~10 nm, which corresponds to the exciton diffusion length.

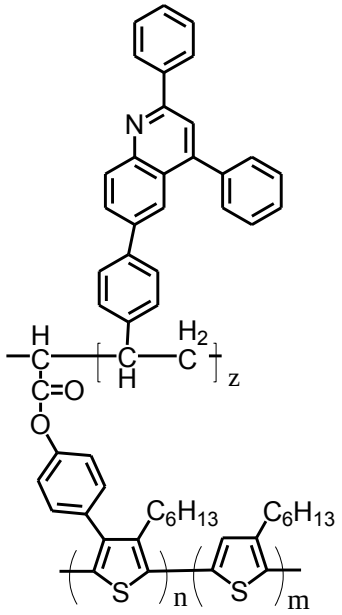

Figure 1.27: Structure of thiophene quinoline brush-type copolymers.

1.8 Project Overview

π-conjugated polymers have attracted considerable attention over the past three decades on account of their special properties, which include electronic conductivity, electroluminescence and light-harvesting. Conjugated polymers can be used as electron donors and their combination with electron acceptors can lead to efficient photovoltaic devices. Bulk heterojunctions of polymer donors and acceptors would appear to be a requirement in order to efficiently dissociate

photo-generated excitons, the diffusion length of which is estimated to be tens of nano meters. It is well known that block copolymers form a variety of different morphologies in the solid state depending on the length and nature of the blocks. In most instances nano-meter-scale phase separation can be obtained between the two different block domains. These would seem ideal structures for designing bulk heterojunction polymeric devices. Copolymers containing donor and acceptor blocks can be used directly or used as compatibilizers to control film morphologies. [72, 76-83] Graft copolymers based on conjugated backbones and non-conjugated side chains have been demonstrated using a combination of post-functionalization of polythiophenes followed by TEMPO-assisted free radical polymerization.[76]

The thesis research focuses on the synthesis of new copolymers and materials by post-functionalization of polythiophenes, and methods to control phase segregation, film morphology and their opto-electronic properties. Blending post-functionalized polythiophenes with acceptors is demonstrated as a convenient way to produce desired phase segregation with nano-structures.

Chapter 2 presents the synthesis of a triazole monomer and its nitroxide-mediated radical polymerization, the synthesis of a macroinitiator consisting of a polythiophene backbone bearing nitroxide groups, and the synthesis of a graft copolymer consisting of a polythiophene backbone bearing polyvinyl triazole moieties. This chapter introduces a new strategy that using π-conjugated polymer bearing graft chains that are compatible with a fullerene that is chemically modified with a similar motif so as to promote their intimate mixing at

the nanoscopic level. The chemical similarity of the triazole functionality attached to P3HT and the fullerene leads to the formation of films with uniform, stable, nanophase morphologies.

Chapter 3 investigates the synthesis of perylene-functionalized P3HT and its solution casting in the presence of perylene diimide (PDI). The strategy is demonstrated with P3HT, partially functionalized at the 4-position with N-(1-hexylheptyl)-N'-(12-carboxylicdodecyl)perylene-3,4,9,10-tetracarboxylbisimide (PP3HT). A unique film morphology is accomplished via the growth of 1-D assemblies of PDI, which are hundreds of nanometers wide, 10 – 20 nm thick, several microns in length, and run parallel to the surface of the substrate. Nano-sized domains of the polymer and the n-type material are in intimate contact. These domains encapsulate 1-D assemblies of nanocrystallites. The research offers an alternative route for the fabrication of innovative supramolecular structures for optoelectronic applications.

Chapter 4 contains a summary of the work and describes future studies related to the thesis topic.

1.9 Reference List

[1] C. K. Chiang, C. R. Fincher, Y. W. Park, A. J. Heeger, H. Shirakawa, E. J. Louis, S. C. Gau, A. G. Macdiarmid. *Physical Review Letters* **1977**, *39*(17), 1098-1101.

[2] H. Shirakawa, E. J. Louis, A. G. Macdiarmid, C. K. Chiang, A. J. Heeger. *Journal of the Chemical Society-Chemical Communications* **1977**, (16), 578-580.

[3] K. F. Schoch. *Ieee Electrical Insulation Magazine* **1994**, *10*(3), 29-32.

[4] M. Angelopoulos. *Ibm Journal of Research and Development* **2001**, *45*(1), 57-75.

[5] J. E. Frommer, R. R. Chance. *Encyclopedia of Polymer Science and Engineering, Vol. 5,* Wiley: New York, **1986**.

[6] R. H. Friend, R. W. Gymer, A. B. Holmes, J. H. Burroughes, R. N. Marks, C. Taliani, D. D. C. Bradley, D. A. Dos Santos, J. L. Bredas, M. Logdlund, W. R. Salaneck. *Nature* **1999**, *397*(6715), 121-128.

[7] J. H. Burroughes, D. D. C. Bradley, A. R. Brown, R. N. Marks, K. Mackay, R. H. Friend, P. L. Burns, A. B. Holmes. *Nature* **1990**, *347*(6293), 539-541.

[8] F. Garnier, R. Hajlaoui, A. Yassar, P. Srivastava. *Science* **1994**, *265*(5179), 1684-1686.

[9] N. S. Sariciftci, L. Smilowitz, A. J. Heeger, F. Wudl. *Science* **1992**, *258*(5087), 1474-1476.

[10] S. Hotta, D. D. V. Rughooputh, A. J. Heeger, F. Wudl. *Macromolecules* **1987**, *20*(1), 212-215.

[11] J. Roncali. *Chemical Reviews* **1997**, *97*(1), 173-206.

[12] S. Sun, L. Dalton. *Introduction to Organic Electronic and Optoelectronic Materials and Devices,* CRC Press, FL, **2007**, p. 191.

[13] J. Roncali. *Chemical Reviews* **1992**, *92*(4), 711-738.

[14] R. D. McCullough. *Advanced Materials* **1998**, *10*(2), 93-116.

[15] T. A. Chen, X. Wu, R. D. Rieke. *Journal of the American Chemical Society* **1995**, *117*(1), 233-244.

[16] Y. Ohmori, M. Uchida, K. Muro, K. Yoshino. *Japanese Journal of Applied Physics Part 2-Letters* **1991**, *30*(11B), L1941-L1943.

[17] T. Sugimoto, T. Nagatomi, H. Ando, Z. Yoshida. *Angewandte Chemie-International Edition in English* **1988**, *27*(4), 560-561.

[18] M. Leclerc, F. M. Diaz, G. Wegner. *Makromolekulare Chemie-Macromolecular Chemistry and Physics* **1989**, *190*(12), 3105-3116.

[19] R. D. Mccullough, R. D. Lowe. *Journal of the Chemical Society-Chemical Communications* **1992**, (1), 70-72.

[20] R. D. Mccullough, R. D. Lowe, M. Jayaraman, D. L. Anderson. *Journal of Organic Chemistry* **1993**, *58*(4), 904-912.

[21] W. B. Smith. *Journal of Organic Chemistry* **1961**, 26, 4206-4209.

[22] R. S. Loewe, S. M. Khersonsky, R. D. McCullough. *Advanced Materials* **1999**, *11*(3), 250-253.

[23] R. S. Loewe, P. C. Ewbank, J. S. Liu, L. Zhai, R. D. McCullough. *Macromolecules* **2001**, *34*(13), 4324-4333.

[24] T. A. Chen, R. D. Rieke. *Synthetic Metals* **1993**, *60*(2), 175-177.

[25] T. A. Chen, R. D. Rieke. *Journal of the American Chemical Society* **1992**, *114*(25), 10087-10088.

[26] E. I. Negishi. *Accounts of Chemical Research* **1982**, *15*(11), 340-348.

[27] N. Miyaura, A. Suzuki. *Journal of the Chemical Society-Chemical Communications* **1979**, (19), 866-867.

[28] N. Miyaura, K. Yamada, A. Suzuki. *Tetrahedron Letters* **1979**, (36), 3437-3440.

[29] S. Guillerez, G. Bidan. *Synthetic Metals* **1998**, *93*(2), 123-126.

[30] M. Rehahn, A. D. Schluter, G. Wegner, W. J. Feast. *Polymer* **1989**, *30*(6), 1054-1059.

[31] T. Yamamoto, A. Yamamoto. *Chemistry Letters* **1977**, (4), 353-356.

[32] A. A. Pud. *Synthetic Metals* **1994**, *66*(1), 1-18.

[33] C. Barbero, M. C. Miras, B. Schnyder, O. Haas, R. Kotz. *Journal of Materials Chemistry* **1994**, *4*(12), 1775-1783.

[34] J. Yue, Z. H. Wang, K. R. Cromack, A. J. Epstein, A. G. Macdiarmid. *Journal of the American Chemical Society* **1991**, *113*(7), 2665-2671.

[35] M. Besbes, G. Trippe, E. Levillain, M. Mazari, F. Le Derf, I. F. Perepichka, A. Derdour, A. Gorgues, M. Salle, J. Roncali. *Advanced Materials* **2001**, *13*(16), 1249-1252.

[36] Y. N. Li, G. Vamvounis, J. F. Yu, S. Holdcroft. *Macromolecules* **2001**, *34*(10), 3130-3132.

[37] Y. N. Li, G. Vamvounis, S. Holdcroft. *Macromolecules* **2001**, *34*(2), 141-143.

[38] Y. N. Li, G. Vamvounis, S. Holdcroft. *Macromolecules* **2002**, *35*(18), 6900-6906.

[39] D. A. Skoog, F. J. Holler, T. A. Nieman. *Principles of Instrmental Analysis,* Hardcourt Brane College Publishes, FL, **1998**.

[40] J.Guillet. *Photophysics and Photochemistry,* London, Cambridge University Press, **1985**.

[41] D. F. Eaton. *Pure and Applied Chemistry* **1988**, *60*(7), 1107-1114.

[42] N. Kasai, M. Kakudo. *X-ray diffraction by macromolecules,* Kodansha, Tokyo ; Springer, New York, **2005**.

[43] W. L. Ma, C. Y. Yang, X. Gong, K. Lee, A. J. Heeger. *Advanced Functional Materials* **2005**, *15*(10), 1617-1622.

[44] B. Fultz, J. Howe. *Transmission Electron Microscopy and Diffractometry of Materials,* Springer, NY, **2007**.

[45] J. M. Li, L. Lu, O. M. Lai, B. Ralph. *Image-based Fractal Description of Microstructures,* Kluwer Academic, Netherlands, **2003**.

[46] J. J. Vanbenschoten, J. Y. Lewis, W. R. Heineman, D. A. Roston, P. T. Kissinger. *Journal of Chemical Education* **1983**, *60*(9), 772-776.

[47] P. T. Kissinger, W. R. Heineman. *Journal of Chemical Education* **1983**, *60*(9), 702-706.

[48] R. Cervini, X. C. Li, G. W. C. Spencer, A. B. Holmes, S. C. Moratti, R. H. Friend. *Synthetic Metals* **1997**, *84*(1-3), 359-360.

[49] N. S. Sariciftci, L. Smilowitz, A. J. Heeger, F. Wudl. *Science* **1992**, *258*(5087), 1474-1476.

[50] C. J. Brabec, G. Zerza, G. Cerullo, S. De Silvestri, S. Luzzati, J. C. Hummelen, S. Sariciftci. *Chemical Physics Letters* **2001**, *340*(3-4), 232-236.

[51] C. W. Tang. *Applied Physics Letters* **1986**, *48*(2), 183-185.

[52] J. J. M. Halls, K. Pichler, R. H. Friend, S. C. Moratti, A. B. Holmes. *Applied Physics Letters* **1996**, *68*(22), 3120-3122.

[53] M. Theander, A. Yartsev, D. Zigmantas, V. Sundstrom, W. Mammo, M. R. Andersson, O. Inganas. *Physics Review B: Condensed Matter* **2000**, *61*(19), 12957-12963.

[54] J. J. M. Halls, C. A. Walsh, N. C. Greenham, E. A. Marseglia, R. H. Friend, S. C. Moratti, A. B. Holmes. *Nature* **1995**, *376*(6540), 498-500.

[55] G. Yu, J. Gao, J. C. Hummelen, F. Wudl, A. J. Heeger. *Science* **1995**, *270*(5243), 1789-1791.

[56] S. Gunes, H. Neugebauer, N. S. Sariciftci. *Chemical Reviews* **2007**, *107*(4), 1324-1338.

[57] Lee J, W. L. Ma, C. J. Brabec, Yuen J, Moon J S, Kim J Y, K. Lee, Bazan C, A. J. Heeger. *Journal of the American Chemical Society* **2008**, 130, 3619-3628.

[58] H. Y. Chen, J. H. Hou, S. Q. Zhang, Y. Y. Liang, G. W. Yang, Y. Yang, L. P. Yu, Y. Wu, G. Li. *Nature Photonics* **2009**, *3*(11), 649-653.

[59] J. H. Hou, H. Y. Chen, S. Q. Zhang, R. I. Chen, Y. Yang, Y. Wu, G. Li. *Journal of the American Chemical Society* **2009**, *131*(43), 15586-15587.

[60] C. R. Newman, C. D. Frisbie, D. A. da Silva, J. L. Bredas, P. C. Ewbank, K. R. Mann. *Chemistry of Materials* **2004**, *16*(23), 4436-4451.

[61] J. Nakamura, C. Yokoe, K. Murata, K. Takahashi. *Journal of Applied Physics* **2004**, *96*(11), 6878-6883.

[62] R. de Bettignies, Y. Nicolas, P. Blanchard, E. Levillain, J. M. Nunzi, J. Roncali. *Advanced Materials* **2003**, *15*(22), 1939-1943.

[63] F. Wurthner. *Chemical Communications* **2004**, (14), 1564-1579.

[64] T. van der Boom, R. T. Hayes, Y. Y. Zhao, P. J. Bushard, E. A. Weiss, M. R. Wasielewski. *Journal of the American Chemical Society* **2002**, *124*(32), 9582-9590.

[65] S. G. Liu, G. D. Sui, R. A. Cormier, R. M. Leblanc, B. A. Gregg. *Journal of Physical Chemistry B* **2002**, *106*(6), 1307-1315.

[66] R. A. Segalman, B. McCulloch, S. Kirmayer, J. J. Urban. *Macromolecules* **2009**, *42*(23), 9205-9216.

[67] G. Krausch, R. Magerle. *Advanced Materials* **2002**, *14*(21), 1579-1583.

[68] M. Szwarc. *Journal of Polymer Science Part A-Polymer Chemistry* **1998**, *36*(1), IX-XV.

[69] E. E. Malmstrom, C. J. Hawker. *Macromolecular Chemistry and Physics* **1998**, *199*(6), 923-935.

[70] C. J. Hawker. *Accounts of Chemical Research* **1997**, *30*(9), 373-382.

[71] T. E. Patten, K. Matyjaszewski. *Advanced Materials* **1998**, *10*(12), 901-915.

[72] U. Stalmach, B. de Boer, C. Videlot, P. F. van Hutten, G. Hadziioannou. *Journal of the American Chemical Society* **2000**, *122*(23), 5464-5472.

[73] J. F. Ding, C. Chuy, S. Holdcroft. *Macromolecules* **2002**, *35*(4), 1348-1355.

[74] J. F. Ding, C. Chuy, S. Holdcroft. *Chemistry of Materials* **2001**, *13*(7), 2231-2233.

[75] J. F. Ding, C. Chuy, S. Holdcroft. *Advanced Functional Materials* **2002**, *12*(5), 389-394.

[76] X. W. Chen, B. Gholamkhass, X. Han, G. Vamvounis, S. Holdcroft. *Macromolecular Rapid Communications* **2007**, *28*(17), 1792-1797.

[77] M. Sommer, A. S. Lang, M. Thelakkat. *Angewandte Chemie-International Edition* **2008**, *47*(41), 7901-7904.

[78] S. M. Lindner, S. Huttner, A. Chiche, M. Thelakkat, G. Krausch. *Angewandte Chemie-International Edition* **2006**, *45*(20), 3364-3368.

[79] Y. Kim, S. A. Choulis, J. Nelson, D. D. C. Bradley, S. Cook, J. R. Durrant. *Applied Physics Letters* **2005**, *86*(6).

[80] T. Erb, U. Zhokhavets, G. Gobsch, S. Raleva, B. Stuhn, P. Schilinsky, C. Waldauf, C. J. Brabec. *Advanced Functional Materials* **2005**, *15*(7), 1193-1196.

[81] K. Sivula, Z. T. Ball, N. Watanabe, J. M. J. Frechet. *Advanced Materials* **2006**, *18*(2), 206-210.

[82] S. P. Economopoulos, C. L. Chochos, V. G. Gregoriou, J. K. Kallitsis, S. Barrau, G. Hadziioannou. *Macromolecules* **2007**, *40*(4), 921-927.

[83] C. Park, J. Yoon, E. L. Thomas. *Polymer* **2003**, *44*(22), 6725-6760.

2: STABILIZING BICONTINUOUS NANOPHASE SEGREGATION IN Π-CONJUGATED POLYMER-C_{60} DONOR-ACCEPTOR BLENDS

Sections of this chapter have been reproduced in part with permission from:

Journal of the American Chemical Society **2008**, 130, 11711-11718,

2.1 Introduction

π -Conjugated polymers (πCPs) are currently under investigation as active materials in photovoltaic devices.[1-3] The mechanism of energy conversion involves the absorption of photons, diffusion of excitons, dissociation of excitons into positive and negative charges, and migration and capture of the charges at electrodes.[4] Since the exciton diffusion length in conjugated polymers is typically measured in the tens of nanometers, the donor/acceptor (D/A) system must be designed so that the exciton reaches the D/A interface within this length scale.[5, 6] The conversion efficiency of polymer photovoltaic cells is thus strongly related to the length scale of phase segregation between donor and acceptor domains. The development of bulk D/A heterojunction structures, possessing interpenetrating, bicontinuous networks, has been found to be a potential strategy for maximizing the conversion of photons to charges while facilitating charge carrier transport through acceptor and donor domains.[7-9] Electron-donating polymers, such as poly(3-hexylthiophene) (P3HT) and poly[2-methoxy-5-(2′-ethyl-hexyloxy)-1,4-phenylene vinylene] (MEH-PPV), have been widely used as hole carriers in conjunction with soluble fullerenes, such as [6,6]-phenyl-C61-butyric acid methyl ester (PCBM), which serve as the electron acceptor and electron transporting material.

Increasing the purity of the phase domains of electron donors and acceptors should provide an advantage in that the electron acceptor molecules are not isolated in the donor, and vice versa, which may circumvent charge trapping and improve device performances.[10] Various methods have been

developed to increased crystallinity of the P3HT and more distinguishable D/A phase morphologies, which results in improved solar cell performance. Various methods have been developed to optimize phase segregation. For example, Forrest et al. used organic vapor-phase deposition (OVPD) to control the consecutive crystalline growth of donor and acceptor layers.[11] Control of the extent of crystallization and morphology resulted in a low resistance, ordered, interdigitated interfaces that significantly improved solar cell efficiency. Holdcroft and co-workers developed a technique using π-conjugated polymers bearing a thermally cleavable solubilizing group to obtain pure, nanostructured phase domains of donors and acceptors.[12] Thermal annealing[13, 14] or solvent annealing[15] of P3HT-PCBM produces increased crystallinity of the P3HT and more distinguishable D/A phase morphologies, which results in improved solar cell performance. Recently, Heeger et al. showed that larger interconnected regions of a low band gap donor material and a bicontinuous network could be formed by the incorporation of additives.[16] Loo et al. reported improved efficiencies by incorporating nonvolatile transition metal complexes into blends of P3HT:PCBM. These additives selectively partition into the P3HT phase, effectively increasing phase separation between the P3HT and PCBM.[17] Cumulatively, these studies indicate photovoltaic performance is improved for systems that improve the phase purity of the donor and acceptor phases, form a bicontinuous network, and produce relatively small D/A domains.

Due to the need to develop systems in which phase segregation of D/A domains can be controlled, the block and graft copolymer approach is attracting

increasing interest because of their capability of forming self-assembled, well-ordered micro and nanostructured morphologies.[18-20] For example, Jenekhe et al. reported the self-assembling behaviour of rod-coil block conjugated copolymers and their encapsulation of fullerenes.[21, 22] McCullough and co-workers reported on the self-assembly of regioregular polythiophene block copolymers and their electrical conductivities.[23] Mezzenga et al. studied self-assembly of PPV based rod-coil block copolymers by varying the volume fraction of the blocks and the annealing temperature.[24, 25] A block polymer is also reported in which one block is compatible with the surface of colloidal particles while the other block serves as a matrix for a doped conducting polymer, so that a single, continuous conducting phase is formed, providing a low percolation threshold for electric conductivity.[26] Several other groups have studied π-conjugated block copolymers in the context of forming bulk heterojunction PV devices. An early example is that reported by the Hadziioannou group of a diblock copolymer consisting of poly(p-phenylene vinylene) (PPV) and a nonconjugated block bearing C_{60} moieties.[27-31] More recently, copolymers combining various donor and acceptor motifs have been reported that modify the morphology of the films. For example, Frechet and co-workers reported a side chain diblock polymer possessing oligothiophene donor blocks and a C_{60} acceptor block, which enhances the stability of the film morphology as a compatiblizer.[32] Lindner et al. described a block polymer with donor and acceptor blocks that form a self-assembled nanostructure which can improve charge separation.[33] Kallitsis et al. described the synthesis of copolymers based

on a polythiophene backbone and a poly(vinyl quinoline) graft chain,[34] whereas Holdcroft and co-workers described the synthesis of polythiophene onto which C_{60}-bearing side chains are grown.[35]

Despite these significant advances, the tailoring of π-conjugated copolymers for the purpose of controlling phase segregation is in its infancy, and systematic studies with model systems are required in order to delineate the role of the polymer structure on the morphology and to determine the role played by morphology on the properties of D/A blends. Furthermore, there is a need to investigate and develop strategies to control the ratio of donor-to-acceptor groups and to further control the size and formation of continuous nanophases that are required for charge migration and collection in PV devices.[23, 29, 35]

In this chapter, a strategy is described for controlling the size, contiguous nature, and extent of phase segregation of donor and acceptor domains. This strategy involves the synthesis of a π-conjugated polymer bearing graft chains that are compatible with a fullerene, chemically modified with a similar motif so as to promote their intimate mixing at the nanoscopic level as shown in Scheme 2.1. This concept is demonstrated with model polymers through the synthesis of a polythiophene backbone bearing poly(vinyl triazole) graft chains and by its blending with C_{60} bearing a similar triazole moiety. The structures of the polymer and $TAZC_{60}$ are described in **Scheme 2.2**. Pendant triazole chains were chosen because they have been shown to enhance electron transport properties in OLEDs.[36-39] The synthesis and properties of C_{60} modified with a triazole group ($TAZC_{60}$) have recently been reported by Holdcroft's group.[40] It is found that

$TAZC_{60}$ possesses optical and electrochemical properties that are similar to those of both C_{60} and PCBM. $TAZC_{60}$ possesses good electron transport properties, but electron mobility values are an order of magnitude lower than that of PCBM.[40] Thus, while $TAZC_{60}$ serves as an acceptable model demonstrating the use of an affinity fullerene with a π-conjugated polymer, it is not expected to yield PV devices with high photoconversion efficiencies.

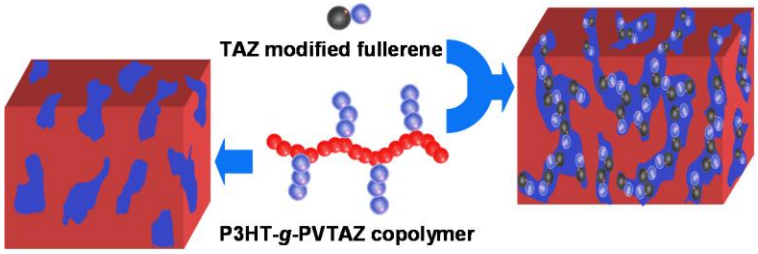

Scheme 2.1: Stabilizing bicontinous nano-phase segregation in graft copolymer and chemically modified fullerene donor-acceptor blends.

The synthesis of graft polythiophenes builds on previous contributions on postfunctionalization of P3HT, wherein partial bromination at the 4-position of the thienyl ring, followed by Pd-catalyzed coupling, enables the covalent attachment of a wide variety of functional groups.[41-43] In the present work, P3HT is functionalized with a nitroxide and is used to initiate the nitroxide-mediated radical polymerization (NMRP) of a vinyl triazole. The synthesis and polymerization of the vinyl triazole, the synthesis, characterization, and morphology of the novel graft copolymer, and the optical and morphological characterization of its blends with $TAZC_{60}$, are described.

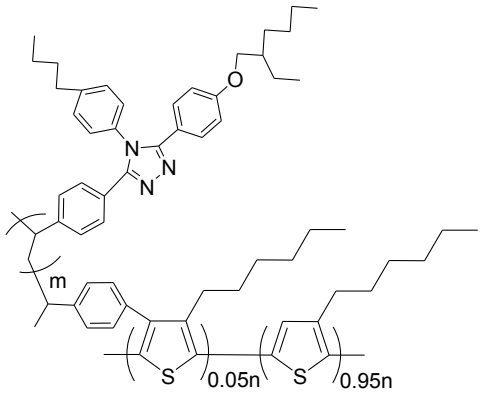

P3HT-*g*-PVTAZ (11)

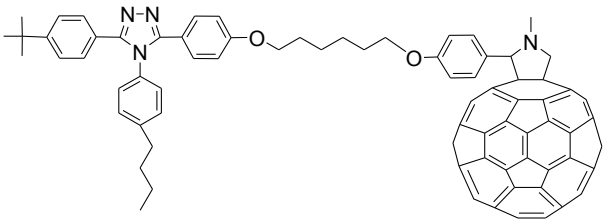

TAZC60

Scheme 2.2: Structures of the graft polymer and affinity fullerene used in this work.

2.2 Experimental

2.2.1 Chemicals

Solvents, reagents, and chemicals were purchased from Aldrich Chemical Co. and used without further purification unless otherwise stated. RR-P3HT possessing >95% regioregularity was synthesized for postfunctionalization, as described below. P3HT possessing ~92% regioregularity was purchased from Rieke Metals, Inc. (M_n = 28000; polydispersity = 1.86) and was only used for preparing blends with $TAZC_{60}$. The latter was preferred as a reference material over RR-P3HT with >95% regioregularity because of its widespread use in photovoltaic applications. THF and toluene were dried over Na/benzophenone

and freshly distilled prior to use. DMF was dried over barium oxide and freshly distilled prior to use.

2.2.2 Synthesis

1-(p-Anisoyl) 2-(4'-bromo)benzoyl hydrazide (1). A solution of 4-bromobenzoyl hydrazine (25.0 g, 116 mmol) and sodium carbonate (12.3 g, 116 mmol) in dioxane (300 mL) was stirred and heated to 40 °C under nitrogen. A solution of p-anisoyl chloride (19.8 g, 116 mmol) in dioxane (50 mL) was added dropwise and the mixture allowed to react at ambient temperature for 24 h. After the reaction was completed, 300 mL of 3 M aqueous HCl was added to precipitate the crude product. The precipitate was collected by filtration, washed with deionized water and dried under vacuum overnight. The yield was 76.2 % (30 g). ^{1}H NMR (DMSO-d_6), δ (ppm): 10.58 (1H, s), 10.43 (1H, s), 7.94 (2H, d), 7.89 (2H, d), 7.75 (2H, d), 7.06 (2H, d), 3.83 (3H, s).

3-(4'-Anisyl)-4-(4'-n-butylphenyl)-5-(4'-bromophenyl)-1,2,4-triazole (2). A solution of 4-*n*-butylaniline (60 mL, 0.38 mol) in *o*-dichlorobenzene (80 mL) was stirred under nitrogen, and a solution of phosphorous chloride (13.9 g, 0.10 mol) in o-dichlorobenzene (40 mL) added dropwise. The mixture was allowed to heat at 100 °C for 1 h. A suspension of **(1)** (30 g, 85.9 mmol) in *o*-dichlorobenzene (80 mL) was added to the solution and the mixture refluxed at 180 °C for 3 h. Residual solvent was removed by azeotropic distillation with added water. The solid was filtered and dried. Recrystallization from ethyl acetate gave 32.5 g of a white solid (yield 82.1 %). ^{1}H NMR (CD_2Cl_2), δ (ppm): 7.44 (2 H,

d), 7.35 (2 H, d), 7.30 (2 H, d), 7.26 (2 H, d), 7.07 (2 H, d), 6.82 (2 H, d), 3.78 (3 H, s), 2.68 (2 H, t), 1.63 (2 H, quintet), 1.36 (2 H, sextet), 0.94 (3 H, t).

3-(4'-Phenoyl)-4-(4'-n-butylphenyl)-5-(4'-bromophenyl)-1,2,4-trizole (3). Boron tribromide (3.5 mL, 37 mmol) in 10 ml dichloromethane was added dropwise to a suspension of **(2)** (8.6 g, 19 mmol) in dichloromethane (50 ml) at -78°C under nitrogen. The mixture was allowed to warm to room temperature and subsequently stirred overnight. The clear solution was poured into water and the precipitate filtered, and dried over vacuum to yield 7.5 g of product (yield 90%). ^{1}H NMR (500 MHz, DMSO-d6), δ(ppm): 9.96 (1 H, s), 7.53 (2 H, d), 7.26 (2 H, d), 7.15 (2 H, d), 6.66 (2 H, d), 2.58 (2 H, t), 1.51 (2 H, quintet), 1.21 (2 H, sextet), 0.84 (3 H, t).

3-(4'-(2''-ethylhexyloxy)phenyl)-4-(4'-n-butylphenyl)-5-(4'-bromophenyl)-1,2,4-trizole (4). A mixture of **(3)** (8.40 g, 18.9 mmol), 2-ethylhexylbromide (4.40 g, 22.7 mmol) and potassium carbonate (14.9 g, 75.6 mmol) in 150 mL DMSO and 30 mL toluene was stirred at 120°C overnight, equipped with a Dean-Stark trap. After cooling, the mixture was poured into water. The precipitate was filtered and recrystallized from ethyl acetate:hexane to provide 9.09 g (yield 85.8%) of a white solid. ^{1}H NMR (500 MHz, CD_2Cl_2), δ(ppm): 7.45 (d, 2 H), 7.26-7.36 (6 H, 6 peaks), 7.07 (2 H, d), 6.82 (2 H, d), 3.84 (2 H, d), 2.69 (2 H, t), 1.32-1.74 (13 H, m), 0.89-0.97 (9 H, m).

3-(4'-(2''-ethylhexyloxy)phenyl)-4-4'-n-butylphenyl)-5-(4'-vinylphenyl)-1,2,4-triazole (5). A mixture of 3-(4'-(2''-ethylhexyloxy)phenyl)-4-4'-n-butylphenyl)-5-(4'-bromophenyl)-1,2,4-triazole. (**4**) (1.00 g, 1.78 mmol),

vinyltributyltin (0.71 g, 2.24 mmol) and $Pd(PPh_3)_4$ (21 mg) in 30 mL toluene was heated at 110 °C under nitrogen for 24 h. After cooling, the mixture was diluted with toluene, washed with brine, and dried over $MgSO_4$. Purification by column gave 0.66 g of a white product (yield 72.8%). ^1H NMR (500 MHz, CD_2Cl_2), δ (ppm): 7.30~7.40 (6 H, m), 7.249 (2 H, d), 7.075 (2 H, d), 6.808 (2 H, d), 6.692 (1 H, q), 5.780 (1 H, d), 5.293 (1 H, d), 3.830 (2 H, d), 2.676 (2 H, t), 1.59~1.71 (1 H, m), 1.21~1.39 (8 H, m), 0.88~0.96 (6 H, m). Analysis: Calcd $C_{34}H_{41}N_3O$: C, 80.43, H, 8.14, N, 8.28. Found C, 80.07, H, 8.11, N, 8.40.

PVTAZ (6). The nitroxide-mediated radical polymerization (NMRP) technique[44, 45] was used for the polymerization of **5**. Solution polymerization was carried out in argon using p-xylene as the solvent. TEMPO initiator (**7**) (20 mg, 0.008 mmol), acetic anhydride 0.3 mL, and (**5**) (0.20 g, 0.40 mmol) in 1.5 mL p-xylene were heated to 125°C. Samples were extracted every 90 minutes for analyses of the molecular weight. After the reaction, the solvent was dried under vacuum and dissolved in chloroform, followed by precipitation in methanol.

1-Phenyl-1-(2',2',6',6'-tetramethyl-1'-piperidinyloxy)-ethane (7). Using a similar method described in the literature[46], ethylbenzene (50 mL), di-tert-butylperoxide (2.5 g, 16.5 mmol) and TEMPO (5.25 g, 33.0 mmol) were refluxed under nitrogen overnight and evaporated the excessive ethylbenzene to get dry crude product. The crude product was purified by flash chromatography using hexane, with gradual addition of ethyl acetate. The colourless oil was recrystallized from cold ethanol (-78 °C) to give a white solid (2.1 g, 24% yield).

^{1}H NMR (500 MHz, CD_2Cl_2), δ(ppm): 0.66, 1.03, 1.17, 1.38 (each br s, 12H), 1.23-1.58 (m, 6H), 1.47 (d, 3H,), 4.79 (q, 1H), 7.25-7.35 (m, 5H).

1-[4-(4'-trimethylene-1,3,2-dioxaborolan-2-yl)phenyl]]-1-(2,2,6,6-tetramethyl-1-piperidinyloxyl)–ethane (8). It was synthesized according to the method reported in literature[35], ^{1}H NMR (CD_2Cl_2), δ(ppm): 0.61, 1.01, 1.16, 1.28 (each s, 12 H), 1.26-1.58 (m, 6 H), 1.45 (d, 3 H), 2.04 (quintet, 2 H), 4.13 (t, 4 H), 4.76 (q, 1 H), 7.29 (d, 2 H), 7.66 (d, 2 H).

Regioregular Poly(3-hexylthiophene) (RR-P3HT). RR-P3HT was synthesized and purified according to the method reported in literature,[47] except that Ni(dppe)Cl_2 catalyst was used instead of Ni(dppp)Cl_2. The RR-P3HT sample obtained possessed a regioregularity of >95% according to ^{1}H NMR analysis as shown in **Figure 2.1**: M_n = 25 000 Da; polydispersity index = 1.70; ^{1}H NMR (δ/ppm, $CDCl_3$) 6.99 (s, 1H), 2.79 (t, 2H), 1.72 (m, 2H), 1.34 (m, 5H), 0.90 (t, 3H).

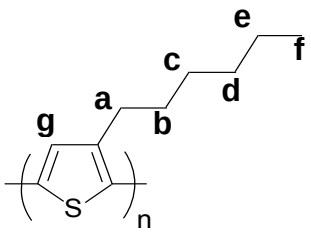

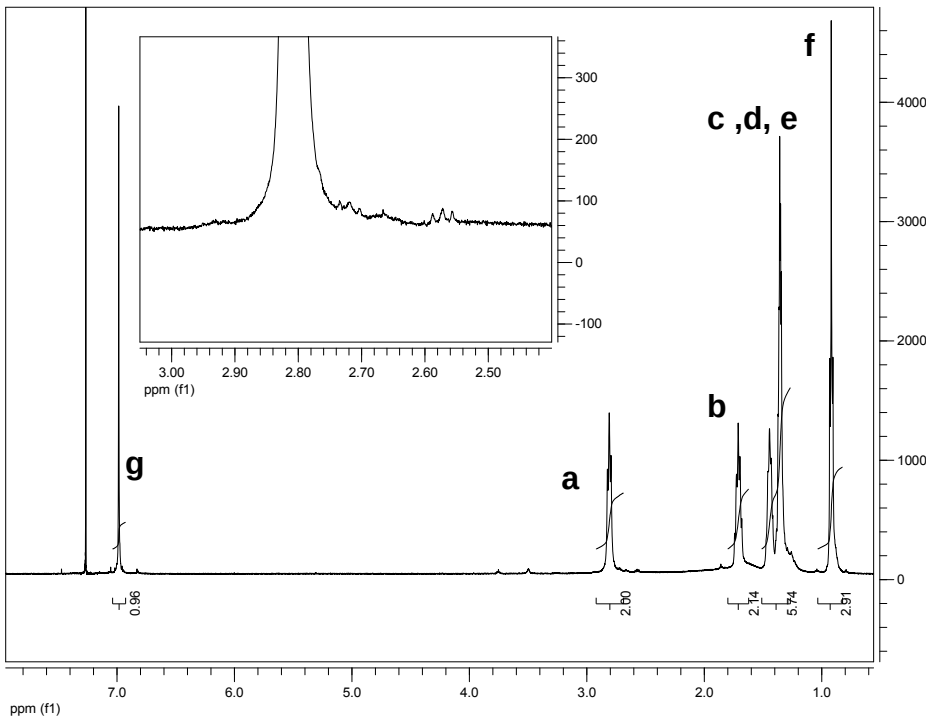

Figure 2.1: NMR spectrum of regioregular P3HT in $CDCl_3$.

5%BrP3HT (9). To a flask containing **RR-P3HT** (0.20 g, 1.20 mmol) in chloroform (14 mL) was added NBS (11.0 mg, 0.06 mmol). The solution was stirred at room temperature for 15 h and heated at 50 °C for 2 h. The reaction mixture was poured into a saturated $NaHCO_3$ solution (50 mL). The organic layer was washed with water five times and dried over $MgSO_4$. Precipitation into methanol gave a black solid (0.18 g, yield: 90%) ^{1}H NMR: ($CDCl_3$) as shown in **Figure 2.2**, δ(ppm) 2.78 (br, methylene), 2.62 (br, methylene), 1.60 (br), 1.33 (br), 1.28 (br), 0.87 (br, C*H*3). GPC: Mn, 27,000 Da; Polydispersity, 1.74.

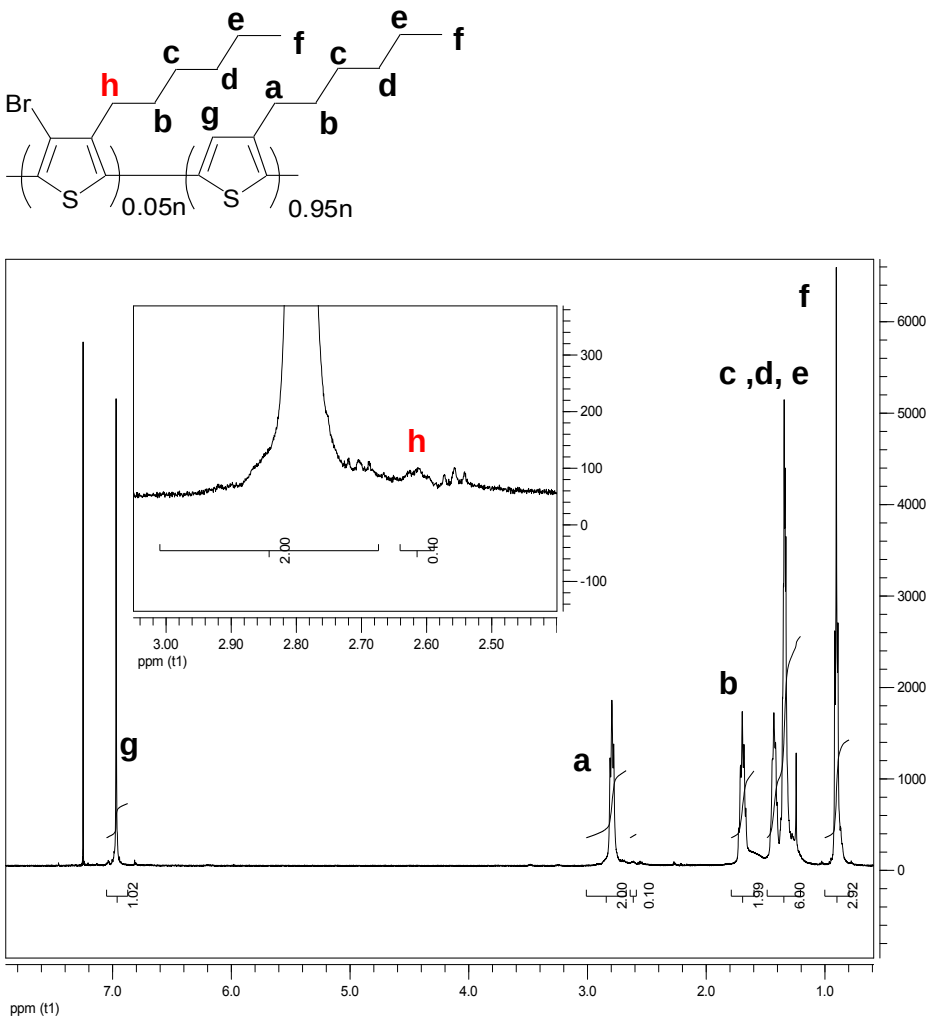

Figure 2.2: NMR spectrum of brominated P3HT (9) in $CDCl_3$.

5%TEMPO-P3HT (10). 5%BrP3HT (**9**) (150 mg, 0.90 mmol) was dissolved in 15 mL THF. **8** (0.155 g, 0.045 mmol) and 2 M Na_2CO_3 aqueous solution (0.6 mL, 1.2 mmol) were added. The mixture was de-oxygenated by bubbling nitrogen for 30 min. $Pd(PPh_3)_4$ (5 mg, 0.004 mmol) was added and the flask heated at 60 °C for 3 days under nitrogen. The mixture was concentrated and precipitated into methanol. The solid was purified by Soxhlet extraction with methanol and precipitated again into methanol from a chloroform solution, and dried in a vacuum oven. 120 mg of a black solid was obtained (yield 80%). ^1H

NMR: ($CDCl_3$) as shown in **Figure 2.3**, δ(ppm) 2.71 (br, methylene), 1.60 (br), 1.33 (br), 1.28 (br), 0.87 (br, C*H*3). GPC: Mn, 31,000 Da; Polydispersity, 1.84.

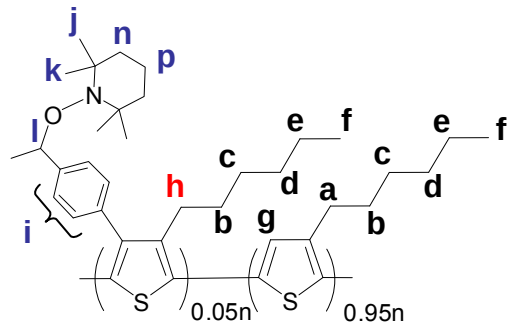

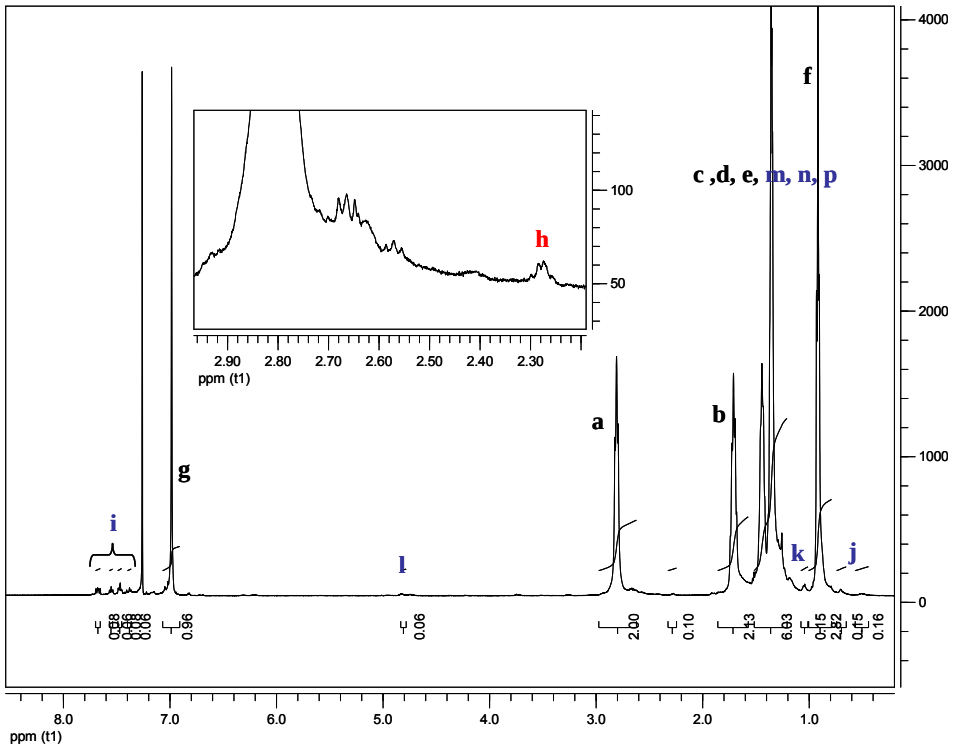

Figure 2.3: NMR spectrum of macroinitiator (10) in $CDCl_3$.

P3HT-*g*-PVTAZ (11a). Macroinitiator (**10**) (100 mg, 0.60 mmol), acetic anhydride (0.4 mL), vinyl TAZ monomer (**5**) (0.06 g, 0.12 mmol) were added to 6.5 ml p-xylene. The mixture was deoxygenated by three freeze-pump-thaw

cycles, maintained under argon, and placed in an oil bath at 125 °C. After 2 days at 125°C, the mixture was cooled and solvent was dried under vacuum. The polymer purified on a silica gel column using ethyl acetate. After work up, 118 mg of brown solid was obtained. GPC: M_n, 39,200 Da, Polydispersity, 1.85.

P3HT-*g*-PVTAZ (11b). Macroinitiator (**10**) (80 mg, 0.48 mmol), acetic anhydride (0.4 mL), vinyl TAZ monomer (**5**) (0.13 g, 0.26 mmol) were added to 6.5 ml p-xylene. The mixture was deoxygenated by three freeze-pump-thaw cycles, maintained under argon, and placed in an oil bath at 125 °C. After 2 days at 125°C, the mixture was cooled and solvent was dried under vacuum. The polymer purified on a silica gel column using ethyl acetate and precipitated in to methanol and acetone mixture (1:1). After work up, 82 mg of brown solid was obtained. GPC: M_n, 58,000 Da, Polydispersity, 1.70.

P3HT-*g*-PVTAZ (11c). Macroinitiator (**10**) (80 mg, 0.48 mmol), acetic anhydride (0.4 mL), vinyl TAZ monomer (**5**) (0.32 g, 0.64 mmol) were added to 7.5 ml p-xylene. The mixture was deoxygenated by three freeze-pump-thaw cycles, maintained under argon, and placed in an oil bath at 125 °C. After 2 days at 125°C, the mixture was cooled and solvent was dried under vacuum. The polymer purified on a silica gel column using ethyl acetate and precipitated in to methanol and acetone mixture (1:1). After work up, 95 mg of brown solid was obtained. GPC: M_n, 99,000 Da, Polydispersity, 1.65.

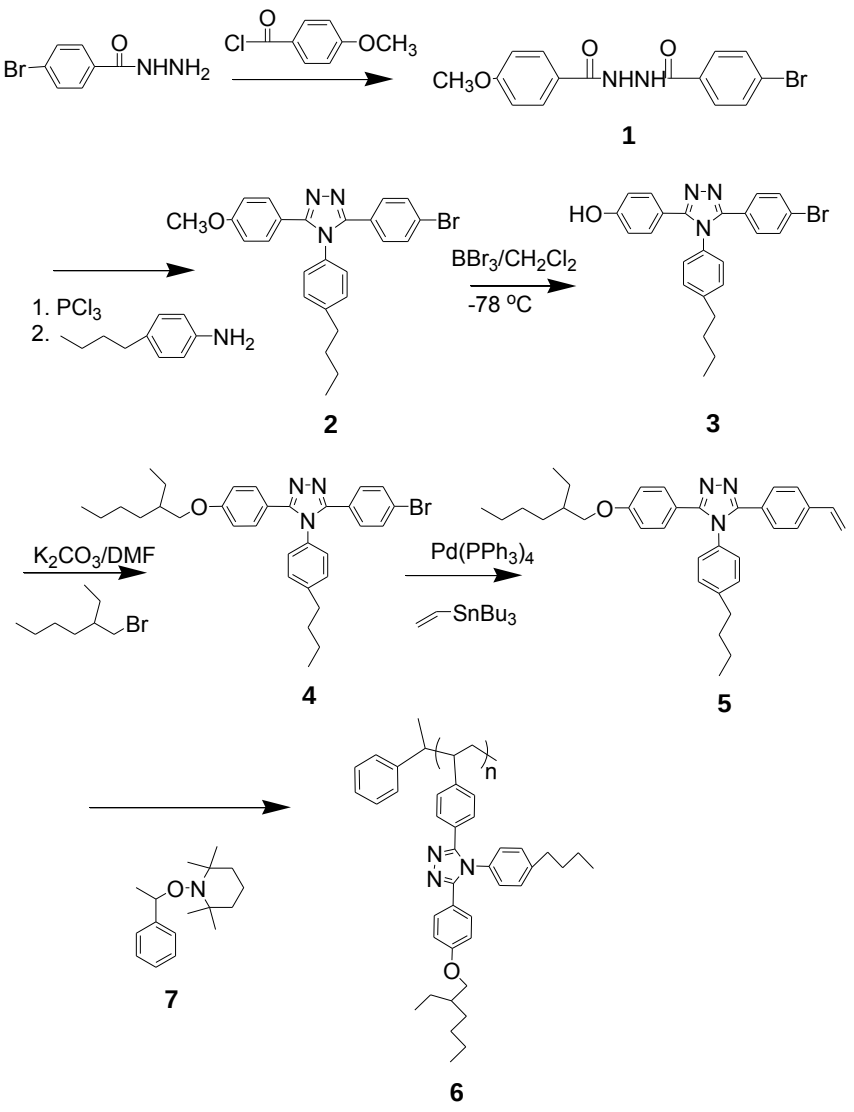

Scheme 2.3: Synthetic route for the vinyl triazole monomer (5) and the polymerization 5 by NMRP to PVTAZ (6).

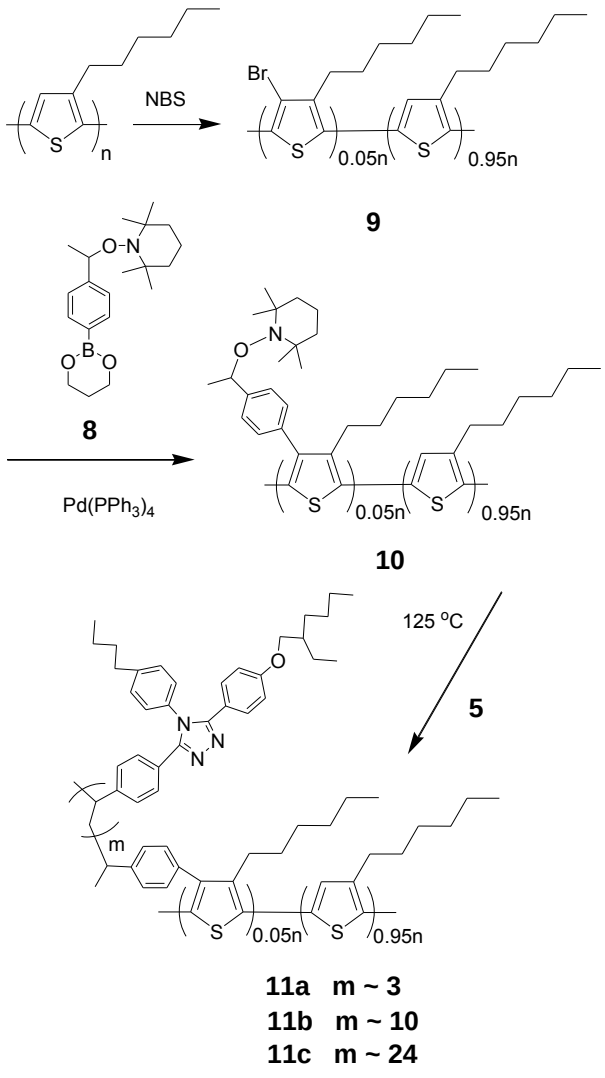

Scheme 2.4: Synthetic route for the polythiophene-graft-polyvinyltriazole.

2.2.3 Measurements

^{1}H NMR spectra were obtained on a 500 MHz Varian AS500 spectrometer; chemical shifts are reported in parts per million (ppm), referenced to CD_2Cl_2 (1H: δ=5.32) or $CDCl_3$ (1H: δ=7.26). Molecular weights were measured by gel permeation chromatography (GPC) (Waters model 1515 isocratic pump) equipped with μ-Styragel columns against polystyrene standards. Polymers were

eluted with THF using a flow rate of 1.0 mL/min and detected with a UV-Vis detector (Waters model 2487) at 254 nm. Elemental analyses were using a Carlo Erba model 1106 CHN analyzer. UV-Vis absorption spectra were recorded on a Cary 3EI (Varian) spectrophotometer. Polymeric films were prepared from either spin-coating 5 mg/mL THF or polymer with various $TAZC_{60}$ in chlorobenzene solution of 15 mg/mL concentration at 700 rpm. Photoluminescence (PL) spectra and quantum efficiency measurement were recorded with a Photon Technology International QuantumMaster model QM-4 equipped with an integrating sphere. Film thickness and surface roughness was measured by KLA-Tencor Alpha-Step IQ Surface Profiler. Ra (roughness avarge) is the arithmetic average deviation from the mean line within the assessment length. Cyclic voltammetry was carried out using a potentiostat/galvanostat Model 263A from Princeton Applied Research. A one compartment, three-electrode cell was used with a glassy-carbon disk coated with polymer, and Pt wires as working and counter electrodes, respectively. The reference electrode consisted of a Pt wire in an acetonitrile solution of 0.1 M Bu_4NI/ 0.05 M I_2, which was separated from the working electrode compartment by a glassy frit. The electrolyte was a solution of 0.1 M Bu_4NClO_4 in dry acetonitrile deoxygenated by bubbling with nitrogen. The potential scan rate was 50 mV/s. Ferrocene was added to the electrolyte after the voltammetry of the polymers and served as an internal standard for calibrating the potential of the reference electrode. Transmission Electron Microscope (TEM) images were performed on a Hitachi H7600 TEM or Tecnai 20 FEI STEM. A layer of poly(styrene sulfonic acid)-doped poly(3, 4-ethylenedioxythiophene)

(PEDOT, Bayton®P VP AI4083) was spin cast on cleaned glasses at 5000 rpm and annealed at 140 °C for 10 min. Onto this surface, polymers and polymer blends were spin cast, and films dried in air. The film and substrate were immersed into water, and the polymer films picked up with Cu grids from the surface of the water. All the films on Cu grids were stained for 15 min using RuO_4 vapor prepared in situ with 0.5 % ruthenium (III) chloride in a sodium hypochlorite solution (containing ≥4% chlorine in solution). X-ray diffractometry was performed on a Bruker-AXS D8 Discover High-Resolution Diffractometer system using Cu Ka wavelength (about 1.544 Å). Polymer films were prepared on silicon wafer substrate by the same spin casting method described before.

2.2.4 Device fabrication and characterization

Patterned indium-tin oxide (ITO) glass (Merck, Taiwan) was cleaned with detergent, ultrasonicated in acetone and isopropyl alcohol. A layer of poly(styrene sulfonic acid)-doped poly(ethylenedioxythiophene) (PEDOT, AI4083, from H. C. Starck) (~40 nm) was spin-coated on top of the ITO. The substrate was dried for 10 min at 140 ºC in air. **11a** (10mg/mL) plus $TAZC_{60}$ (10mg/mL) or P3HT (10mg/mL) plus $TAZC_{60}$ (10mg/mL) in chlorobenzene was spin-casting at 700 rpm on top of the PEDOT layer to form an active layer ~100 nm. Then a layer of aluminum (100 nm) was thermally deposited in a vacuum chamber at 2×10^{-6} Torr pressure through a shadow mask. Current-voltage characteristics of the photovoltaic devices were measured using a Keithley 2400 source meter under illumination with an ozone free Xenon 300 W lamp through 1 AM 1.5 filter from Newport. The power was adjusted to be 80 mW/cm^2,

measured by calibrated Radiant Power Meter (model 70260) combined with a model 70268 Probe.

2.3 Results and Discussion

2.3.1 Monomer and Polymer Synthesis

The vinyl triazole monomer **(5)** was synthesized according Scheme 2.3. Following condensation of 4-bromobenzoyl hydrazine and p-anisoyl chloride, 1-(p-anisoyl) 2-(4'-bromo)benzoyl hydrazide **(1)** was formed as evidenced by the 2 hydrazide proton peaks at 10.4 and 10.6 ppm in the ^{1}H NMR spectrum of **1**. Other NMR peaks due to **1** are observed at 7.0-8.0 (aryl, 8H), and 3.8 ppm (anisoyl, 3H). **1** was reacted with 4-*n*-butylaniline to form 3-(4'-anisoyl)-4-(4'-n-butylphenyl)-5-(4'-bromophenyl)-1,2,4-triazole (**2)**. The ^{1}H NMR spectrum indicates that the 2 peaks at 10.4 and 10.6 ppm due to hydrazide had disappeared. **2** possessed peaks at 6.8-7.5 (aryl, 12H), 2.7, 1.7, 1.4 (methylene, 6H), and 3.8 ppm (anisoyl, 3H), 0.9 (methyl, 3H). In order to enhance the solubility of the triazole compound**,** the anisoyl group was converted to a hydroxide group to form 3-(4'-phenoyl)-4-(4'-n-butylphenyl)-5-(4'-bromophenyl)-1, 2, 4-trizole (**3**), which was confirmed by the disappearance of the ^{1}H NMR peak at 3.8 ppm due to anisoyl, and the emergence of a peak at 9.95 ppm due to the hydroxide group. The ethylhexyl group was attached using the Williamson reaction to form 3-(4'-(2''-ethylhexyloxy)phenyl)-4-(4'-n-butylphenyl)-5-(4'-bromophenyl)-1,2,4-trizole **(4)**. The ^{1}H NMR spectrum of **4** indicated that the

hydroxide peak at 9.95 ppm was absent and peaks due to -OCH_2- (3.70 ppm) and the ethylhexyl group (0.9-1.8 ppm, 15H) were present. A Stille coupling of vinyltributyltin to **4** afforded the vinyl triazole monomer, 3-(4'-(2''-ethylhexyloxy)phenyl)-4-4'-n-butylphenyl)-5-(4'-vinylphenyl)-1,2,4-triazole **(5).** The ^{1}H NMR spectrum of **5** revealed three peaks due to the vinyl group at 6.70, 5.78 and 5.29 ppm, in addition the peaks due to the triazole moiety.

Since **5** is a monomer prepared for the first time, intended to be polymerized onto RR-P3HT by NMRP, a demonstration of its NMRP of **5** was warranted. The polymerization of **5** to its polymer (**6**) was initiated by a TEMPO compound (**7**). The evolution of the GPC traces of **6** is shown in **Figure 2.4a**, as is a plot of the molecular weight versus polymerization time (**Figure 2.4b**). The molecular weight of **6** increased linearly with reaction time and the polymers possessed a polydispersity index between 1.05-1.15, indicating typical pseudo-controlled, radical polymerization behavior. The synthetic scheme for the graft copolymers **11a, 11b** and **11c** are shown in **Scheme 2.4**. The molecular weight, composition, and optical properties of P3HT, macroinitiator(**10**) and graft copolymers (**11a, 11b** and **11c**) are listed in **Table 2.1**. The aim was to substitute only 5% of the 4-thienyl protons with a graft chain since previous studies[43] have shown that much larger degrees of substitution with bulky functional groups disrupt the coplanarity of the π-conjugated backbone leading to reduced polycrystallinity of the P3HT - resulting in a large shift in the absorption spectrum and, potentially, reduced hole conductivity. Frechet and coworkers reported a surprising result that P3HT with 4% of disubstituent hexyl on the thienyl group

can result in better thermal stability of solar cell devices due to stabilising the morphology.[48] For similar reasons of promoting organized structures with the highest hole mobilities and lowest-energy absorption spectra, regioregular RR-P3HT was used as the starting material. The ^{1}H NMR spectrum of the poly(3-hexylthiophene) (RR-P3HT) prepared indicated that the regioregularity was > 95% (see **Figure 2.1**). The spectrum shows peaks corresponding to α-methylene protons at 2.78 ppm, which are indicative of hexyl chains on adjacent thienyl units linked head-to-tail; only a very small peak is observed at 2.58 ppm, which is attributed to head-to-head linkages. RR-P3HT was brominated at the 4-position via electrophilic substitution to 5 mol% (based on the thienyl ring). The α-methylene protons, for which bromine is located on the same thienyl ring, are observed at 2.62 ppm. (see **Figure 2.2**) Integration of the α-methylene protons peak at 2.62 ppm indicated that 5% of the RR-P3HT backbone was brominated.

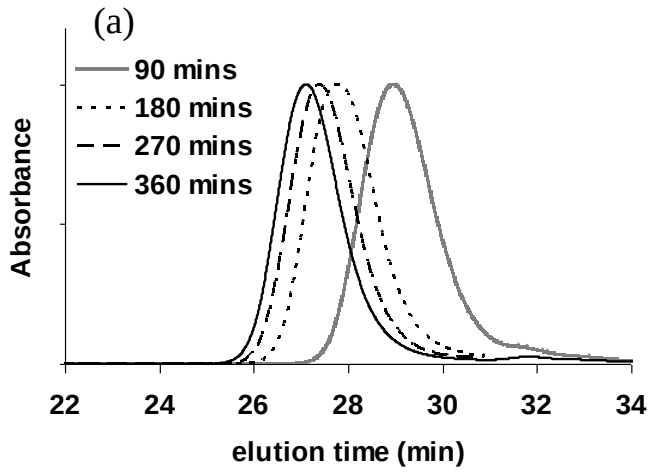

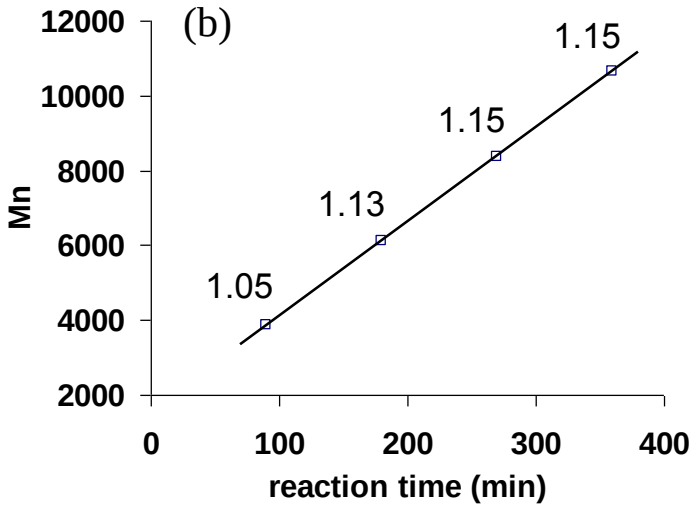

Figure 2.4: (a) Evolution of GPC peaks of homopolymer (6) with reaction time. (b) Polymer chain growth vs. reaction time for (6). Polydispersity indices are shown above data points.

Partially brominated P3HT (**9**) was used in the Suzuki cross-coupling reaction with a boronic ester of a nitroxide to form the macroinitiator (**10**), comprising of a polythiophene bearing a TEMPO group on thienyl ring, following the reported method for fully postfunctionalization of the P3HT.[35] Previous studies of 100% post-functionalization of P3HT backbone with various functional groups indicate a phenyl ring attached to the 4-position of an alkyl-substituted thiophene shifts the α-methylene peak from 2.78 to 2.26 ppm.[41] The peak at 2.26 ppm in the ^{1}H NMR spectrum of **10** is thus assigned to α-methylene protons associated with a thienyl ring bearing a TEMPO group. (see **Figure 2.3**) Some of the signals from TEMPO group, which are almost at the same position as compound (**8**), can be observed by NMR. By integrating the peak at 2.26 ppm, it is found that 5 mol% of the RR-P3HT backbone was functionalized, i.e., conversion of the bromo- to nitroxide-group is quantitative. The macroinitiator

(**10**) was used to initiate the NMRP of **5**, so as to grow poly(vinyl triazole) from the conjugated polymer backbone. The polymerization was carried out at 125 °C under argon. Graft copolymers, **11a, 11b and 11c** were synthesized using a monomer **(5)** to initiator with various ratios. Gel permeation chromatograms of the macroinitiator (**10**) and the graft polymers (**11a, 11b and 11c)** are shown in **Figure 2.5**. Each possessed single and narrow molecular weight distributions. GPC analysis, using THF as eluent and polystyrene calibration standards, indicates that M_n for **10, 11a, 11b** and **11c** are 31000 (Polydispersity: 1.84), 39200 (Polydispersity: 1.85) Da, 58,000 (Polydispersity: 1.70) and 99,000 (Polydispersity: 1.65).

The ^{1}H NMR spectra of **11a, 11b** and **11c** are shown in **Figure 2.6**. The spectra reveal protons associated with the P3HT backbone and PVTAZ side chain. Of note, the peaks due to α-methylenes and aromatic protons of the P3HT backbone appear at 2.78 (m, 2H) and 6.98 ppm (s, 1H), respectively. **11a, 11b** and **11c** possess signature peaks at 6.7-7.3 (aryl, 12H), 3.70 (–OCH_2-, 2H), and 2.63 ppm (α-methylene, 2H). Protons at 5.78 and 5.29 ppm, due to the vinyl group, and previously observed for **5**, are notably absent. For **11a**, the molar ratio of thienyl units to TAZ groups calculated from the integrals of the peaks at 2.78 ppm (α-methylene of 3-hexylthienyl and 3.70 ppm (–OCH_2-, TAZ group) was 6:1. Given that the α-methylene and –OCH_2- integrals possess 2 protons per group, and as 5 mol% of the thienyl units bear graft chains the average degree of polymerization of **5** onto the main chain was 3.3 (3). Thus the side chain is an oligomer rather than a polymer, but for the purpose of consistency the term

polymer is used throughout. In the same way, the molar ratio of thienyl units to TAZ groups for **11b** and **11c** are 2:1 and 1: 1.2 respectively. For **11b** and **11c**, the average degree of polymerization of **5** onto the main chain was 10 and 24, respectively. The molar ratio and weight percentages of P3HT in the graft copolymers are listed in **Table 2.1**.

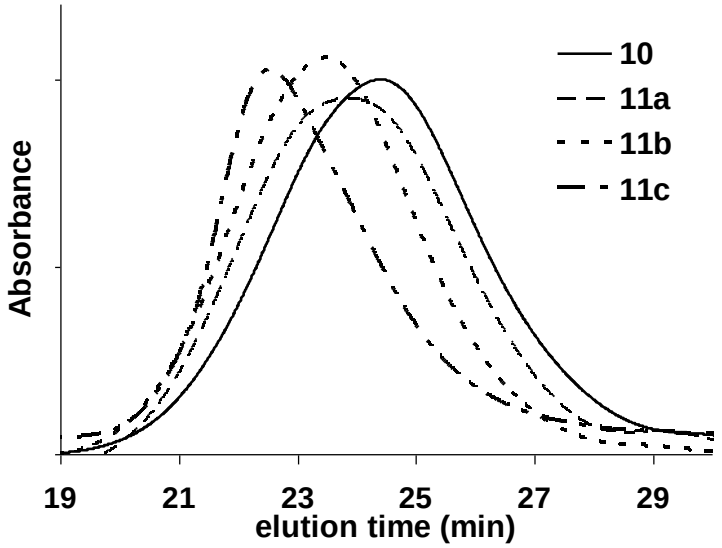

Figure 2.5: GPC trace of TEMPO-P3HT macroinitiator (10), the graft copolymer P3HT-g-PVTAZ (11a, 11b, and 11c).

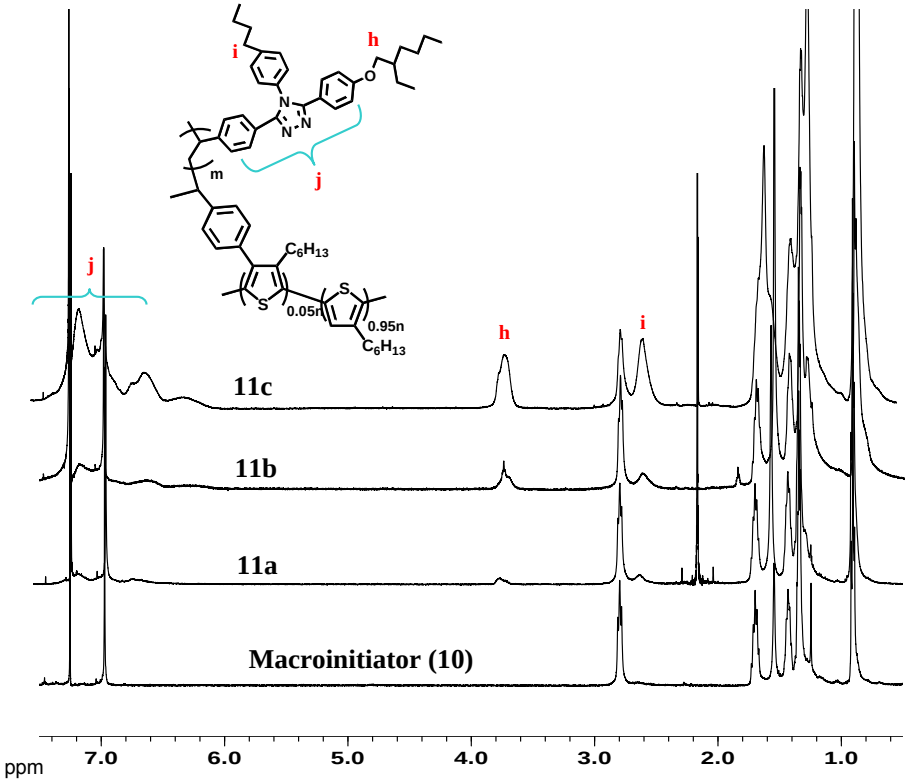

Figure 2.6: ^{1}H NMR spectra of macroinitiator (10), and the resulting graft copolymer P3HT-g-PVTAZ (11a, 11b and 11c).

	$\overline{M}_n$ 10^4 Da	PDI	Molar ratio of thienyl to TAZ	Thienyl Wt.-%	$\overline{DP}$	Solution			Film		
						λ_{abs} nm	λ_{em} nm	Φ	λ_{abs} nm	λ_{em} nm	Φ
P3HT	25000	1.70	__	__	__	445	572	0.26	559	728	0.020
10	31000	1.84	__	__	__	445	572	0.24	559	728	0.023
11a	39200	1.85	6:1	67%	3	445	572	0.24	524	728	0.051
11b	58000	1.70	2:1	40%	10	445	572	0.23	500	662	0.060
11c	99000	1.65	1:1.2	22%	24	445	572	0.23	461	606	0.082

Table 2.1: Molecular weights, composition and optical properties of polymers.

2.3.2 Optical Properties

Absorption and emission maxima of the polymers are listed in **Table 2.1**. The spectra were normalized so that the maximum absorbance and fluorscence are equal to 1.0. Normalized UV-Vis spectra of **RR-P3HT, 10**, **11a, 11b** and **11c** in solution possess almost identical absorption spectra (λ_{max} 445 nm) (see **Figure 2.7**). Thus the electronic structure of isolated π-conjugated polymer chains in solution are unperturbed by the presence of the PVTAZ side chain. Similarly, the PL spectra of **RR-P3HT, 10**, **11a, 11b** and **11c** exhibit identical emission maxima (λ_{max} 572 nm) (see **Figure 2.8**) indicating that the PVTAZ side chains do not perturb the excited state structure of π-conjugated polymer chains in solution relative to ~95% rr P3HT. In contrast, differences are observed in the solid state spectra. As observed in **Figure 2.9**, the absorption due to the triazole in **11a** occurs at 278 nm. The absorption maximum of **11a** due to the π- π^* transition is blue-shifted 35 nm compared to both **RR-P3HT** and **10**, and the vibronic splitting, observed as the shoulder at 603 nm, diminishes in the order **RR-P3HT >10> 11a**, indicating a decreasing degree of ordering in the solid state. **11b** and **11c** possess maxima at 500 nm and 461 nm. This blue-shift may be the result of the bulky side graft, which induces torsion on the backbone. The photoluminescence of films of **RR-P3HT**, **10**, and **11a** (see **Figure 2.10**) showed very similar maximum emission wavelengths, 728 nm, indicating that the short graft side chain does not perturb the electronic structure of the emitting exciton associated with the main chain. While for **11b** and **11c** blue shifted maxima indicates long

side graft may have more interferes with long-range structural order of P3HT. The quantum yields of fluorescence, $\Phi_{fl,}$ for films of **RR-P3HT**, **10**, **11a**, **11b** and **11c** are 0.020, 0.023, 0.051, 0.060 and 0.082 respectively. The value for **RR-P3HT** is typical,[27] and the values for **11a, 11b** and **11c** are consistent for functionalized P3HTs, which exhibit higher fluorescence efficiency because the 4-functionality increases the distance between stacks of chains, thereby reducing self-quenching.[43]

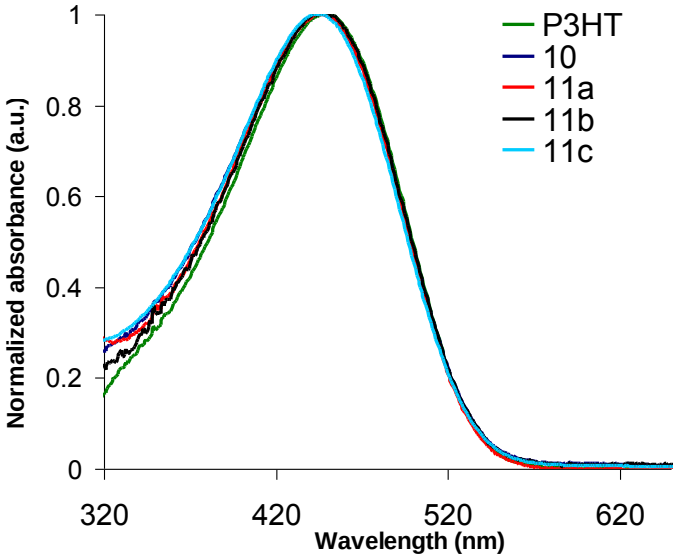

Figure 2.7: UV-vis absorption spectra of P3HT, 10, 11a, 11b and 11c in THF solution.

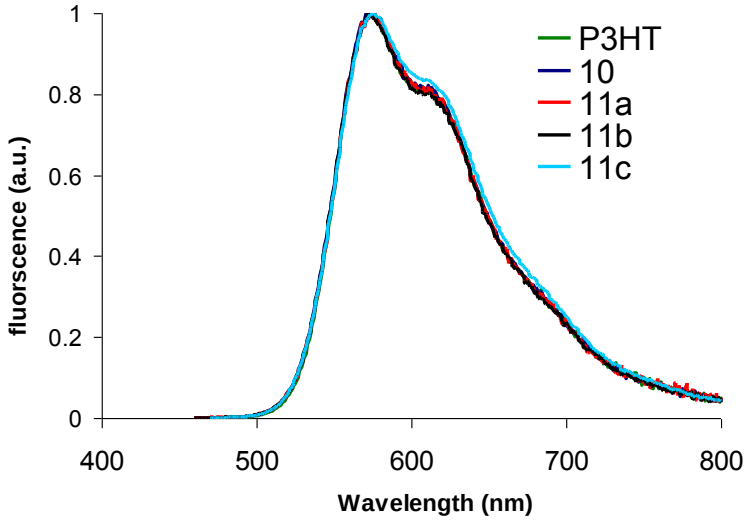

Figure 2.8: photoluminescence spectra of P3HT, 10, 11a, 11b and 11c in THF solution.

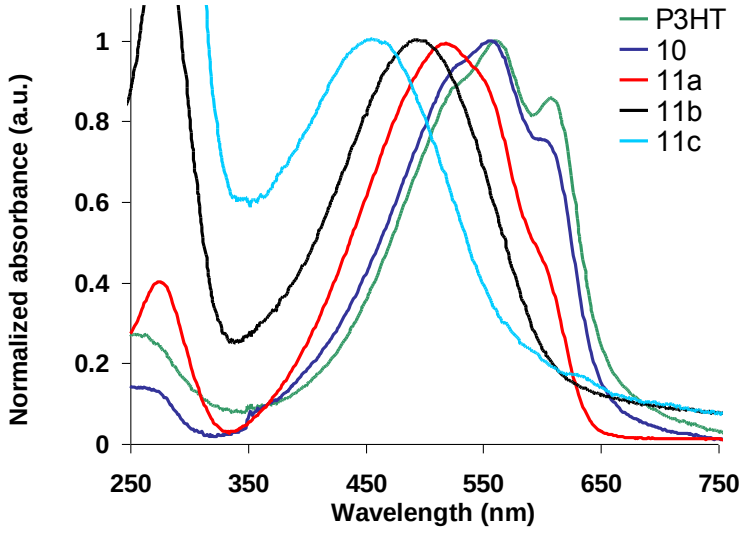

Figure 2.9: UV-Vis spectra of RR-P3HT, 10, 11a, 11b and 11c films.

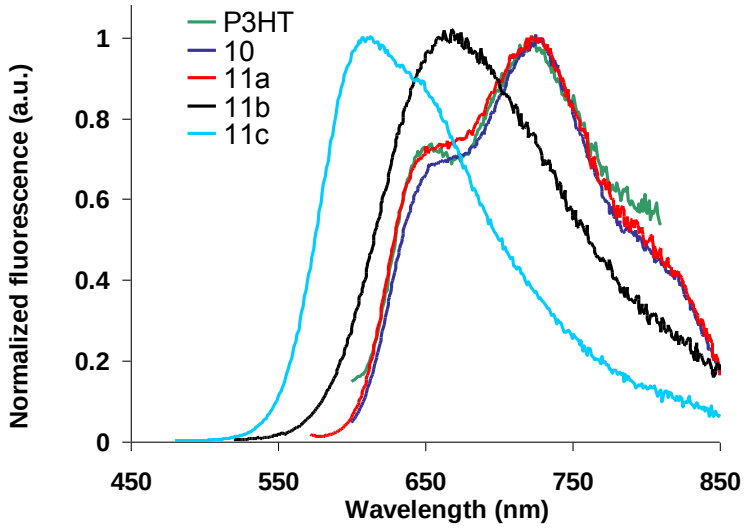

Figure 2.10: PL spectra of RR-P3HT, 10, 11a, 11b and 11c films.

2.3.3 Redox Properties

CVs of **RR-P3HT, 10**, **11a**, **11b** and **11c** are shown in **Figure 2.11**, from which HOMO and LUMO energy levels can be approximated by considering the onset potential of oxidation or reduction. Redox energy levels were measured against the Fc/Fc^+ redox couple, which is 4.8 eV with respect to an electron *in vacuo*.[49] The onset of oxidation for **RR-P3HT**, **10,** and **11a** are +0.08 V vs. Fc/Fc^+, indicating a HOMO level ~4.9 eV. Furthermore, a clear n-doping process with an onset potential at –2.24 V is observed, that is reversible. This indicates the polymers exhibit both p-type and n-type behavior, which is consistent with the observation that π-conjugated polymers are generally ambipolar from field effect transistor studies.[50] The electron affinities for the 3 polymers are estimated to be ~2.6 eV. While for **11b** and **11c**, the onset of oxidation are +0.31 V vs. Fc/Fc^+ and +0.36 V vs. Fc/Fc^+. This indicates **11b** and **11c** have HOMO level at 5.1 and

5.2, respectively. The CV didn't show a clear n-doping and dedoping process for **11b** and **11c**.

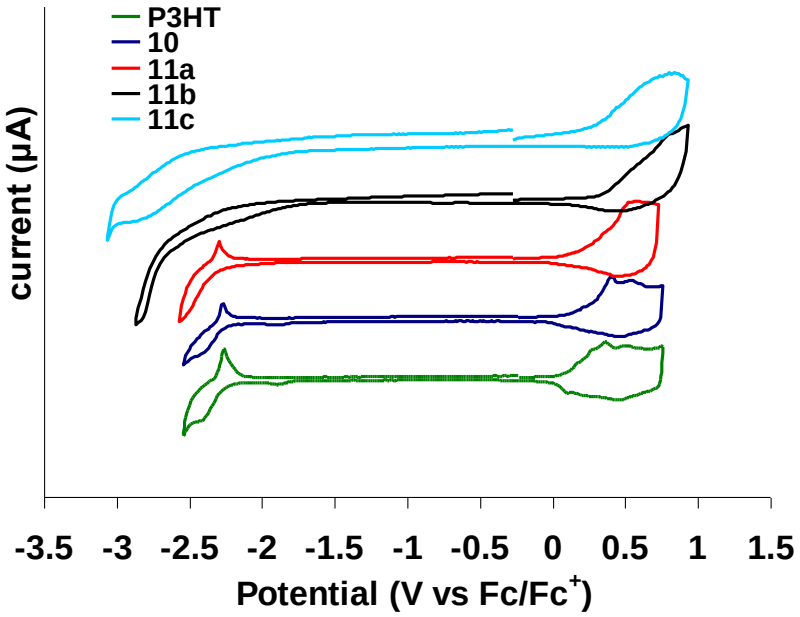

Figure 2.11: Cyclic voltammograms of films of RR-P3HT, 10, 11a, 11b and 11c.

2.3.4 Morphology of Polymer Thin Films and of Its Blends with $TAZC_{60}$

11a was designed in order to investigate the role of the graft chain on the formation of blends with $TAZC_{60}$. The morphologies of the graft copolymers and its blends with $TAZC_{60}$ were studied by TEM. The staining agent, RuO_4 preferentially oxidizes P3HT domains (oxidation potential ~4.9 eV) rather than TAZ domains (oxidation potential ~6.3 eV) or $TAZC_{60}$ domains (oxidation potential ~5.9 eV)[40], producing highly scattering RuO_2.[51, 52] The dark regions of the TEM images therefore represent P3HT domains; the lighter regions, PVTAZ side chain or $TAZC_{60}$ domains. Films of **11a**, and **11a:**$TAZC_{60}$ blends consisting of 1:1 and 1:2 wt ratios, were prepared. Micrographs are shown in **Figure**

2.12(a), (b) and (c) and reveal that films of **11a**, and its blends, possess uniform, phase-segregated morphologies. They also reveal that the lighter regions in micrographs of **11a**, grow in relative size with increasing $TAZC_{60}$ content, providing strong evidence that $TAZC_{60}$, with its polar TAZ functionality (similar to the graft structure of **11a)** mixes with the PVTAZ domains associated with **11a**. As a control experiment, unmodified P3HT (~92% regioregularity) was blended with $TAZC_{60}$ and the morphology examined. All attempts to form uniform, miscible films of P3HT and $TAZC_{60}$ failed - as exemplified by the TEM of the 1:1 wt blend shown in **Figure 2.12**, which shows large scale (micron-sized) phase separation of P3HT-rich phase surrounded by $TAZC_{60}$-rich phase. Furthermore, the average surface roughness of blends of **11a**, determined by surface profilometry, was <2 nm, while for blends of P3HT and $TAZC_{60}$, the roughness was >18 nm.

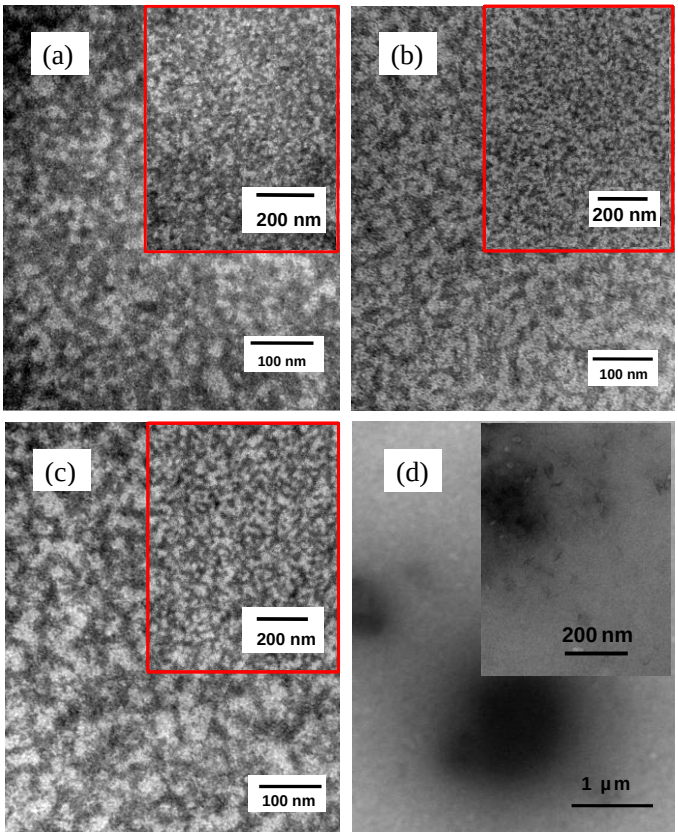

Figure 2.12: TEM of (a) 11a, (b) 11a:TAZC$_{60}$ (1:1 in wt blend), (c) 11a: TAZC$_{60}$ (1:2 in wt blend), (d) P3HT:TAZC$_{60}$ (1:1 in wt blend). Inset images are taken in different magnification.

The UV-Vis absorption spectra of films of P3HT:TAZC$_{60}$ and **11a**:TAZC$_{60}$ blends were similar. The concomitant change in UV-Vis spectra absorption spectra of **11a** and P3HT with increasing TAZC$_{60}$ content is shown in **Figure 2.13a** and **b**. With increasing TAZC$_{60}$ content, the extinction coefficient of the polymer blends (**11a**: TAZC$_{60}$ and P3HT:TAZC$_{60}$) decreases, λ_{max} blue shifts, and the vibronic features are less observable. This indicates intermolecular inter-chain interactions of the π-conjugated system were weakened with increasing TAZC$_{60}$ content in the blends.

Both sets of blends were subsequently annealed at 140 °C for 1 hour. λ_{max} of **P3HT:** $TAZC_{60}$ blends subsequently red shifted – for example, λ_{max} for a 50:50 blend ratio shifted from 464 nm to 497 nm, and the vibronic features increased in intensity as shown in **Figure 2.14**. In contrast, annealing blends of **11a:** $TAZC_{60}$ did not produce any noticeable change in the UV-Vis spectra. XRD of annealed 50:50 blends of **11a**: $TAZC_{60}$ and P3HT:$TAZC_{60}$ blends (see **Figure 2.15**) revealed an increase in intensity of the peak at 2θ≈5° (corresponding to the interchain spacing in P3HT associated with the interdigitated alkyl chains).[53] The intensity of the XRD peak for the P3HT:$TAZC_{60}$ blend is much stronger than that for the **11a:** $TAZC_{60}$ blend, which indicates much more extensive organization and self-assembly of the P3HT in the former.

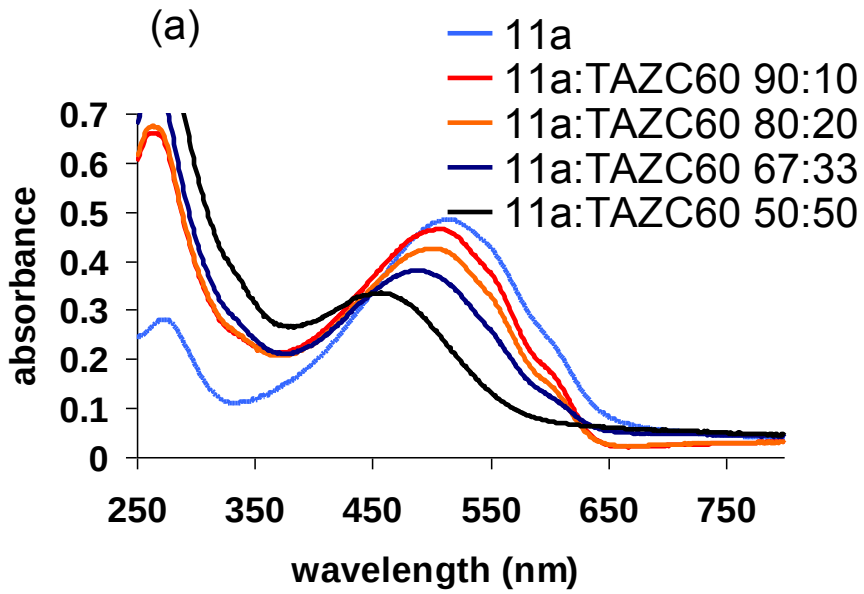

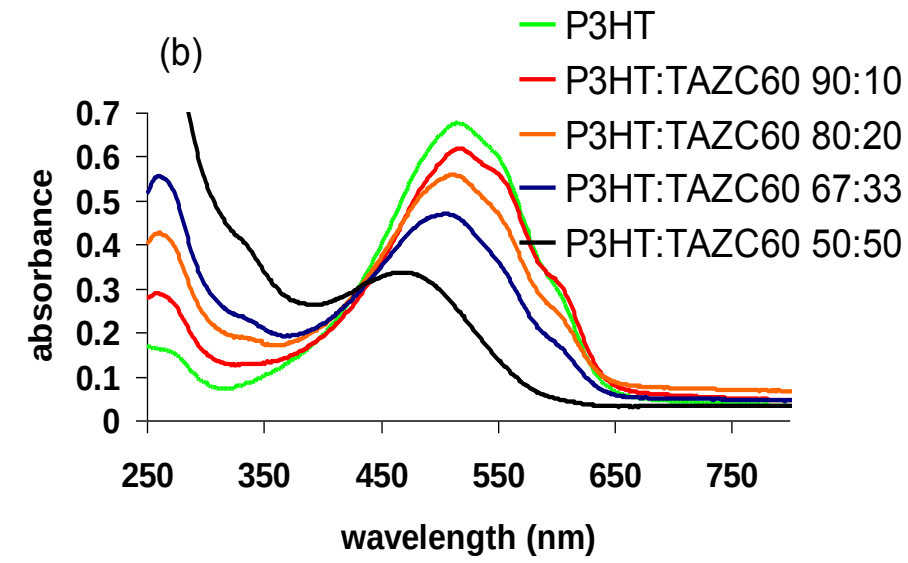

Figure 2.13: UV-vis absorption spectra of films spin cast from (a) 11a and (b) P3HT in chlorobenzene solutions containing various weight ratios of $TAZC_{60}$.

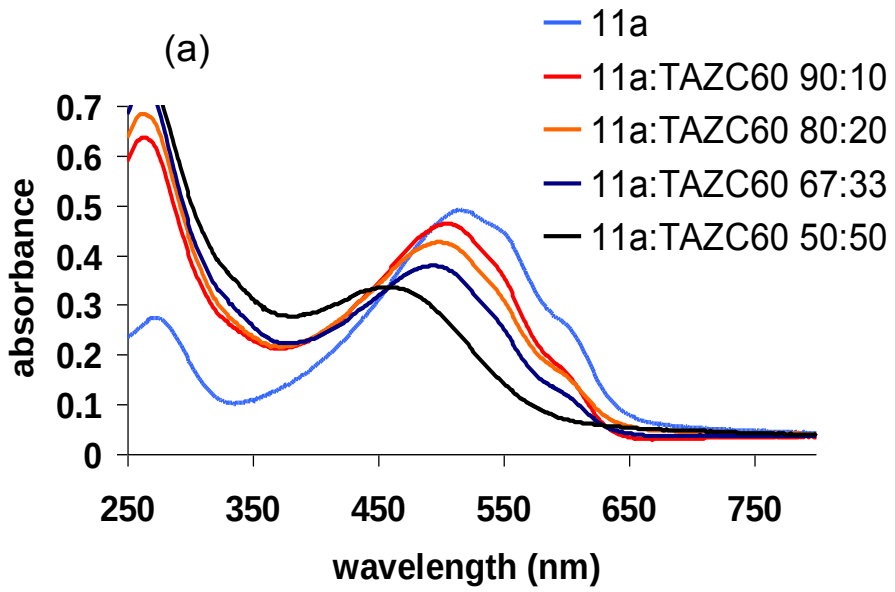

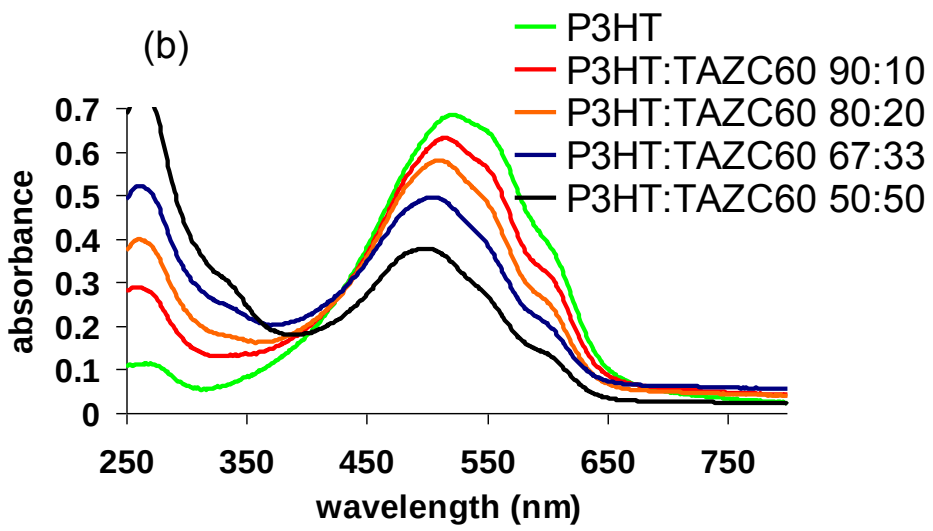

Figure 2.14: UV-vis absorption spectra of films after annealing at 140 °C for 1 hour (a) 11a and (b) P3HT containing various weight ratios of $TAZC_{60}$.

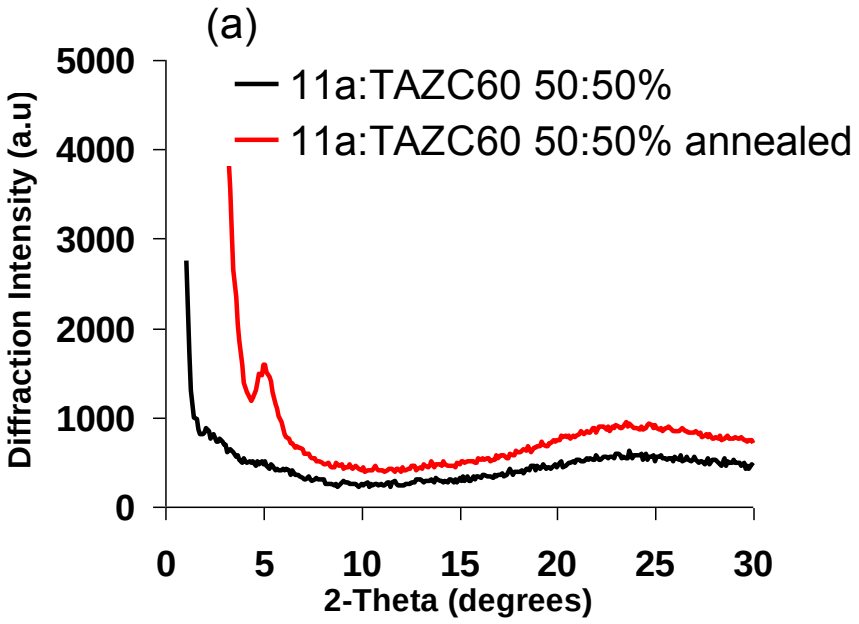

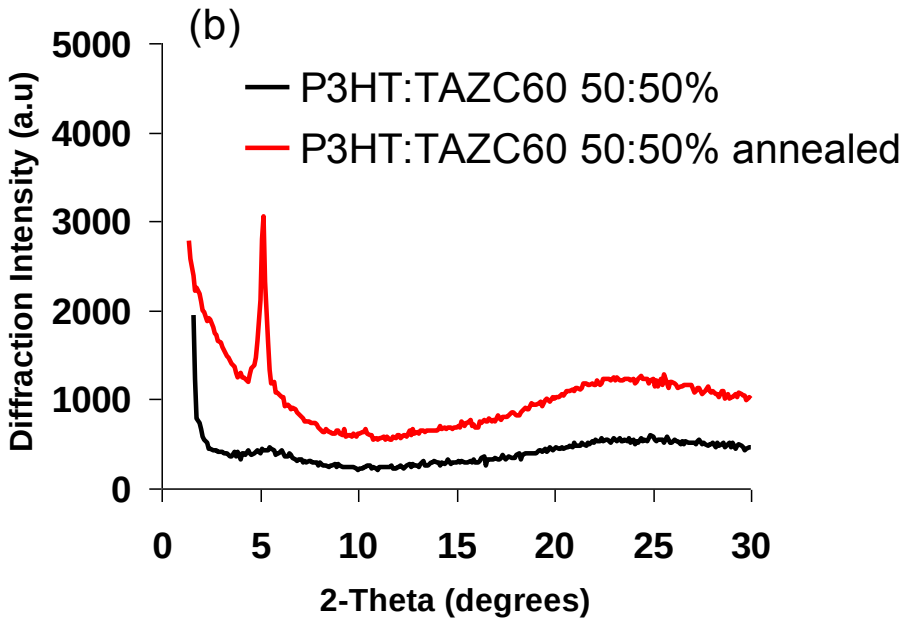

Figure 2.15: XRD spectra of films before and after annealing at 140 °C for 1 hour: (a) 11a, (b) P3HT blended with $TAZC_{60}$.

PL spectra for films of **11a**: $TAZC_{60}$ and P3HT: $TAZC_{60}$ prior to thermal annealing are shown in **Figure 2.16**, as are the corresponding decreases in PL intensity plotted against composition for the two systems (**Figure 2.18**). Both systems are characterized as exhibiting decreasing PL intensity with increasing $TAZC_{60}$ content due to photo-induced electron transfer,[54] but PL quenching is considerably greater for the **11a**: $TAZC_{60}$ systems. For example, in the 90:10 of **11a**: $TAZC_{60}$ blend the PL intensity is only 18% of **11a**; whereas for P3HT: $TAZC_{60}$ with the same composition, PL is still 50% of pure P3HT. Similarly, for a 50:50 blend, emission from **11a** is completely quenched, whereas the P3HT blend maintains 12% of its original PL intensity. After annealing at 140 °C for 1 hour, as shown in **Figure 2.17**, both PL of copolymer **11a** and P3HT decreased, because annealing induces stronger interchain-interlayer interactions of P3HT

chain,[55] however, as shown in **Figure 2.18**, the PL intensity increases for P3HT:TAZC$_{60}$ blends after annealing, while, for blends of **11a**:TAZC$_{60}$, the increase in PL with annealing was much more modest for 90:10, 80:20 and 67:33 in wt blends and PL remained absent for 50:50 blends. This, again, showed after annealing, in P3HT:TAZC$_{60}$, the P3HT showed substantial re-organization, whereas blends of **11a**, which intimately mixes with TAZC$_{60}$, were morphologically stable. These data suggest that in the case of P3HT:TAZC$_{60}$ films, mixing of TAZC$_{60}$ with P3HT occurs to some degree (despite TEMs of solution cast films indicting large scale phase separation) thereby lowering PL by photo-induced electron transfer; and that upon annealing, the TAZC$_{60}$ is expelled from the P3HT domains, which become more ordered (see XRD data) yet more fluorescent. The latter can only be explained by a reduction in the rate of photo-induced electron transfer from P3HT to TAZC$_{60}$ as a result of the phase domains of P3HT and TAZC$_{60}$ becoming larger, and more distant, since an increased molecular order of P3HT is normally associated with a lowering of PL intensity. In contrast, PL intensities in films of **11a**:TAZC$_{60}$ remain constant and low after annealing, which suggests the domains remain much more stabilized.

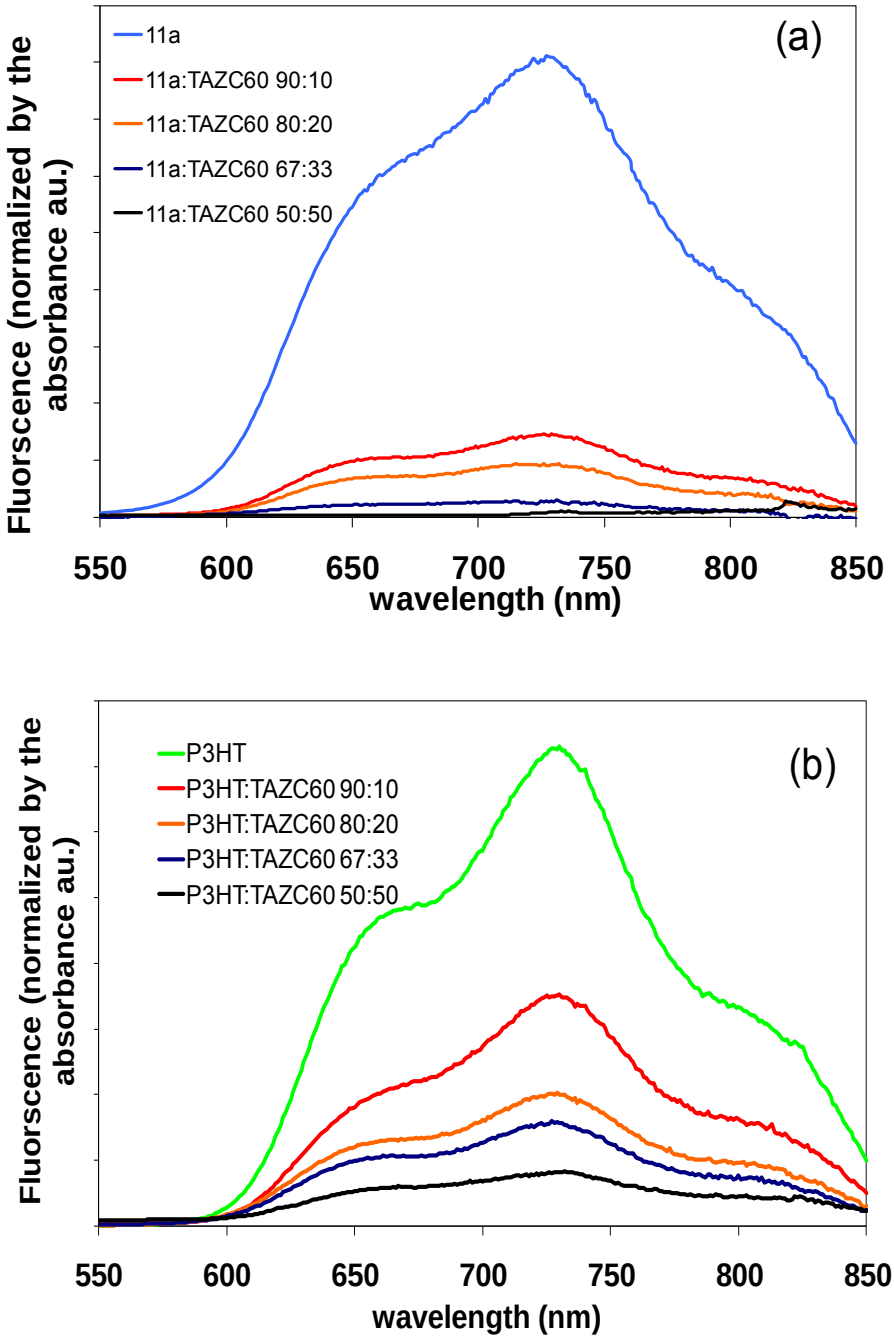

Figure 2.16: Photoluminescence spectra of films spin cast from: (a) 11a, (b) P3HT in chlorobenzene solutions containing various weight ratios of $TAZC_{60}$, spectra normalized to absorbance at 480 nm.

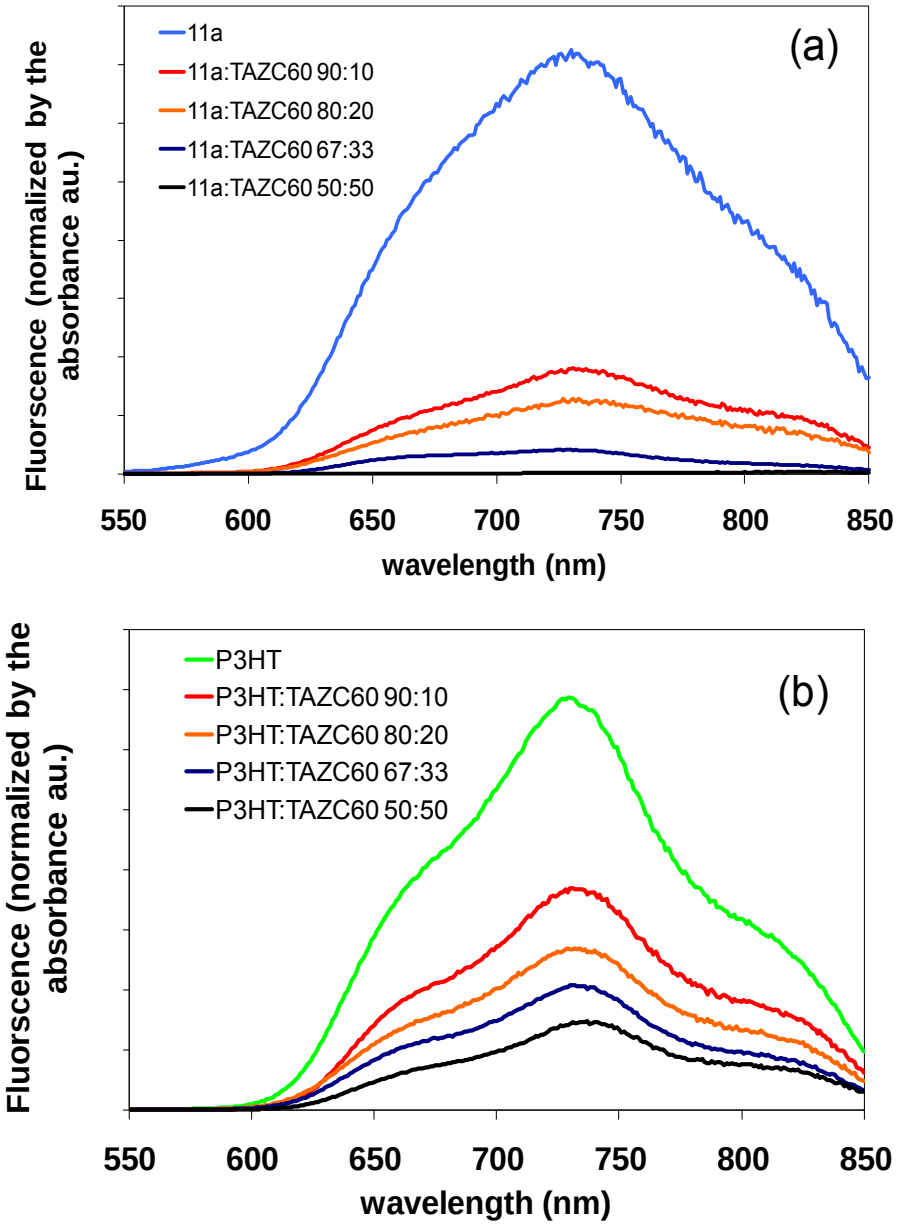

Figure 2.17: Photoluminescence spectra of films after annealing at 140 °C for 1 hour: (a) 11a, (b) P3HT containing various weight ratios of $TAZC_{60}$, spectra normalized to absorbance at 480 nm.

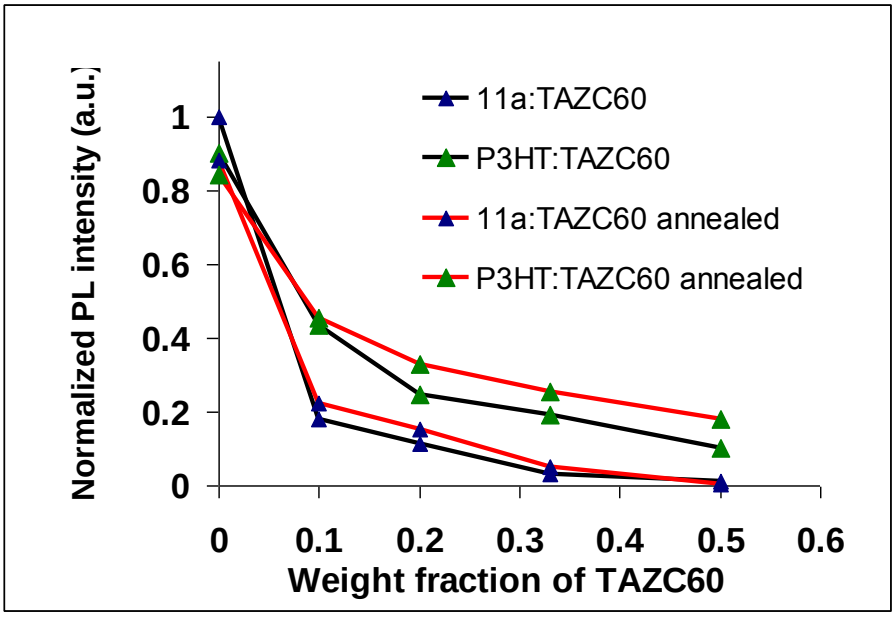

Figure 2.18: Photoluminescence intensity normalized to absorbance at 480 nm.

TEM morphologies of polymers **11a,** and its blends with $TAZC_{60}$, after annealing, are shown in **Figure 2.19**. After annealing, the contrast becomes stronger: dark regions (P3HT), in general, appear darker; light regions (TAZ), lighter. The morphology of blends of the **11a**:$TAZC_{60}$ become more distinguishable, although the phase domains remain in the region of ~10 nm, indicating both improved phase purity and kept the nano-phase separation. Of note, these morphologies bear strong resemblance to the morphologies of films of P3HT (~92 % regioregular):PCBM blends after annealing.[13] In contrast to **11a**:$TAZC_{60}$ blends, P3HT:$TAZC_{60}$ blends maintained large scale phase separation after annealing.

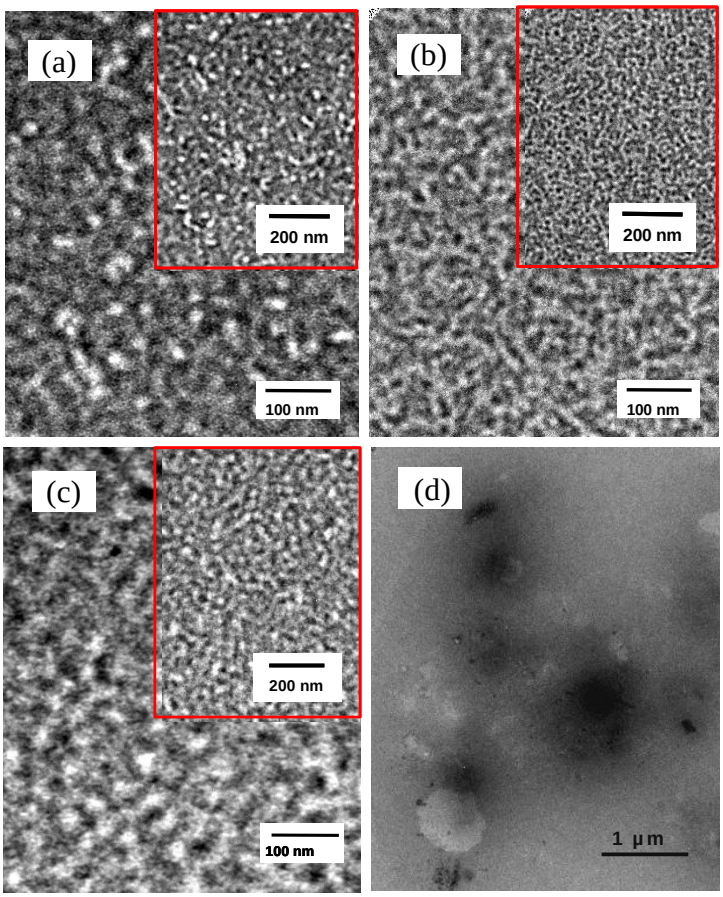

Figure 2.19: Transmission electron micrographs for films after annealing at 140 °C for 1 hour: (a) 11a, (b) 11a:$TAZC_{60}$ (1:1 in wt blend), (c) 11a: $TAZC_{60}$ (1:2 in wt blend), (d) P3HT:$TAZC_{60}$ (1:1 in wt blend).

2.3.5 PV Devices

While PV devices prepared using $TAZC_{60}$ were not anticipated to provide high power conversion efficiencies (PCE) compared to PCBM-based devices because of their inherent lower electron mobilities,[40] it was useful to compare PCEs of the various blends. The following device structure was used: ITO/PEDOT:PSS/polymer-$TAZC_{60}$/Al. As in **Figure 2.20**, the short circuit current, J_{sc}, and open circuit voltage, V_{oc}, for the **11a**:$TAZC_{60}$ PV was 0.42 mA/cm^2 and 0.5 V, respectively and for the P3HT: $TAZC_{60}$ device the values were 0.11 mA/cm^2 and 0.27 V. Power conversion efficiencies under AM 1.5 (80 mW/cm^2)

irradiation for the devices were 0.07% and 0.007% for the **11a**:$TAZC_{60}$ and P3HT:$TAZC_{60}$, respectively. When these values are corrected for reflection from by ITO glass, the PCEs are 0.11% and 0.011% respectively. Under all examinations, the **11a**:$TAZC_{60}$ PV devices displayed much better performance than P3HT:$TAZC_{60}$ devices. Given the similar optical and electronic properties of the **11a**:$TAZC_{60}$ and P3HT:$TAZC_{60}$ blends it can be inferred that improved performance of the former may be due to its nano-phase segregated morphology, although the efficiencies are much lower than state of the art devices.

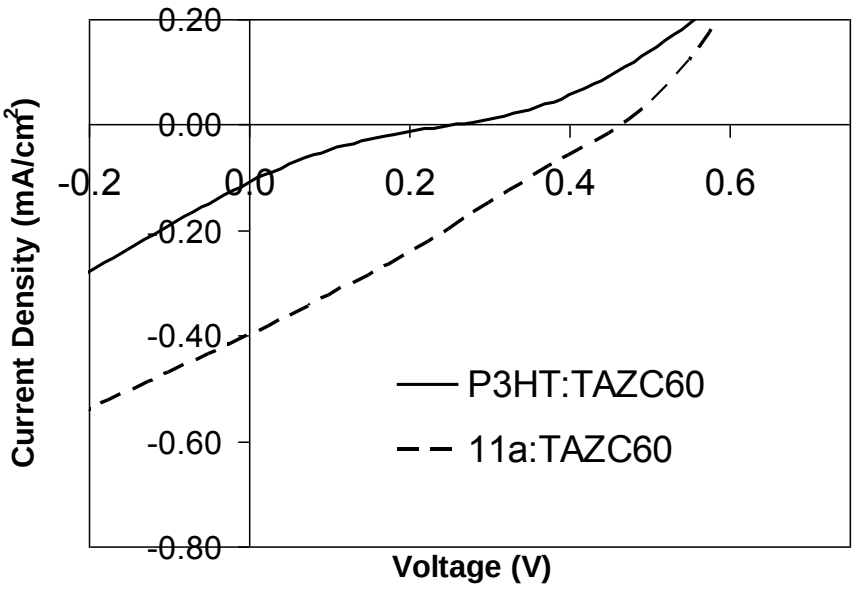

Figure 2.20: Current voltage characteristics of ITO/PEDOT:PSS/11a:$TAZC_{60}$/Al (dashed line); ITO/PEDOT:PSS/P3HT:$TAZC_{60}$/Al (solid line).

2.4 Conclusions

In summary, this work describes the synthesis of a triazole monomer **(5**) and its NMRP; the synthesis of a macroinitiator (**10)** consisting of a polythiophene backbone bearing nitroxide groups; the synthesis of graft copolymers consisting of a polythiophene backbone bearing polyvinyl triazole moieties (**11a**, **11b** and **11c**); and the preparation of blends of a graft copolymer **11a** with a fullerene possessing a chemically similar motif ($TAZC_{60}$). **11a** possesses similar optical and electrochemical properties to P3HT (~92 % regioregular), the latter being a preferred polymer for study in photovoltaic device, but it is found that the miscibility of the blend with $TAZC_{60}$ is substantially different. **11a** forms a bicontinous phase and one phase is compatible with the fullerene modified by the similar triazole. The **11a**-$TAZC_{60}$ blends form interconnected phase domains on the 10 nm scale, by virtue of the attachment of TAZ groups to polymer, as demonstrated by TEM, UV-Vis, PL quenching and XRD measurements. P3HT, in contrast, is not miscible with $TAZC_{60}$ and phase separates into micro-sized domains.

While the incorporation of short, oligomer side chains onto regioregular P3HT facilitates the formation of a bicontinuous 10 nm scale network, it is noted that the result is that the P3HT component of **11a** adopts a degree of twisting (non-coplanarity) when blended with $TAZC_{60}$, as evidenced by the blue-shift in the absorption spectrum and the absence of a strong XRD patterns. P3HT in P3HT:$TAZC_{60}$ blends also adopts a degree of non-coplanarity but annealing the P3HT:$TAZC_{60}$ blends enables the P3HT to adopt a more organized, semi-

crystalline structure. However, annealing blends of the **11a**:TAZC$_{60}$ does not produce a more organized, semi-crystalline P3HT component. The conclusion of this work therefore is three-fold: the incorporation of oligomer side chains onto regioregular P3HT facilitates the formation of a bicontinuous 10 nm scale network; the structure of the P3HT in blends of the **11a**:TAZC$_{60}$ is relatively stable; but the P3HT component is not able to adopt a highly organized, semi-crystalline structure. The latter may potentially be mitigated by manipulating the microstructure of the polymer through the sequence length distribution of grafts along the main chain (graft density) and the length of the side chains (graft length), in a manner previously shown for proton conducting graft copolymers.[56] The results of this work are intended to stimulate further examination of the role of molecular architecture of π-conjugated polymers on the evolution of controlled nano-segregated, donor-acceptor morphologies.

2.5 References

[1] B. J. de Gans, P. C. Duineveld, U. S. Schubert. *Advanced Materials* **2004**, *16*(3), 203-213.

[2] S. R. Forrest. *Nature* **2004**, *428*(6986), 911-918.

[3] S. E. Shaheen, C. J. Brabec, N. S. Sariciftci, F. Padinger, T. Fromherz, J. C. Hummelen. *Applied Physics Letters* **2001**, *78*(6), 841-843.

[4] C. W. Tang. *Applied Physics Letters* **1986**, *48*(2), 183-185.

[5] J. J. M. Halls, K. Pichler, R. H. Friend, S. C. Moratti, A. B. Holmes. *Applied Physics Letters* **1996**, *68*(22), 3120-3122.

[6] M. Theander, A. Yartsev, D. Zigmantas, V. Sundstrom, W. Mammo, M. R. Andersson, O. Inganas. *Physical Review B* **2000**, *61*(19), 12957-12963.

[7] J. J. M. Halls, C. A. Walsh, N. C. Greenham, E. A. Marseglia, R. H. Friend, S. C. Moratti, A. B. Holmes. *Nature* **1995**, *376*(6540), 498-500.

[8] P. Peumans, S. Uchida, S. R. Forrest. *Nature* **2003**, *425*(6954), 158-162.

[9] G. Yu, J. Gao, J. C. Hummelen, F. Wudl, A. J. Heeger. *Science* **1995**, *270*(5243), 1789-1791.

[10] J. J. Dittmer, E. A. Marseglia, R. H. Friend. *Advanced Materials* **2000**, *12*(17), 1270-1279.

[11] F. Yang, M. Shtein, S. R. Forrest. *Nature Materials* **2005**, *4*(1), 37-41.

[12] X. Han, X. W. Chen, S. Holdcroft. *Advanced Materials* **2007**, *19*(13), 1697-1702.

[13] W. L. Ma, C. Y. Yang, X. Gong, K. Lee, A. J. Heeger. *Advanced Functional Materials* **2005**, *15*(10), 1617-1622.

[14] S. Xiao, M. Nguyen, X. Gong, Y. Cao, H. B. Wu, D. Moses, A. J. Heeger. X. Han, X. W. Chen, S. Holdcroft. *Advanced Functional Materials* **2007**, *19*(13), 1697. **2003**, *13*(1), 25-29.

[15] G. Li, Y. Yao, H. Yang, V. Shrotriya, G. Yang, Y. Yang. *Advanced Functional Materials* **2007**, *17*(10), 1636-1644.

[16] Lee J, W. L. Ma, C. J. Brabec, Yuen J, Moon J S, Kim J Y, K. Lee, Bazan C, A. J. Heeger. *Journal of the American Chemical Society* **2008**, 130, 3619-3623.

[17] C. S. Kim, L. L. Tinker, B. F. DiSalle, E. D. Gomez, S. Lee, S. Bernhard, Y. L. Loo. *Advanced Materials* **2009**, *21*(30), 3110-3112.

[18] F. S. Bates. *Science* **1991**, *251*(4996), 898-905.

[19] A. K. Khandpur, S. Forster, F. S. Bates, I. W. Hamley, A. J. Ryan, W. Bras, K. Almdal, K. Mortensen. *Macromolecules* **1995**, *28*(26), 8796-8806.

[20] M. Muthukumar, C. K. Ober, E. L. Thomas. *Science* **1997**, *277*(5330), 1225-1232.

[21] S. A. Jenekhe, X. L. Chen. *Science* **1998**, *279*(5358), 1903-1907.

[22] S. A. Jenekhe, X. L. Chen. *Science* **1999**, *283*(5400), 372-375.

[23] J. S. Liu, E. Sheina, T. Kowalewski, R. D. McCullough. *Angewandte Chemie-International Edition* **2001**, *41*(2), 329-332.

[24] N. Sary, L. Rubatat, C. Brochon, G. Hadziioannou, J. Ruokolainen, R. Mezzenga. *Macromolecules* **2007**, *40*(19), 6990-6997.

[25] N. Sary, R. Mezzenga, C. Brochon, G. Hadziioannou, J. Ruokolainen. *Macromolecules* **2007**, *40*(9), 3277-3286.

[26] R. Mezzenga, J. Ruokolainen, G. H. Fredrickson, E. J. Kramer, D. Moses, A. J. Heeger, O. Ikkala. *Science* **2003**, *299*(5614), 1872-1874.

[27] B. de Boer, U. Stalmach, P. F. van Hutten, C. Melzer, V. V. Krasnikov, G. Hadziioannou. *Polymer* **2001**, *42*(21), 9097-9109.

[28] T. Heiser, G. Adamopoulos, M. Brinkmann, U. Giovanella, S. Ould-Saad, C. Brochon, K. van de Wetering, G. Hadziioannou. *Thin Solid Films* **2006**, *511*, 219-223.

[29] U. Stalmach, B. de Boer, C. Videlot, P. F. van Hutten, G. Hadziioannou. *Journal of the American Chemical Society* **2000**, *122*(23), 5464-5472.

[30] K. van de Wetering, C. Brochon, C. Ngov, G. Hadziioannou. *Macromolecules* **2006**, *39*(13), 4289-4297.

[31] M. H. van der Veen, B. de Boer, U. Stalmach, K. I. van de wetering, G. Hadziioannou. *Macromolecules* **2004**, *37*(10), 3673-3684.

[32] K. Sivula, Z. T. Ball, N. Watanabe, J. M. J. Frechet. *Advanced Materials* **2006**, *18*(2), 206-210.

[33] S. M. Lindner, S. Huttner, A. Chiche, M. Thelakkat, G. Krausch. *Angewandte Chemie-International Edition* **2006**, *45*(20), 3364-3368.

[34] S. P. Economopoulos, C. L. Chochos, V. G. Gregoriou, J. K. Kallitsis, S. Barrau, G. Hadziioannou. *Macromolecules* **2007**, *40*(4), 921-927.

[35] X. W. Chen, B. Gholamkhass, X. Han, G. Vamvounis, S. Holdcroft. *Macromolecular Rapid Communications* **2007**, *28*(17), 1792-1797.

[36] J. Kido, K. Hongawa, K. Okuyama, K. Nagai. *Applied Physics Letters* **1993**, *63*(19), 2627-2629.

[37] M. Strukelj, T. M. Miller, F. Papadimitrakopoulos, S. Son. *Journal of the American Chemical Society* **1995**, *117*(48), 11976-11983.

[38] M. Strukelj, F. Papadimitrakopoulos, T. M. Miller, L. J. Rothberg. *Science* **1995**, *267*(5206), 1969-1972.

[39] L. S. Yu, S. A. Chen. *Advanced Materials* **2004**, *16*(8), 744-748.

[40] X. W. Chen, C. Y. Liu, T. H. Jen, S. A. Chen, S. Holdcroft. *Chemistry of Materials* **2007**, *19*(21), 5194-5199.

[41] Y. N. Li, G. Vamvounis, J. F. Yu, S. Holdcroft. *Macromolecules* **2001**, *34*(10), 3130-3132.

[42] Y. N. Li, G. Vamvounis, S. Holdcroft. *Macromolecules* **2001**, *34*(2), 141-143.

[43] Y. N. Li, G. Vamvounis, S. Holdcroft. *Macromolecules* **2002**, *35*(18), 6900-6906.

[44] C. J. Hawker, A. W. Bosman, E. Harth. *Chemical Reviews* **2001**, *101*(12), 3661-3688.

[45] E. Malmstrom, R. D. Miller, C. J. Hawker. *Tetrahedron* **1997**, *53*(45), 15225-15236.

[46] D. Benoit, V. Chaplinski, R. Braslau, C. J. Hawker. *Journal of the American Chemical Society* **1999**, *121*(16), 3904-3920.

[47] R. S. Loewe, P. C. Ewbank, J. S. Liu, L. Zhai, R. D. McCullough. *Macromolecules* **2001**, *34*(13), 4324-4333.

[48] K. Sivula, C. K. Luscombe, B. C. Thompson, J. M. J. Frechet. *Journal of the American Chemical Society* **2006**, *128*(43), 13988-13989.

[49] J. Pommerehne, H. Vestweber, W. Guss, R. F. Mahrt, H. Bassler, M. Porsch, J. Daub. *Advanced Materials* **1995**, *7*(6), 551-554.

[50] L. L. Chua, J. Zaumseil, J. F. Chang, E. C. W. Ou, P. K. H. Ho, H. Sirringhaus, R. H. Friend. *Nature* **2005**, *434*(7030), 194-199.

[51] J. S. Trent, J. I. Scheinbeim, P. R. Couchman. *Macromolecules* **1983**, *16*(4), 589-598.

[52] S. Hong, A. A. Bushelman, W. J. MacKnight, S. P. Gido, D. J. Lohse, L. J. Fetters. *Polymer* **2001**, *42*(13), 5909-5914.

[53] T. A. Chen, X. M. Wu, R. D. Rieke. *Journal of the American Chemical Society* **1995**, *117*(1), 233-244.

[54] N. S. Sariciftci, L. Smilowitz, A. J. Heeger, F. Wudl. *Science* **1992**, *258*(5087), 1474-1476.

[55] J. Cornil, D. Beljonne, J. P. Calbert, J. L. Bredas. *Advanced Materials* **2001**, *13*(14), 1053-1067.

[56] J. F. Ding, C. Chuy, S. Holdcroft. *Advanced Functional Materials* **2002**, *12*(5), 389-394.

3: DIRECTED GROWTH OF 1-D ASSEMBLIES OF PERYLENE DIIMIDE FROM A CONJUGATED POLYMER

Sections of this chapter have been reproduced in part with permission

from: Chemistry of Materials, **2010**, 22(7), 2287-2296,

3.1 Introduction

π-Conjugated organic materials have attracted considerable attention over the past three decades on account of their special properties, which include electronic conductivity, electroluminescence and light-harvesting. The use of these materials in thin-film electronics is a driving force behind the development of new and modified π-conjugated systems; however, a greater understanding of structure-property relationships is vital to reaching this goal. Recently, research has focused on the formation of nanosized structures by molecular self-assembly of tailored, supramolecular building blocks. Through non-covalent interactions (e.g., hydrophobic, electrostatic, π-π stacking, hydrogen bonding)[1-6] a variety of supramolecular architectures (e.g., spherical micelles, vesicles, fibers, supramolecular helices, nanoribbons and nanotubes)[7-13] have been fabricated. Although research in this field has led to a greater understanding of the requirements for supramolecular engineering,[1] the creation of supramolecular architectures with well-defined shapes, structure and functions continues to be a significant challenge.

Among the many types of supramolecular building blocks, the most widely studied systems are rod-coil oligomers and polymers consisting of rigid, rod-like and flexible, coil-like blocks within the same molecular backbone. These materials are excellent candidates for creating supramolecular structures due to mutual repulsion of the dissimilar blocks that result in microphase segregation of rod and coil segments into ordered periodic arrays.[14] Recently, triblock

copolymers which can exist as either coilrod-coil or rod-rod-rod conformations were reported by Mezzenga et al. The transition between configurations, triggered either thermally or via variation in solvent composition, result in lamellar ordering or clustering, respectively.[15] Alternatively, ordered structures may be obtained from crystalline-crystalline diblock copolymers. For example, regioregular poly(3-butylthiophene)-b-poly(3-octylthiophene) in various compositions was found to self-assemble into crystalline nanowires from solution and, from the melt phase, to microphase-separate into two distinct crystalline domains possessing a lamellar structure.[16] Sary et al. have also reported on blends of a rod-type homopolymer with rod-coil block copolymers in which long-range lamellar clusters percolate throughout the entire sample. It was noted that such ordering was not observed upon blending the rod-type polymer with the coil-type homopolymer thus attributing the ordered lamellar clusters to π-π interactions between rod segments.[17]

Dendritic materials have also garnered a great deal of attention in the drive to develop ordered structures for optoelectronic applications.[18] For example, Stupp et al. have incorporated dendritic blocks into rod-coil materials at the end of the rod segment (e.g., **1** in **Scheme 3.1**). The relative size of the dendron with respect to the rod-coil segment significantly influences the packing, either promoting or inhibiting long range molecular assembly.[19] A number of one-dimensional nanostructures based on flat and helical nanoribbons have been assembled using dendron-rod-coil molecules. Furthermore, introduction of functionality onto the dendritic block in the form of hydroxyl groups or

electronically conductive substitutents provides nano-assemblies with potential applications as biomaterials, nonlinear optics and nanowires.[10] Similarly, Lee et al. have demonstrated that 1-D cylindrical assemblies may be formed from wedge-coil molecules. As opposed to dendron-rod-coil systems, these materials possess tunable properties triggered by external stimuli such as solvent polarity.[20] For example, as the solvent polarity is changed from water to hexane, the self-assembled nanofibers of molecule **2** become inverted resulting in conversion of highly flexible, coil-like to stiff, rod-like cylinders. Such structural inversions may be utilized in applications such as encapsulation and smart surfaces.[20] Besides solvent effects, enhanced π-π interactions significantly influence the self-assembly of 1-D nanostructures as is observed with **3**, in which aggregation into twisted helical ribbons with regular periodicity occurs.[21]

Attachment of bulky dendrons to both ends of a rigid rod, such as the dumbbell molecule **4**, promotes π-π stacking of the aromatic groups. In this case, mutual rotation to relieve steric hindrance due to the bulky dendrons results in aggregation into regular helical arrangements.[7] Furthermore, transformation of the helical strands into nanocages can be achieved through addition of aromatic guest molecules. The authors attribute this to intercalation of the guest molecule between the rod segments via π-π interactions, thus partially relieving steric repulsion between the bulky dendrons and illustrating the impact π-π interactions can impart on the aggregation of molecules.[7] Similarly, the shape dependent organization of perylene diimides (PDI) has been reported by Würthner et al. in which the wedge-shaped PDI **5** assembles into small micellar aggregates and

the dumbbell-shaped PDI **6** forms nanorod aggregates.[22] Interestingly, the authors found that mixtures of wedge-shaped and dumbbell shaped PDIs formed hollow vesicles due to coassembly. In other words, alternation between a bulky symmetric PDI with an unsymmetric wedge-shaped PDI decreases the curvature with respect to the micelle formed by **5** alone and increases the curvature with respect to the nanorods of **6**, thus vesicles are formed over micelles or nanorods. Collectively, these structural effects on morphology provide a guideline for the rational design of particular morphologies.[22]

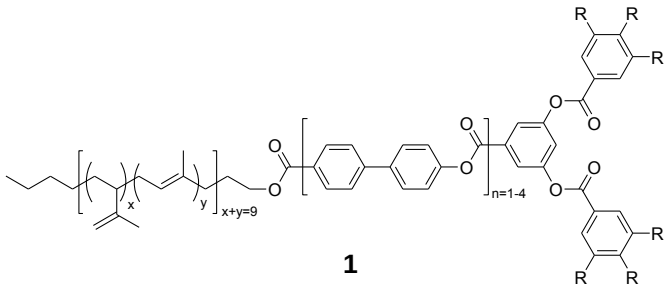

1

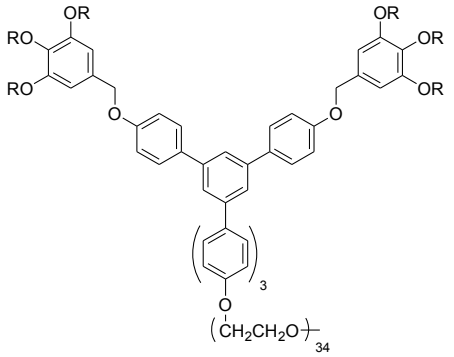

2

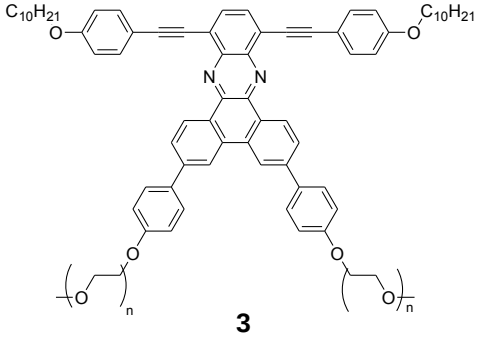

3

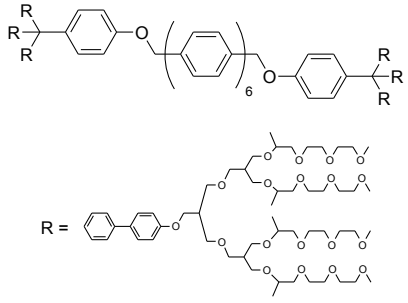

4

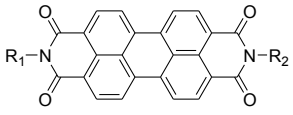

5: R_1 = Ph(O$_3$)$_3$ R_2 = O$_6$O(C=O)C(=C)

6: $R_1 = R_2$ = Ph(O$_3$)$_3$

7: $R_1 = R_2$ = C_6H_{13} / C_6H_{13}

8: R_1 = C_6H_{13} / C_6H_{13} R_2 = O$_{10}$OH

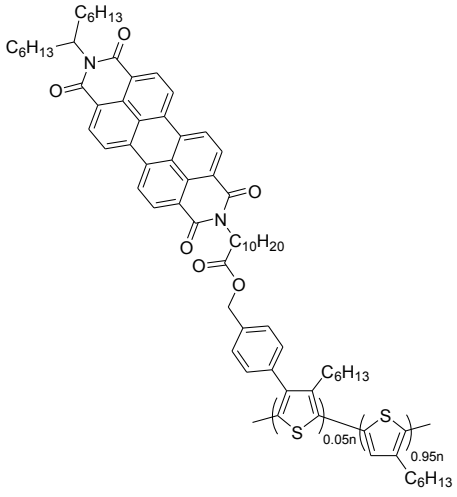

9: PP3HT

Scheme 3.1: Structures of various molecules showing self-assembly behavior and PP3HT (9) used in this work.

The planar π-conjugated framework of PDI molecules coupled with their inherent n-type semiconductor characteristics and high thermal and photo-stability make these ideal candidates for supramolecular self-assembly into 1-D nanoarchitectures through strong π-π interactions. Their potential use in device applications provides the impetus for optimization of the molecular structure to achieve shape-defined 1-D assemblies with desired optoelectronic properties. Thus, fabrication of 1-D nanostructures, based on PDI, with controllable size and morphology has been investigated by Zang and coworkers. Their research has demonstrated that assembly of PDI into 1-D structures requires cofacial π-π stacking between molecular skeletons to predominate over lateral association caused by the hydrophobic interaction among the side chain substituents.[23] Through a variety of techniques (e.g., phase transfer, vapour diffusion, seeded growth) Zang et al. have been successful at generating nanobelts, nanowires and nanofibers from PDI systems that would otherwise form bulky aggregates.[23] Under similar conditions, other research groups have also isolated PDI nanowires and nanofibers by phase transfer and solvent-vapor annealing, respectively.[24, 25] Recently, a new class of polymeric multichromophoric arrays in which PDI molecules are linked to a polymeric backbone via small peptidic spacers has been reported.[26] In these perylene polyisocyanides, the PDI moieties have rotational and translational freedom to allow for rearrangement on the molecular scale; however, on a larger scale they form highly defined arrays along the polymer backbone through π-π stacking. This “locking in” of the PDI molecules, essentially forming π-stacks along the polymer backbone, confers

electronic and optical function to the architecture.[27, 28] Interestingly, blends of the perylene functionalized polymer with PDI have shown that, depending on the polarity of the solvent and substrate, the two components either influence each others morphology or self assemble independently. Thus interplay between the polymer and PDI could be controlled by tuning the solvent or substrate polarity.[29] Alternatively, perylene diimides may be incorporated as electron-acceptors with π-conjugated polymers; such polymers have been reported wherein PDI has been incorporated as block copolymers,[30-35] in the main chain,[36] or as pendant groups.[28, 37] These donor-acceptor polymers are specifically designed to enable energy transfer in the electronically excited state of the polymer, thereby imparting useful optoelectronic properties. Furthermore, inclusion of PDI in donor-acceptor polymers results in microphase separated morphologies and photoluminescence quenching, both attractive features for photovoltaic applications.

In this chapter, combining the formation of 1-D nanowires, fabricated from PDI small molecules, with π-conjugated polymers containing pendant perylene moieties was demonstrated. It is hypothesized that during film formation free PDI molecules in solution will interact with pendant perylene attached to a conjugated polymer backbone and, upon slow evaporation of solvent, molecular templating by the pendant perylene will initiate π-π stacking of the PDI small molecules, as illustrated in **Figure 3.1**. In other words, polymer-assisted crystal growth of PDI may be accomplished through blending PDI small molecules with a conjugated polymer functionalized with perylene diimide. The influence of the pendant

perylene moieties on the self-assembly and crystallization of PDI, and the resulting effects on thin film morphology and structure-function were investigated. This strategy involves the synthesis of a π-conjugated polymer bearing PDI side groups attached via alkyl chain spacers that allows for the rotational and translational freedom required for self-assembly. This builds on previous reported work on post-functionalization of preformed poly(3-hexylthiophene) (P3HT), wherein partial bromination at the 4-position of the thienyl ring, followed by Pd-catalyzed coupling, enables the covalent attachment of a wide variety of functional groups.[38-41] Previous studies have shown that ~5 mol% postfunctionality of P3HT is optimal, i.e., 1 in 20 thienyl groups, as larger degrees of substitution disrupt the coplanarity of the π-conjugated backbone leading to reduced crystallinity in thin films.[40, 42] In the chapter, the preparation of 5 mol% post-functionalized P3HT bearing PDI moieties (PP3HT, **9**) is reported. Comparative studies of the electronic properties of **9** by cyclic voltammetry, UV-visible and fluorescence spectroscopy using molecular blends of P3HT and PDI molecules (**7**) and blends of **9** and **7** reveal striking effects illustrating the importance of the pendant perylene moiety on the morphology and properties of the thin films formed.

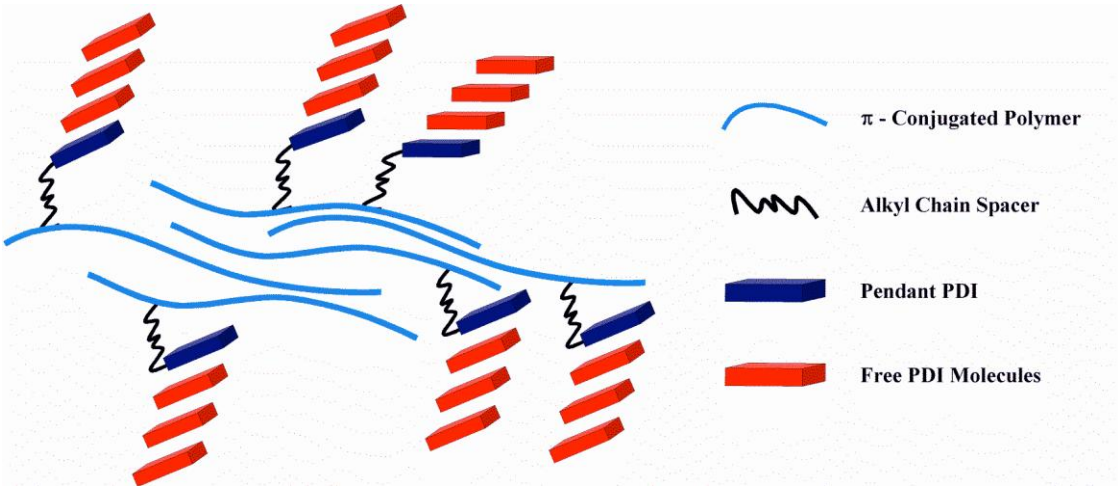

Figure 3.1: Schematic representation illustrating polymer-assisted crystal growth of PDI from pendant perylene moieties attached to a π-conjugated polymer.

3.2 Experimental

3.2.1 Chemicals

All reagents were obtained commercially from Sigma-Aldrich and used as received. All solvents were of at least reagent grade. All reactions were performed under an inert atmosphere of either argon or nitrogen. RR-P3HT possessing >98% regioregularity was synthesized for post-functionalization, as described below.

3.2.2 Synthesis

N,N'-bis(1-hexylheptyl)perylene-3,4,9,10-tetracarboxylbisimide (7) was synthesized according to the method reported in literature.[43] ^{1}H NMR (δ/ppm, $CDCl_3$): 0.79 (t, 12H), 1.18-1.30 (m, 32 H), 1.84 (m, 4H), 2.23 (m, 4H), 5.16 (m, 2H), 8.62-8.75 (m, 8H).

N-(1-hexylheptyl)-N'-(12-carboxylicdodecyl)perylene-3,4,9,10 tetracarboxylbisimide (8) was synthesized according to the method reported in literature.[43] ^{1}H NMR (δ/ppm, $CDCl_3$): 0.82 (t, 6H), 1.29 (m, 32H), 1.64 (quint, 2H), 1.77 (quint, 2H), 1.88 (m, 2H), 2.27 (m, 2H), 2.36 (t, 2H), 4.20 (t, 2H), 5.18 (m, 1H), 8.68 (dd, 8H).

Regioregular poly(3-hexylthiophene) (P3HT) was synthesized and purified according to the method reported in literature,[44] except that Ni(dppe)Cl_2 catalyst was used instead of Ni(dppp)Cl_2. The RR-P3HT sample obtained possessed a regioregularity of >98% according to 1H NMR analysis as shown in **Figure 3.2**. ^{1}H NMR (δ/ppm, $CDCl_3$): 6.99 (s, 1H), 2.79(t, 2H), 1.72 (m, 2H), 1.34 (m, 5H), 0.90 (t, 3H). GPC: M_n, 22,000 Da; Polydispersity, 1.85.

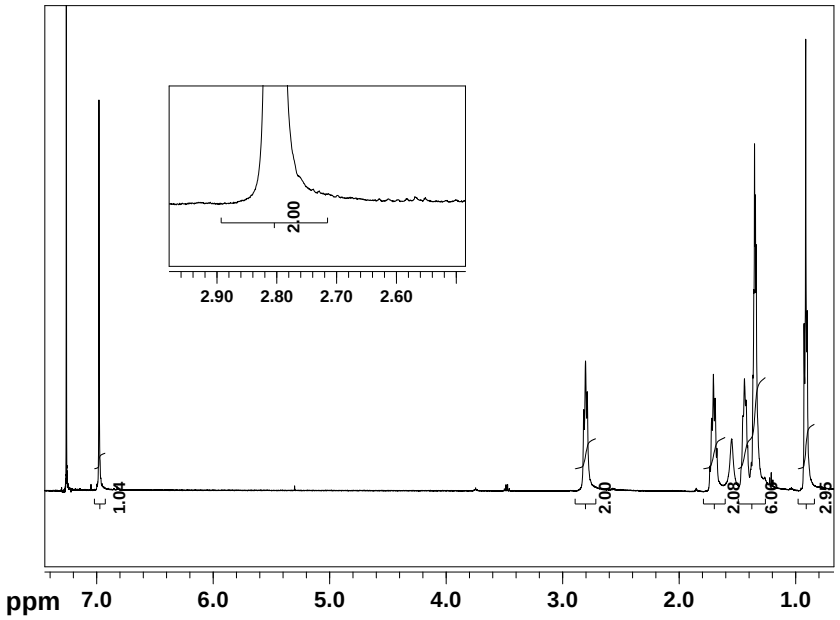

Figure 3.2: ^{1}H NMR spectrum of regioregular poly(3-hexylthiophene) (RR-P3HT) in $CDCl_3$.

5 mol% BrP3HT (10). NBS (11.0 mg, 0.06 mmol) was added to a flask containing P3HT (0.20 g, 1.2 mmol) in chloroform (16 mL). The solution was stirred at room temperature for 15 h then heated at 50 °C for 2 h. The reaction mixture was poured into a saturated $NaHCO_3$ solution (60 mL). The organic layer was extracted then washed with water five times and dried over $MgSO_4$. Precipitation into methanol afforded a black solid (0.18 g, yield: 90%). ^{1}H NMR (δ/ppm, $CDCl_3$) as shown in **Figure 3.3**: 6.99 (s) 2.80 (br, methylene), 2.60 (br, methylene), 1.60 (br), 1.33 (br), 1.28 (br), 0.87 (br, CH3). GPC: M_n, 23,000 Da; Polydispersity, 1.87.

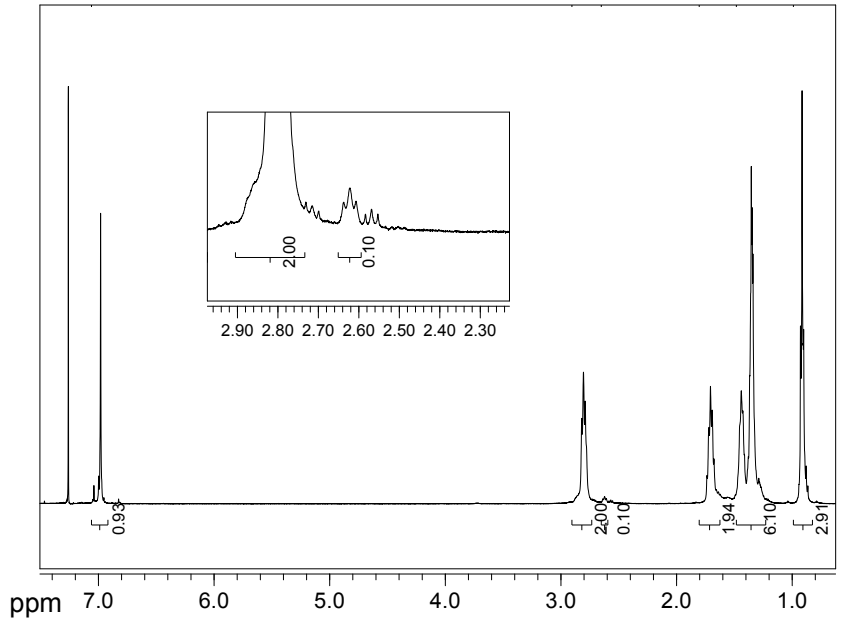

Figure 3.3: ^{1}H NMR spectrum of 5 mol% brominated P3HT (10) in $CDCl_3$.

5 mol% OH-P3HT (11). 4-(Hydroxymethyl)phenylboronic acid (0.011 g, 0.072 mmol) in 2.0 M Na_2CO_3 aqueous solution (1.0 mL, 2.0 mmol) was added at a solution of **10** (120 mg, 0.72 mmol) in THF (16 mL). Following de-oxygenation (nitrogen bubbled through solution for 30 min), $Pd(PPh_3)_4$ (5 mg, 0.004 mmol)

was added and the reaction mixture was heated at 60 °C for 2 days. Upon cooling, the solution was concentrated then precipitated into methanol. The resulting solid was purified by Soxhlet extraction with methanol and precipitated again into methanol from a chloroform solution, then dried in a vacuum oven affording 96 mg of a black solid (yield 80%). ^{1}H NMR (δ/ppm, $CDCl_3$) as shown in **Figure 3.4**: 6.99 (s), 4.72 (d), 2.78 (br, methylene), 2.39 (br, methylene) 1.60 (br), 1.33 (br), 1.28 (br), 0.87 (br, CH_3). GPC: M_n, 23,000 Da; Polydispersity, 2.00.

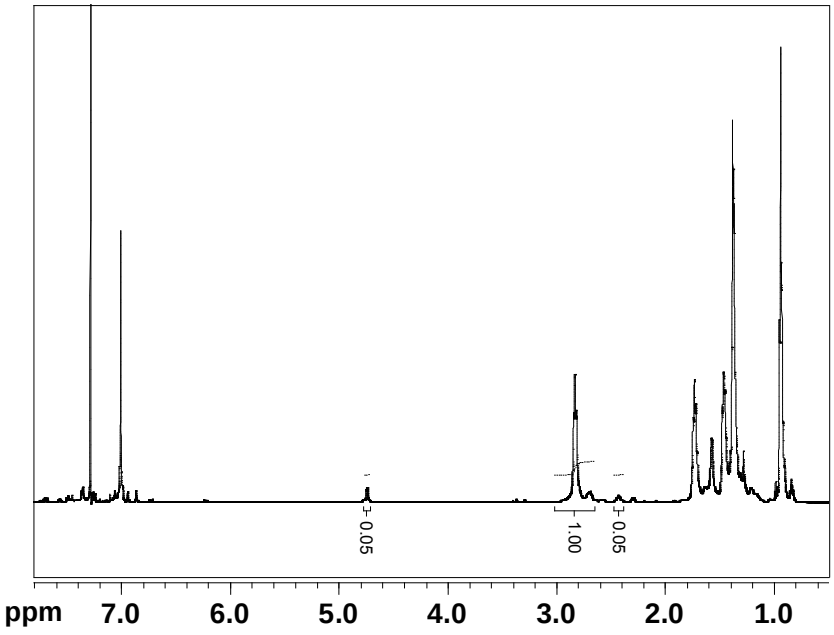

Figure 3.4: ^{1}H NMR spectrum of 5 mol% OH-P3HT (11) in $CDCl_3$.

PP3HT (9). A solution of **8** (34 mg, 0.045 mmol), **11** (100 mg, 0.60 mmol), DMAP (3 mg, 0.025 mmol) and dicyclohexylcarbodiimide (DCC, 15 mg, 0.054 mmol) in dichloromethane (12 ml) was stirred for 24 h at RT then filtered and the solvent removed under reduced pressure. The resulting residue was purified by

column chromatography (silica gel and celite) with chloroform then precipitated into methanol afforded the desired product as a dark purple solid (90 mg, 68%). ^{1}H NMR (δ/ppm, $CDCl_3$) as shown in **Figure 3.5**: 8.68 (br), 6.99 (s), 5.18 (m), 5.12 (d), 4.20 (t), 2.78 (br), 2.35-2.40 (br), 2.27 (m), 1.58-1.88 (br), 1.21-1.38 (br), 0.82-0.87 (br). ^{13}C NMR ($CDCl_3$): 177.3, 163.5, 140.1, 134.7, 133.9, 131.6, 130.7, 129.6, 128.1, 127.6, 126.5, 123.0, 65.6, 41.1, 34.6, 33.7, 33.1, 32.8, 31.7, 30.8, 29.4, 28.3, 27.1, 24.8, 22.7, 14.5. Anal. Calcd for $C_{255}H_{340}N_2O_6S_{20}$: C, 73.47; H, 8.20; N, 0.67. Found: C, 73.09; H, 8.09; N, 0.49. GPC: M_n, 29,000 Da; Polydispersity, 2.01.

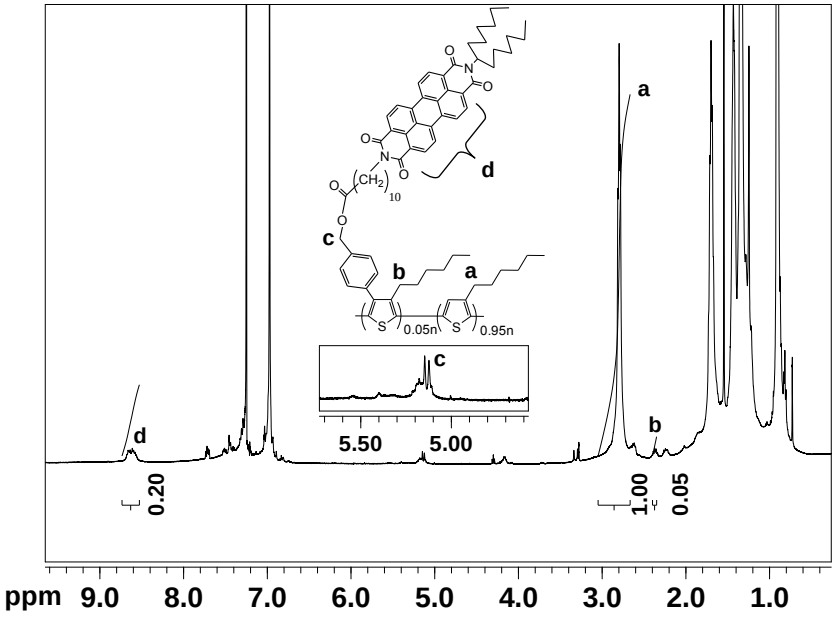

Figure 3.5: ^{1}H NMR spectrum of PP3HT (9) in $CDCl_3$.

3.2.3 Measurements

^{1}H NMR spectra were obtained on a 500 MHz Varian AS500 spectrometer; chemical shifts are reported in parts per million (ppm), referenced to $CDCl_3$ (^{1}H: δ=7.26). Molecular weights were measured by gel permeation

chromatography (GPC) (Waters model 1515 isocratic pump) equipped with μ-Styragel columns against polystyrene standards. Polymers were eluted with THF using a flow rate of 1.0 mL/min and detected with a UV-vis detector (Waters model 2487) at 254 nm. Elemental analyses were obtained using a Carlo Erba model 1106 CHN analyzer. UV-vis absorption spectra were recorded on a Cary 3EI (Varian) spectrophotometer. Photoluminescence (PL) spectra were recorded with a Photon Technology International QuantumMaster model QM-4 equipped with an integrating sphere. Film thickness and surface roughness were measured on a KLA-Tencor Alpha-Step IQ Surface Profiler with scan rate at 50 μm/s, force at 2.56 mg and stylus radius at 5 μm. Cyclic voltammetry was performed on a Princeton Applied Research Model 263A potentiostat/galvanostat in a one compartment, three-electrode cell in acetonitrile (ACN) solution of 0.1 M n-Bu_4NClO_4 at scan rates of 50 mVs^{-1}. A glassy carbon disk coated with polymer and Pt wire were used as the working and counter electrodes, respectively, and a Pt wire in an ACN solution of 0.1 M Bu_4NI/ 0.05 M I_2, separated from the working electrode compartment by a glassy frit, was used as the reference electrode. An internal reference to ferrocene (Fc/Fc^+ redox couple is 4.8 eV) was used to calibrate the reference electrode. TEM images were performed on a Tecnai 20 FEI STEM. A layer of poly(styrene sulfonic acid)-doped poly(3, 4-ethylenedioxythiophene) (PEDOT, Bayton®P VP AI4083) was spin cast onto clean glass substrates at 5000 rpm then annealed at 140 °C for 10 min. Onto this surface, polymers and polymer blends were fabricated following the “solvent annealing” procedure described above. The film and substrate were immersed in

water and, upon dissolution of the PEDOT layer, the polymer films were removed from the surface of the water by lift-out using uncoated Cu grids. The films were then stained for 15 min using of RuO_4 vapor prepared in situ from 0.5 % ruthenium (III) chloride in a sodium hypochlorite solution (containing ≥4% chlorine in solution). XRD was performed on a Bruker-AXS D8 Discover High-Resolution Diffractometer system using Cu Kα wavelength (~1.544 Å). Polymer films for XRD analysis were prepared on glass substrates by the same spin casting method described below.

3.2.4 Fabrication of Polymer Thin Films

Polymeric films were fabricated following the "solvent annealing" procedure described by Li et al.[45] Dichorobenzene solutions (20 mg/mL) of PP3HT, P3HT, PDI and blends of PP3HT:PDI and P3HT:PDI at various weight ratios were spin-coated at 100 rpm for 1 s, 300 rpm for 1 s and 900 rpm for 20 s onto PEDOT coated glass substrates in a glove box under N_2-filled atmosphere. Following spin-coating, the substrates were left in a covered glass petri dish for one hour to allow for slow evaporation of the solvent resulting in 70 to 80 nm thick films as measured by profilometry.

3.3 Results and Discussion

3.3.1 Polymer Synthesis

Preparation of the desired polymer, PP3HT (**9**, **Scheme 3.2**), began with partial bromination (5 mol%, based on the number of thiophene units) via electrophilic substitution of the 4-thienyl protons of regioregular P3HT (>98%

RRP3HT). As previously reported, the extent of bromination can be monitored by ^{1}H NMR.[39] Integration of the α-methylene protons for which bromine is located on the same thienyl ring indicates that 5 mol% of the RR-P3HT backbone was brominated (**10**, see **Figure 3.3**). Suzuki cross-coupling of **10** with 4-(hydroxymethyl)phenylboronic acid following the reported method for fully functionalized P3HT afforded **11**.[46] Conversion of the bromo- to 4-(hydroxymethyl)phenyl- substituents is quantitative as evidenced by ^{1}H NMR (see **Figure 3.4**).[39]

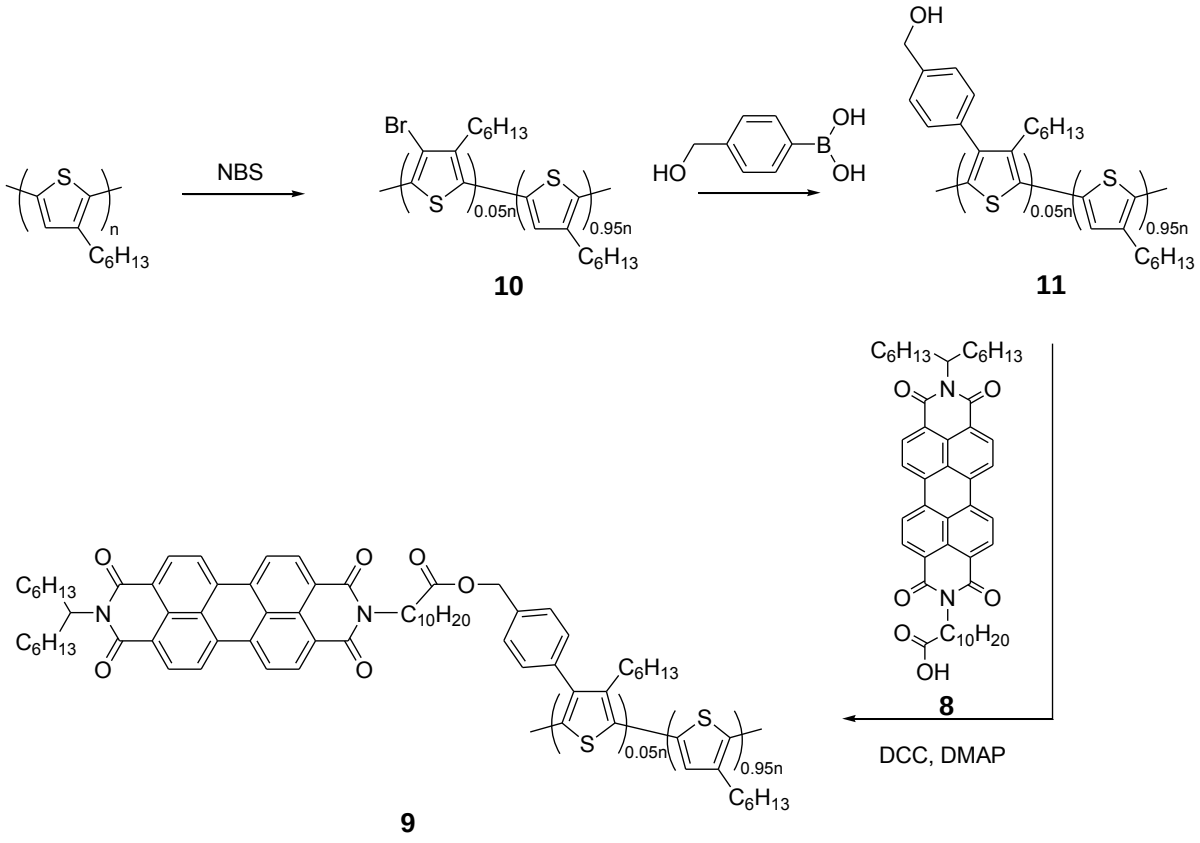

Scheme 3.2: Synthetic route for PP3HT (9).

Following a previously reported method,[47] N,N'-bis(1-hexylheptyl)perylene-3,4,9,10-tetracarboxylbisimide **(7)** and N-(1-hexylheptyl)-N'-(12-carboxylicdodecyl)perylene-3,4,9,10 tetracarboxylbisimide **(8)** were synthesized (see Appendix for details). Briefly, condensation of perylene-3,4,9,10-tetracarboxyldianhydride with 1-hexylheptylamine afforded the symmetric diimide **7**. Partial saponification with KOH led to the monoimide monoanhydride, which, following condensation with 11-aminoundecanoic acid in molten imidazole, afforded **8**, a highly soluble perylene dye bearing a carboxylic acid group.

Steglich esterification of **8** and **11** afforded the desired 5 mol% post-functionalized polymer PP3HT **(9)**. Following purification, the ^{1}H NMR spectrum (see **Figure 3.5**) exhibited peaks attributable to both P3HT and perylene. The shift of the methylene peak from 4.72 ppm (-C*H*$_2$-OH) to 5.12 ppm (-C*H*$_2$-COO), which partially overlaps with the proton at 5.18 ppm (-NC*H*(C_6H_{13})$_2$), suggests complete esterification. Furthermore, integration of the α-methylene protons of P3HT (2.78 ppm) and aromatic protons of perylene (8.68 ppm) confirms that 1 in 20 of the thienyl units was functionalized with PDI. This corresponds to a mass ratio of 4 to 1 for P3HT with respect to PDI.

3.3.2 Spectroscopic Properties in Solution

The optical absorption and emission spectra of dilute tetrahydrofuran (THF) solutions (5.0 mg/L) of PDI **(7)**, P3HT, PP3HT **(9)** and a mixture of P3HT:PDI in a 4:1 wt ratio (corresponding to the weight ratio of PDI moieties relative to P3HT in PP3HT) were investigated. The results, illustrated in **Figure**

3.6 and **Figure 3.7**, reveal a maximum absorption band at 445 nm and a broad emission band at 573 nm with a shoulder at 612 nm observed for P3HT. The absorption and emission spectra of PDI **(7)** exhibit three absorption peaks at 450, 485 and 520 nm and a fluorescence spectrum that is the mirror image of the absorption spectrum with peaks at 530, 570 and 620 nm.[48, 49]

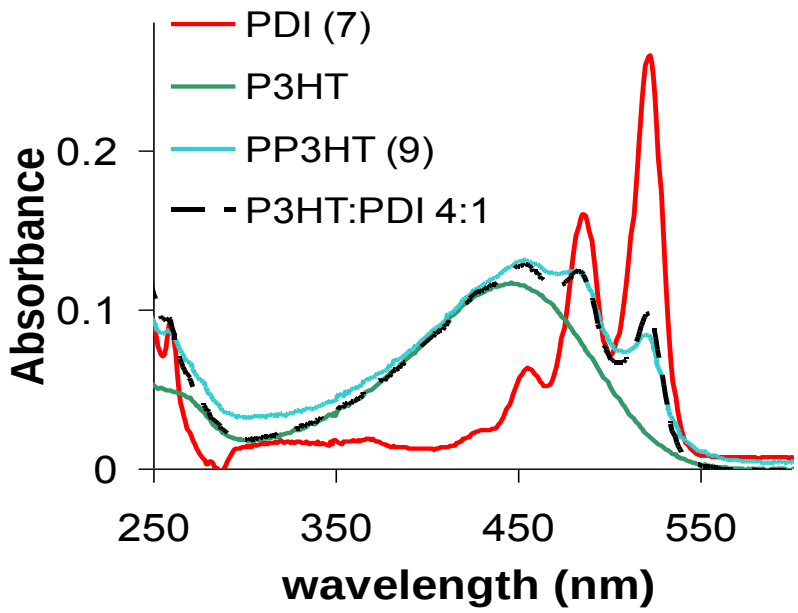

Figure 3.6: Optical absorption spectra of dilute THF solutions (5.0 mg/L) of PDI (7), P3HT, PP3HT (9) and a 4:1 mixture of P3HT:PDI.

Solutions of PP3HT **(9)** and mixtures of P3HT:PDI **(7)** in a 4:1 wt ratio reveal almost identical absorption spectra and contain peaks corresponding to both P3HT and PDI (see **Figure 3.6**). This similarity in absorption spectra, peak position and relative intensity, is indicative of little or no electronic interaction in the ground state between the polymer backbone in **9** and pendant perylene moieties.[26] Comparison of the photoluminescence spectra (PL), however, reveal

a significant difference between solutions of PP3HT and 4:1 wt ratio mixtures of P3HT:PDI (see **Figure 3.7**). In the latter case, the PL spectrum is a simple superposition of the PL spectra of PDI and P3HT. Conversely, the PL spectrum of PP3HT exhibits much weaker emission from both the PDI and P3HT moieties with a quantum yield of 18% (cf. 48% for 4:1 wt ratio P3HT:PDI, 68% for PDI and 26% for P3HT).[46] Photoluminecence quenching observed in solutions of PP3HT **(9)** is indicative of enhanced intramolecular interaction (namely, photo-induced electron transfer) between P3HT and PDI in the excited state, compared to solution blends of P3HT and PDI.[50, 51]

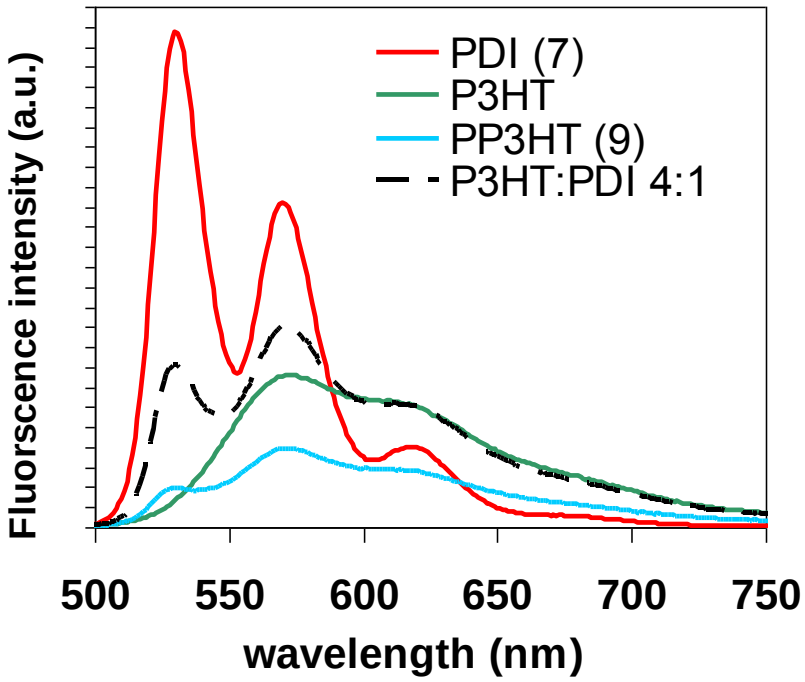

Figure 3.7: Optical emission spectra of dilute THF solutions (5.0 mg/L) of PDI (7), P3HT, PP3HT (9) and a 4:1 mixtureof P3HT:PDI.

3.3.3 Electrochemical and Spectroscopic of Thin Films

The redox properties of thin films of P3HT, PDI **(7)** and PP3HT **(9)** were probed by cyclic voltammetry (CV). The results, illustrated in **Figure 3.8**, provide insight into the electronic structure of the polymers and PDI molecules as estimates of HOMO and LUMO energy levels may be calculated from the onset of redox peaks. As previously reported, thin films of P3HT show quasi-reversible oxidation and reduction waves corresponding to the formation of radical cation and radical anion species, respectively.[52] Onset potentials of +0.08 V for oxidation and -2.24 V for reduction correspond to HOMO and LUMO energy levels of 4.9 eV and 2.6 eV, respectively. Due to the greater electronegative character of PDI **(7)**, a higher onset oxidation potential, at +1.06 V, and lower reduction potential, at -1.05 V, is observed. These potentials correspond to HOMO and LUMO levels of 5.9 eV and 3.7 eV, respectively. As expected, the CV of PP3HT is similar to P3HT with onset potentials of +0.08 V and -2.24 V for oxidation and reduction, respectively. In contrast, however, a small reduction wave due to the presence of perylene diimide moieties was observed with an onset potential at -1.1 V (highlighted by a circle in **Figure 3.8**).

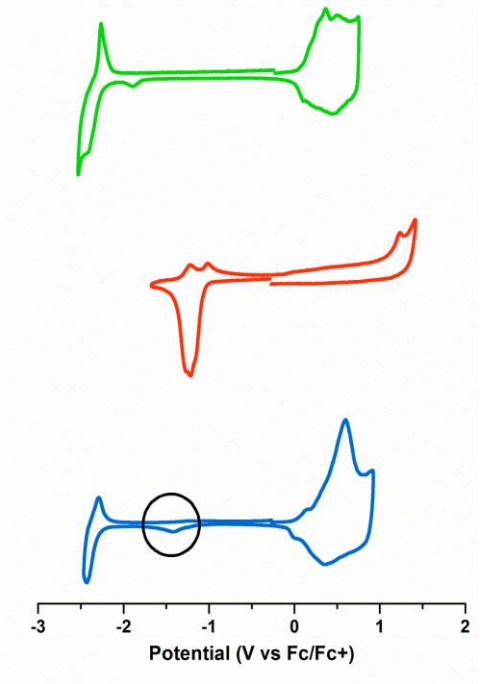

Figure 3.8: CV scans of thin films of P3HT (top), PDI (7) (middle) and PP3HT (9) (bottom) in acetonitrile with n-Bu_4NClO_4 supporting electrolyte.

The optical properties of spin cast thin films of PDI **(7)**, P3HT and PP3HT **(9)** as well as blends of P3HT:PDI and blends of PP3HT:PDI in 1:1, 1:2 and 1:4 wt ratios were probed by UV-vis and PL spectroscopy. All polymeric films were fabricated following the "solvent annealing" procedure previously described for P3HT:PCBM photovoltaic devices – which is reported to afford an extensively self-assembled polymer network.[45] Following spin-coating, this slow growth approach allows the film to stand in the liquid phase while the solvent slowly evaporates (see Experimental Section for more details). Not surprisingly, the absorption spectra of the thin film blends of P3HT:PDI correspond to the direct superposition of P3HT and PDI absorption profiles for a given weight ratio (see **Figure 3.9**). In the case of PP3HT:PDI blends, however, the absorbance at 495

nm remains constant while the peak at 530 nm increases as the concentration of PDI increases. Furthermore, the intensity of the shoulder observed at 597 nm decreases with increasing PDI content indicative of weakening of the intermolecular interchain interactions within the π-conjugated polymer.[53] In fact, for a 1:4 wt ratio blend, the shoulder is no longer present. This may be attributed to increased twisting of the PP3HT polymer backbone or the result of packing phenomenon associated with increasing PDI content as indicated by thin film morphological studies that reveal 1-D nanostructures of the perylene molecules (see section on thin film morphology).

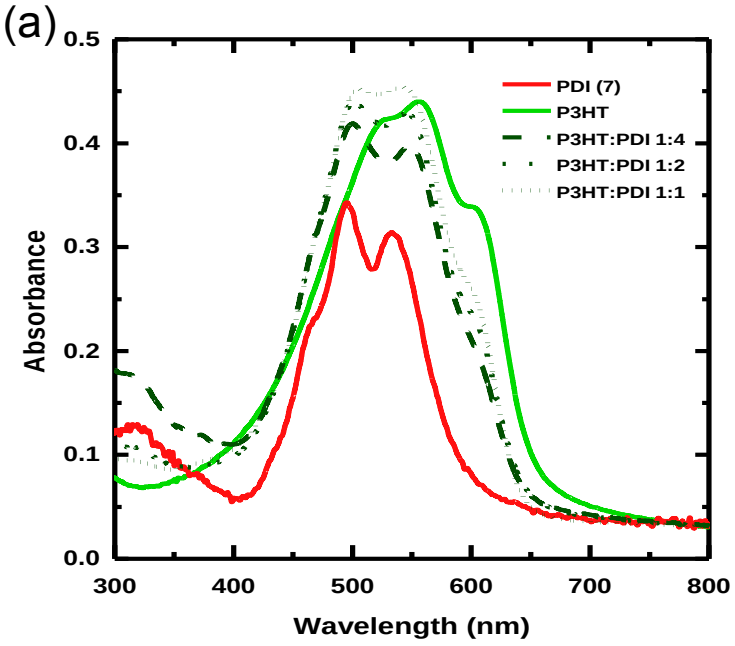

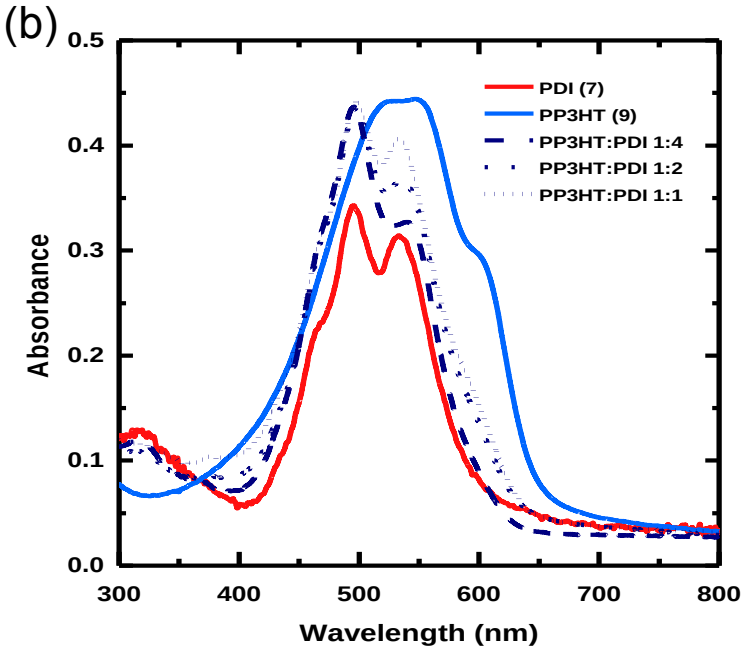

Figure 3.9: The optical absorption spectra of thin films of (a) P3HT, PDI (7) and blends of P3HT:PDI in 1:1, 1:2 and 1:4 wt ratios and (b) PP3HT (9), PDI (7) and blends of PP3HT:PDI in 1:1, 1:2 and 1:4 wt ratios.

Quantum yields of PL (Φ_{PL}), reported in **Table 3.1**, exemplify the fluorescence quenching observed in blends of P3HT:PDI and PP3HT:PDI. Since the Φ_{PL} for PDI is larger than P3HT and PP3HT, increasing PDI content in thin film blends with both P3HT and PP3HT should increase the fluorescence quantum yields if there is little to no molecular interaction between the conjugated polymers and PDI. In blends of P3HT:PDI, the decrease in PL intensity with decreasing PDI content is gradual and is attributed mostly to a lowering of the relative PDI content in the films rather than to quenching from interaction between the PDI molecules and the polymer. On the other hand, thin

film blends of PP3HT:PDI exhibit a significantly greater effect of the polymer on the PL intensity see **Figure 3.10** and **Figure 3.11**. For example, comparison of the PL spectra of 1:4 wt ratio blends of PP3HT:PDI and P3HT:PDI show that fluorescence is quenched to a much greater extent in the PP3HT:PDI blends, e.g., quantum yields for 1:4 blends of PP3HT:PDI and P3HT:PDI are 0.3% vs. 2.1%, respectively. Increased quenching provides further evidence of increased interaction between the conjugated polymer and PDI, but may also be indicative of long-range order (e.g., 1-D nanostructure) of perylene molecules as fluorescence quenching is typically indicative of π-π stacking due to the forbidden low-energy excitonic transition.[54]

Table 3.1:Thin film PL quantum yields for pristine films and blends of P3HT and PP3HT with PDI for various weight ratios.

Blend	P3HT[a]	PP3HT[a]	PDI[a]	P3HT:PDI			PP3HT:PDI		
				1:1[b]	1:2[a]	1:4[a]	1:1[b]	1:2[b]	1:4[a]
Φ (%)	1.9	0.5	5.5	0.3	0.5	2.1	0.07	0.2	0.3

[a] Quantum yield measured directly by integrating sphere (λ_{ex} = 500 nm). [b] Quantum yield calculated using the following equation $\Phi_u = \Phi_{PDI}(I_u/I_{PDI})(A_{PDI}/A_u)$, where subscripts u and PDI refer to the unknown and perylene, respectively; A corresponds to the optical density at the excitation wavelength (λ_{ex} = 500nm); I is the integrated emission.

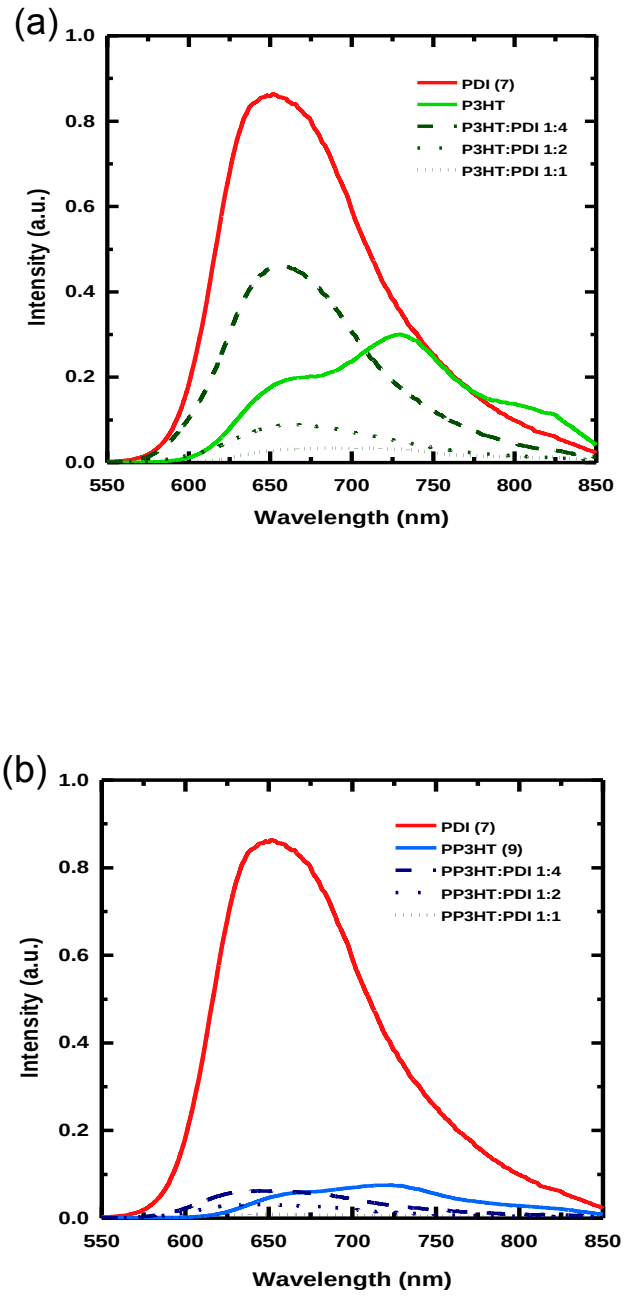

Figure 3.10: Emission spectra (λ_{ex} = 500 nm) of thin films of (a) P3HT, PDI (7) and blends of P3HT:PDI in 1:1, 1:2 and 1:4 wt ratios and (b) PP3HT (9), PDI (7) and blends of PP3HT:PDI in 1:1, 1:2 and 1:4 wt ratios. The spectra are corrected for the optical density at the excitation wavelength.

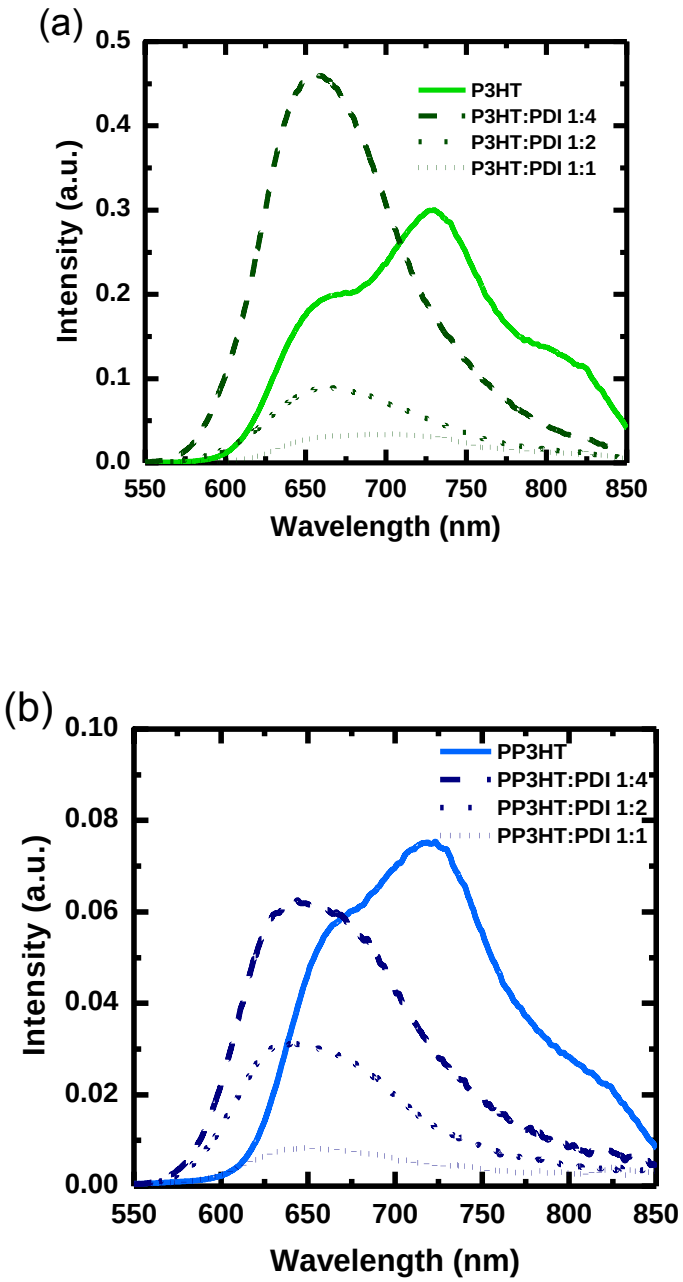

Figure 3.11: Emission spectra (λ_{ex}= 500 nm) of thin films of (a) P3HT and blends of P3HT:PDI in 1:1, 1:2 and 1:4 wt ratios and (b) PP3HT (9) and blends of PP3HT:PDI in 1:1, 1:2 and 1:4 wt ratios. The spectra are corrected for the optical density at the excitation wavelength.

3.3.4 Thin Film Morphology

The thin film morphology of P3HT, PP3HT and their blends with PDI were examined by transmission electron microscopy (TEM). All polymeric films were fabricated following the "solvent annealing" procedure described previously (see Experimental Section for more details).[45] To investigate phase separation, films were stained with RuO_4 which preferentially stains the P3HT domains producing highly scattering RuO_2.[55] The micrographs, shown in **Figure 3.13**, **Figure 3.14** and **Figure 3.14** show light and dark areas representing regions of PDI and P3HT, respectively. The TEM images reveal that films of PP3HT exhibit a feathered lamella pattern with phase segregated domains of ~20 nm. When blended with PDI in a 1:1 wt ratio, intriguing 1-D assemblies of PDI are observed uniformly distributed within the film, ~200 nm wide and several microns in length. Increasing the PDI content by preparing a 1:2 wt ratio PP3HT:PDI film enhances the connectivity and continuity of the network of 1-D PDI. In order to show the reproducibility, more TEM images of blends of PP3HT and PDI are shown in the Appendix. As a control experiment, the morphology of P3HT blended with PDI was investigated. As confirmed by TEM of the 1:1 and 1:2 wt blends of P3HT:PDI, shown in **Figure 3.14**, no 1-D assemblies were observed; but rather, micro-phase segregated morphologies. This clearly illustrates that 1-D self-assemblies of PDI are templated by the perylene molecule attached to P3HT, and not simply by the P3HT backbone.

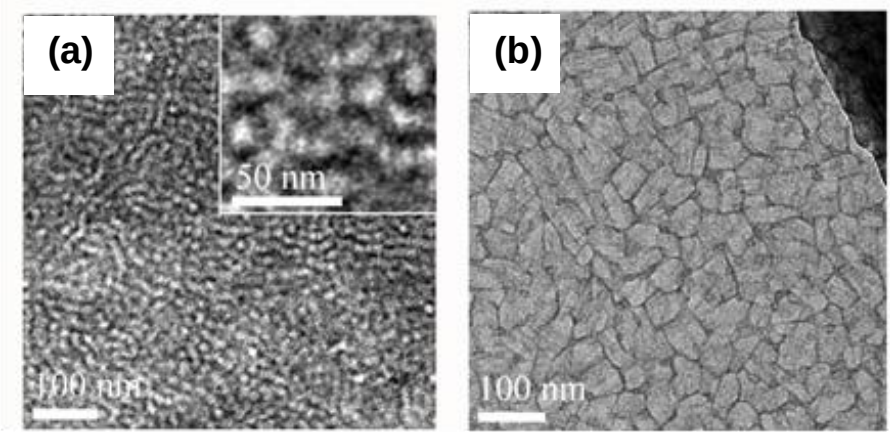

Figure 3.12: TEM micrographs of pristine films of PP3HT (a) and PDI (b).

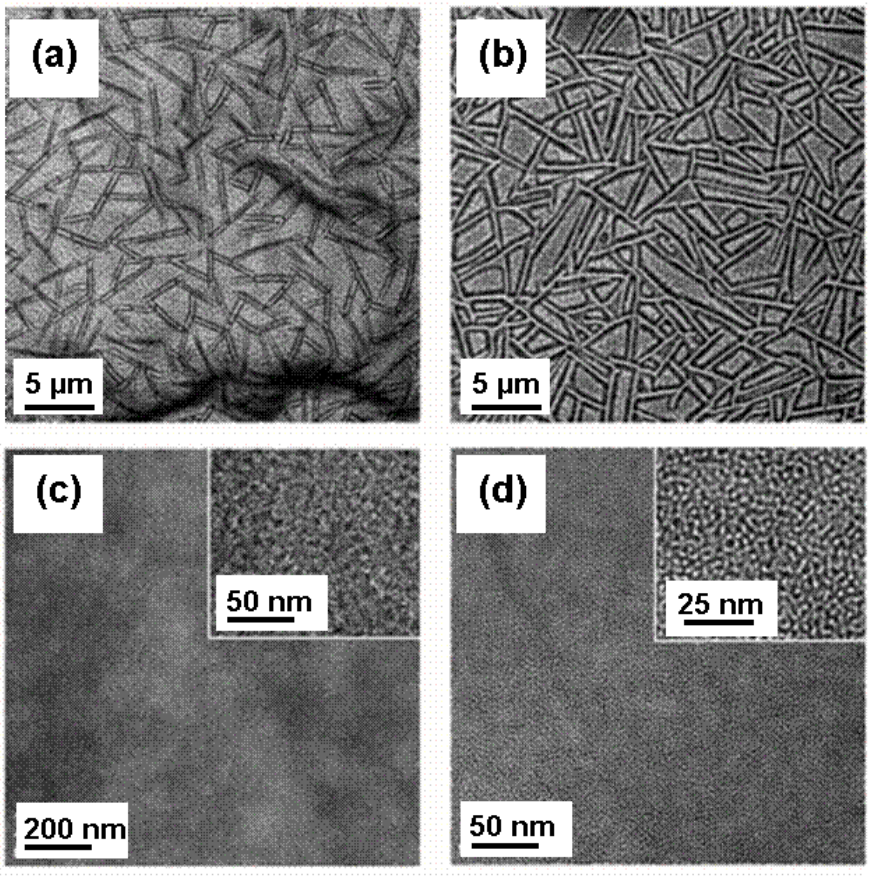

Figure 3.13: Transmission electron micrographs for thin films of PP3HT:PDI for 1:1 (a,c) and 1:2 (b,d) wt ratios; (c,d) represent higher magnification of the interstitial regions.

TEM images of the regions in-between the PDI nanowires formed in PP3HT:PDI blends are shown in **Figure 3.13c and Figure 3.13d**. The images indicate that phase segregation of the conjugated polymer and PDI also exists, but the length scale is much smaller and dependent on the PDI content; i.e., an increase in PDI content from 1:1 to 1:2 results in a decrease in domain size from 8 nm to 4 nm, respectively. In stark contrast, blends of P3HT and PDI form random, micron-sized crystallites **Figure 3.14a and Figure 3.14b**). PDI alone forms polycrystalline films comprised of 50 nm crystallites (**Figure 3.12d**).

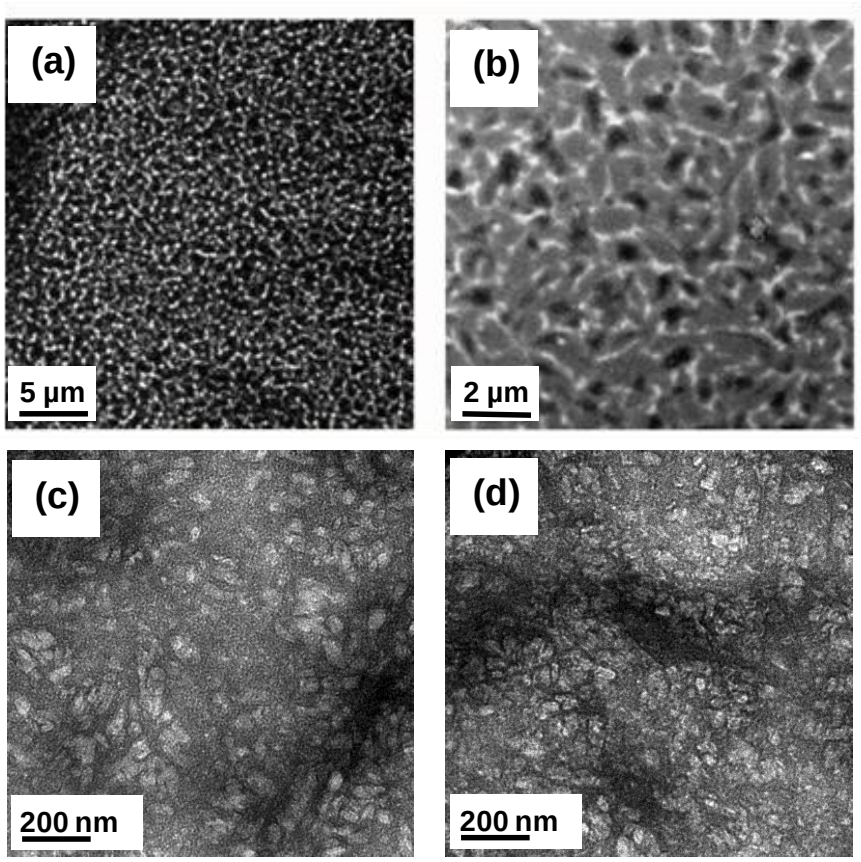

Figure 3.14: Transmission electron micrographs for thin films of P3HT:PDI for 1:1 (a,c) and 1:2 (b,d) wt ratios; (c,d) represent higher magnification.

To further explore the influence of the pendant perylene moieties in PP3HT on the molecular assembly of PDI in thin film blends, TEM images of the cross-sectioned films were obtained. A micrograph of PP3HT:PDI with 1:2 wt ratio, shown in **Figure 3.15**, reveals anisotropic, 10 – 20 nm thick, linear assemblies of PDI running parallel to the surface of the substrate. If the linear arrangement of PDI is driven by π-π interactions, then one may assume PDI π-stacks are formed and, depending on the orientation of the pendant PDI, these π-stacks may arrange perpendicular to the surface of the substrate. Alternatively,

the pendant PDI molecules may arrange perpendicular to the polymer chain thus forming π-stacked columns of PDI running parallel to the substrate surface (see **Figure 3.15c**). In contrast, blends of P3HT:PDI (1:2 wt ratio) form agglomerates (or nanocrystals) of PDI molecules randomly distributed throughout the film - as opposed to linear assemblies. The schematic representation in **Figure 3.15** is provided to illustrate the difference in thin film morphologies when PDI is blended with PP3HT and P3HT.

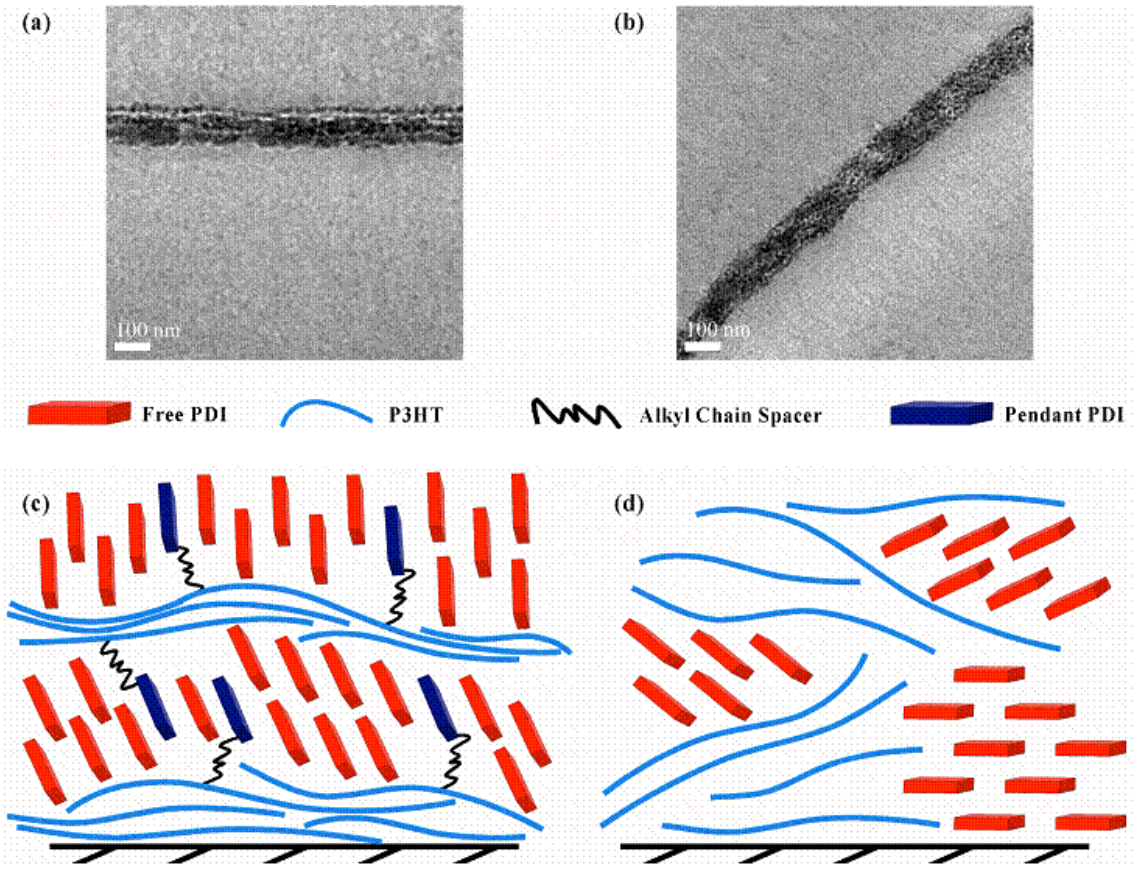

Figure 3.15: Top panel, cross-sectional transmission electron micrographs for thin film blends of PP3HT:PDI (a) and P3HT:PDI (b) in 1:2 wt ratio. Bottom panel, schematic representation illustrating the morphological effect of pendant PDI in PP3HT on blends with free PDI (c) compared with blends of P3HT:PDI (d).

3.3.5 Thin Film X-ray Diffraction

X-ray diffraction (XRD) experiments were carried out to probe the molecular arrangement of free PDI molecules in the films. The XRD pattern (see **Figure 3.16**) for thin films of P3HT and PP3HT exhibit first order reflections at 2θ angles of 5.49° and 5.33°, respectively. The lower diffraction angle observed for PP3HT, compared with P3HT, is indicative of an increased interlamellar spacing as would be expected upon attachment of pendant PDI. In addition to a peak at 4.52°, the XRD pattern for PDI shows clearly resolved peaks corresponding to

first, second, third and fourth order reflections at 2θ angles of 5.01°, 9.99°, 15.0° and 20.04°, respectively. The first and second diffraction peak (with d-spacing of 19.53 Å and 17.6 Å, respectively) are assigned to the edge-to-edge distances between two adjacent PDI molecules. For comparative purposes, XRD experiments were performed on thin film blends of P3HT:PDI in 4:1 and 1:2 wt ratios. Introduction of PDI into a film of P3HT in a 4:1 wt ratio (corresponding to the wt ratio of P3HT:PDI in PP3HT) results in a broad peak between 4.0° – 5.9° with two sharp peaks at 2θ angles of 4.425° and 5.37°. Interestingly, the peak at 5.37° is similar to the diffraction peak observed in thin films of PP3HT (cf. 5.49° for P3HT films) and the peak at 4.425° is observed at very low intensity in pristine films of PDI. Increasing the PDI content, as in the 1:2 P3HT:PDI wt ratio blends, yields a sharp diffraction peak at 5.01° on top of a broad diffraction from 4.0° – 5.9°.

Introduction of PDI into thin film blends with PP3HT, as in the case for 1:1 wt ratio blends, results in a decrease in crystallinity within the PP3HT film (as evidenced by broadening of the diffraction peak from 3.8° – 5.7°). There is, however, a sharp diffraction peak at 4.99° corresponding to ordering of PDI within the blend. Further increasing the PDI content (as in the 1:2 PP3HT:PDI wt ratio blends) increases the degree of crystallinity of PDI as evidenced by the sharp diffraction peaks at 5.01° and 7.71°. The peak at 5.01° corresponds to packing of PDI; however, the new peak observed at 7.71° may be due to interaction between the free PDI molecules and the pendant PDI moieties. The XRD data are consistent with the morphologies observed by TEM upon

increasing the PDI content – i.e., the content of crystalline PDI in the film is increased.

If the PDI molecules are linearly arranged due to π-π interactions, the XRD pattern should exhibit peaks corresponding to a d-spacing of < 5.0 Å (since π-π interactions of ~3.3 – 3.6 Å typically correspond to repeat units of < 5 Å).[48, 56] Unfortunately, inspection of the XRD patterns obtained for blends of PP3HT:PDI in 1:1 and 1:2 wt ratios did not reveal peaks corresponding to π-π interactions. The absence of these diffraction peaks, however, does not strictly imply that π-π interactions are absent, as the films are thin (100 nm) and TEM images reveal the 1-D assemblies to be only 10 – 20 nm thick. Furthermore, XRD measurements were obtained using glass substrates that inherently yield a broad diffraction peak in the region where π-π interactions would be observed.

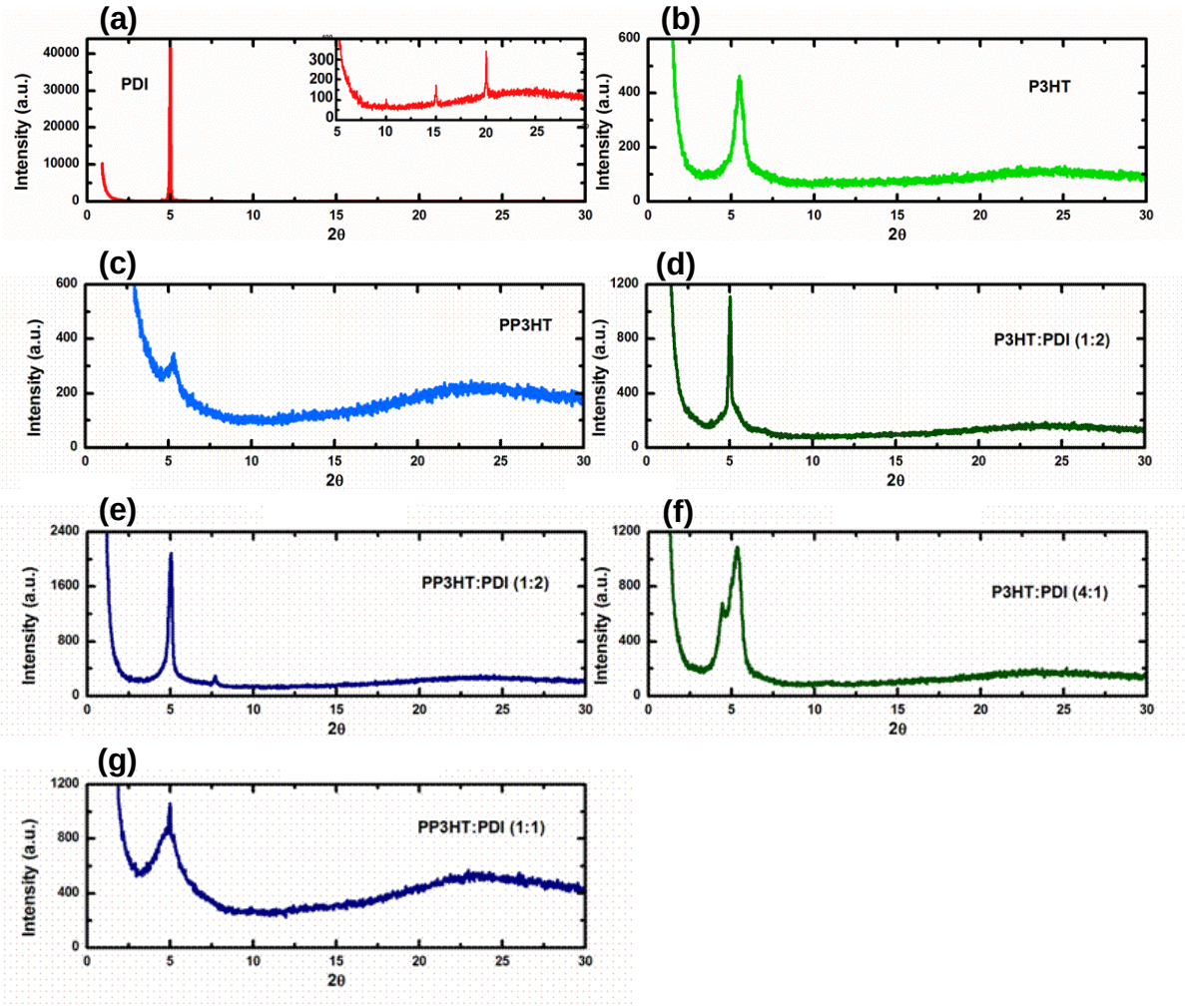

Figure 3.16: Thin film XRD patterns of PDI (a), P3HT (b), PP3HT (c) and blends of P3HT:PDI in 1:2 (d) and 4:1 (f) and PP3HT:PDI in 1:1 (g) and 1:2 (e) wt ratios.

3.3.6 PV Devices

The P3HT:PDI and PP3HT:PDI films were made into PV devices in order to investigate their current-voltage characteristics. Photovoltaic measurements were performed using an AM 1.5 solar simulator and the intensity of the incident light was 100 mW cm^{-2}. The following device structure was used: ITO/PEDOT:PSS/polymer-PDI/Al. As shown in **Figure 3.17**, the short circuit

current, J_{sc}, and open circuit voltage, V_{oc}, for the P3HT:PDI 1:1 PV was 0.41 mA/cm^2 and 0.18 V, respectively and for the P3HT:PDI 1:2 device the values were 0.45 mA/cm^2 and 0.21 V. Power conversion efficiencies under AM 1.5 (80 mW/cm^2) irradiation for the devices were 0.03% and 0.04%. Shin et al. [57] reported that P3HT and PDI were used as the electron donor and electron acceptor respectively in photovoltaic devices and exhibited current-voltage characteristics, which are comparable with the data reported here. The short circuit current, J_{sc}, and open circuit voltage, V_{oc}, for the PP3HT:PDI 1:1 PV was 0.05 mA/cm^2 and 0.42 V, respectively and for the PP3HT:PDI 1:2 device the values were 0.11 mA/cm^2 and 0.30 V. As noted, the open circuit voltages were larger than those of P3HT devices while the short circuit currents were smaller than those of P3HT devices. Power conversion efficiencies for the devices of PP3HT were only 0.006% and 0.01%. Both P3HT and PDI are light-absorbing and charge transporting materials, and contribute the harvesting of sunlight. The absorption spectra for the P3HT:PDI and PP3HT:PDI films are similar as shown in **Figure 3.9**, while photoluminescence spectra shown in **Figure 3.10** are quite different. Fluorescence and quantum yields are much larger for P3HT:PDI blends, which means that a greater fraction of excitons recombine rather than undergo charge separation. However, P3HT:PDI blends exhibit better performance than PP3HT:PDI blends. The lower PV performance for PP3HT device could be due to the 1-D assemblies of PDI running parallel to the surface of the substrate, rather than vertically (or isotropically) as is required for electron transport in PV devices. Structural modification is required to improve the

electron transport ability. For P3HT:PDI devices, the mass ratio of P3HT and PDI exerted a small effect on I_{SC}. However, for PP3HT:PDI devices, the mass ratio of the PP3HT and PDI strongly affected I_{SC}. The I_{SC} for PP3HT:PDI 1:2 device is twice that for PP3HT:PDI 1:1 devices. The ratio of PP3HT and PDI was found to be a critical factor for building continuous and connected networks for the transport of electrons as shown in TEM in **Figure 3.13**. This could be the reason for the increase of I_{SC} in PP3HT:PDI 1:2 device, as improved connectivity of the continuous network of PDI would facilitate electron transport to the electrode. Furthermore, as shown in absorption spectra in **Figure 3.9**, the shoulder at 597 nm is much less distinguishable for PP3HT:PDI blends. This indicates the enhanced miscibility of PDI with P3HT, with respect to P3HT:PDI blends, and this may inhibit the structural ordering of P3HT, and lower rates of hole transport in the conjugated polymer domains. The charge carrier injection and photo voltage critically depend on the interfaces with the electrodes. Generally, the smaller the injection barriers at electrodes are, the smaller contact resistance becomes. Since the LUMO of perylene is 3.7 eV and the work function of Al cathode is 4.3 eV, this relative large barrier may cause low short circuit current. Interfacial layer, such as LiF, may be inserted between the metal cathodes and the organic layer to lower of the barrier.

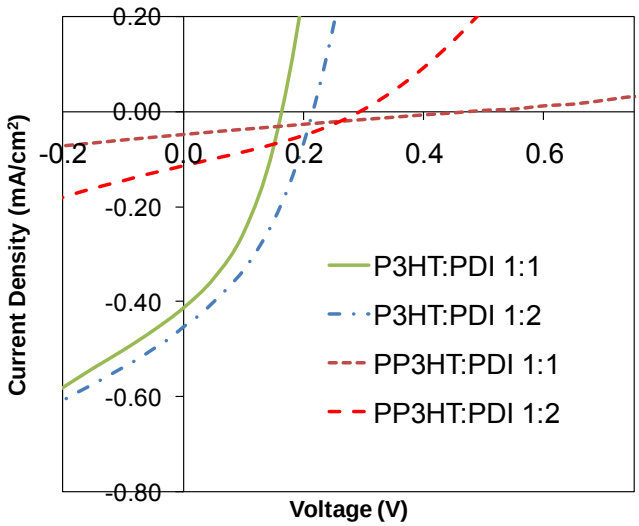

Figure 3.17: Current voltage characteristics of ITO/PEDOT:PSS/polymer:PDI/Al.

3.4 Conclusions

In this chapter, a chemical strategy to form 1-D nanoarchitectures of PDI within a conjugated polymer was shown. The anisotropy of these organized PDI structures is confirmed by cross-sectional TEM, which show the 1-D assemblies aligning parallel to the substrate surface. This work therefore provides evidence of polymer-assisted crystal growth of perylene diimide in which the polymer itself is an opto-electronically active material. The origin of these unique morphologies lies in the difference in solubility of the conjugated polymer and the PDI. The conjugated polymer, being less soluble, nucleates from the casting solution as solvent evaporates – incorporating a fraction of PDI due to the attachment of PDI to the polymer backbone. During the process of polymer deposition, the

crystallization of free PDI by the polymer is templated parallel to the substrate's surface.

Surrounding the 1-D structures of PDI is a heterogeneous PP3HT-PDI blend. The size domain of the polymeric component is substantially reduced in the presence of PDI when compared to pristine PP3HT films. This therefore indicates that the presence of PDI restricts long range organization of the conjugated polymer. In fact, the crystalline domains of the polymer cannot be observed in these blends by XRD as is common for P3HT polymers, although the absorption spectra of PP3HT and its blends are consistent with a highly organized structure. Indeed, excitation energy in thin film blends of PP3HT:PDI is quenched to a much greater extent than direct blends of P3HT and PDI, which is indicative of enhanced electron transfer between the donor and acceptor species. Thus, at one level, nano-sized domains of π-conjugated polymer are in intimate contact with PDI domains (in the sub-10 nm range), but at a higher level micrometer-scale crystallites of PDI domains phase segregate from the conjugated polymer. Studies aimed at investigating these blends as active layers in photovoltaic devices are currently underway by other researchers in Holdcroft's laboratory, as are further investigations into the stacking orientation of PDI molecules within the 1-D arrays. Moreover, the effect of side chain substitution of the PDI molecules on the thin film morphology in PP3HT blends may lead to innovative supramolecular structures that may be tailored for optoelectronic applications.

3.5 Reference

[1] F. J. M. Hoeben, P. Jonkheijm, E. W. Meijer, A. Schenning. *Chemical Reviews* **2005**, *105*, 1491-1546.

[2] V. Berl, M. Schmutz, M. J. Krische, R. G. Khoury, J. M. Lehn. *J. M. Chemistry - A European Journal* **2002**, *8*, 1227-1244.

[3] G. C. L. Wong, J. X. Tang, A. Lin, Y. L. Li, P. A. Janmey, C. R. Safinya. *Science* **2000**, *288*, 2035-2039.

[4] C. F. J. Faul, M. Antonietti. *Advanced Materials* **2003**, *15*, 673-683.

[5] G. Ligthart, H. Ohkawa, R. P. Sijbesma, E. W. Meijer. *Journal of the American Chemical Society* **2005**, *127*, 810-811.

[6] J. M. Lehn. *Science* **2002**, *295*, 2400-2403.

[7] J. H. Ryu, D. J. Hong, M. Lee. *Chemical Communications* **2008**, 1043-1054.

[8] H. J. Kim, Y. B. Lim, M. Lee. *Journal of Polymer Science Part A: Polymer Chemistry* **2008**, *46*, 1925-1935.

[9] A. H. Fuhrhop, T. Y. Wang. *Chemical Reviews* **2004**, *104*, 2901-2937.

[10] L. C. Palmer, S. I. Stupp. *Accounts of Chemical Research* **2008**, *41*, 1674-1684.

[11] M. Lazzari, M. A. Lopez-Quintela. *Advanced Materials* **2003**, *15*, 1583-1594.

[12] T. Shimizu, M. Masuda, H. Minamikawa. *Chemical Reviews* **2005**, *105*, 1401-1443.

[13] M. Antonietti, S. Forster. *Advanced Materials* **2003**, *15*, 1323-1333.

[14] M. Lee, Y. S. Yoo. *Journal of Materials Chemistry* **2002**, *12*, 2161-2168.

[15] L. Rubatat, X. X. Kong, S. A. Jenekhe, J. Ruokolainen, M. Hojeij, R. Mezzenga. *Macromolecules* **2008**, *41*, 1846-1852.

[16] P. T. Wu, G. Q. Ren, C. X. Li, R. Mezzenga, S. A. Jenekhe. *Macromolecules* **2009**, *42*, 2317-2320.

[17] N. Sary, R. Mezzenga, C. Brochon, G. Hadziioannou, J. Ruokolainen. *Macromolecules* **2007**, *40*, 3277-3286.

[18] S. C. Lo, P. L. Burn. *Chemical Reviews* **2007**, *107*, 1097-1116.

[19] L. C. Palmer, Y. S. Velichko, M. O. de la Cruz, S. I. Stupp. *Philosophical Transactions A* **2007**, *365*, 1417-1433.

[20] J. K. Kim, E. Lee, M. Lee. *Angewandte Chemie International Edition* **2006**, *45*, 7195-7198.

[21] E. Lee, Z. Huang, J. H. Ryu, M. Lee. *Chemistry - A European Journal* **2008**, *14*, 6957-6966.

[22] X. Zhang, Z. J. Chen, F. Wurthner. *Journal of the American Chemical Society* **2007**, *129*, 4886.

[23] L. Zang, Y. K. Che, J. S. Moore. *Accounts of Chemical Research* **2008**, *41*, 1596-1608.

[24] G. De Luca, A. Liscio, P. Maccagnani, F. Nolde, V. Palermo, K. Mullen, P. Samori. *Advanced Functional Materials* **2007**, *17*, 3791-3798.

[25] A. L. Briseno, S. C. B. Mannsfeld, C. Reese, J. M. Hancock, Y. Xiong, S. A. Jenekhe, Z. Bao, Y. Xia. *Nano Letters* **2007**, *7*, 2847-2853.

[26] J. Hernando, P. A. J. de Witte, E. van Dijk, J. Korterik, R. J. M. Nolte, A. E. Rowan, M. F. Garcia-Parajo, N. F. van Hulst. *Angewandte Chemie International Edition* **2004**, *43*, 4045-4049.

[27] V. Palermo, M. B. J. Otten, A. Liscio, E. Schwartz, P. A. J. de Witte, M. A. Castriciano, M. M. Wienk, F. Nolde, G. De Luca, J. Cornelissen, R. A. J. Janssen, K. Mullen, A. E. Rowan, R. J. M. Nolte, P. Samori. *Journal of the American Chemical Society* **2008**, *130*, 14605-14614.

[28] C. E. Finlayson, R. H. Friend, M. B. J. Otten, E. Schwartz, J. Cornelissen, R. L. M. Nolte, A. E. Rowan, P. Samori, V. Palermo, A. Liscio, K. Peneva, K. Mullen, S. Trapani, D. Beljonne. *Advanced Functional Materials* **2008**, *18*, 3947-3955.

[29] R. Dabirian, V. Palermo, A. Liscio, E. Schwartz, M. B. J. Otten, C. E. Finlayson, E. Treossi, R. H. Friend, G. Calestani, K. Mullen, R. J. M. Nolte, A. E. Rowan, P. Samori. *Journal of the American Chemical Society* **2009**, *131*, 7055-7063.

[30] S. M. Lindner, S. Huttner, A. Chiche, M. Thelakkat, G. Krausch. *Angewandte Chemie International Edition* **2006**, *45*, 3364-3368.

[31] J. L. Hua, F. S. Meng, J. Li, F. Ding, X. Fan, H. Tian. *European Polymer Journal* **2006**, *42*, 2686-2694.

[32] S. Rajaram, P. B. Armstrong, B. J. Kim, J. M. J. Frechet. *Chemistry of Materials* **2009**, *21*, 1775-1777.

[33] M. Sommer, S. M. Lindner, M. Thelakkat. *Advanced Functional Materials* **2007**, *17*, 1493-1500.

[34] Q. L. Zhang, A. Cirpan, T. P. Russell, T. Emrick. *Macromolecules* **2009**, *42*, 1079-1082.

[35] M. Sommer, A. S. Lang, M. Thelakkat. *Angewandte Chemie International Edition* **2008**, *47*, 7901-7904.

[36] E. E. Neuteboom, S. C. J. Meskers, P. A. van Hal, J. K. J. van Duren, E. W. Meijer, R. A. J. Janssen, H. Dupin, G. Pourtois, J. Cornil, R. Lazzaroni, J. L. Bredas, D. Beljonne. *Journal of the American Chemical Society* **2003**, *125*, 8625-8638.

[37] E. E. Neuteboom, P. A. van Hal, R. A. J. Janssen. *Chemistry-a European Journal* **2004**, *10*, 3907-3918.

[38] Y. N. Li, G. Vamvounis, J. F. Yu, S. Holdcroft. *Macromolecules* **2001**, *34*, 3130-3132.

[39] Z. Y. Zhou, X. W. Chen, S. Holdcroft. *Journal of the American Chemical Society* **2008**, *130*, 11711-11718.

[40] Y. N. Li, G. Vamvounis, S. Holdcroft. *Macromolecules* **2002**, *35*, 6900-6909.

[41] Y. N. Li, G. Vamvounis, S. Holdcroft. *Macromolecules* **2001**, *34*, 141-143.

[42] K. Sivula, C. K. Luscombe, B. C. Thompson, J. M. J. Frechet. *Journal of the American Chemical Society* **2006**, *128*, 13988-13989.

[43] M. W. Holman, R. C. Liu, D. M. Adams. *Journal of the American Chemical Society* **2003**, *125*(41), 12649-12654.

[44] R. S. Loewe, P. C. Ewbank, J. Liu, L. Zhai, R. D. McCullough. *Macromolecules* **2001**, *34*(13), 4324-4333.

[45] G. Li, Y. Yao, H. Yang, V. Shrotriya, G. Yang, Y. Yang. *Advanced Functional Materials* **2007**, *17*, 1636-1644.

[46] X. W. Chen, B. Gholamkhass, X. Han, G. Vamvounis, S. Holdcroft. *Macromolecular Rapid Communications* **2007**, *28*, 1792-1797.

[47] M. W. Holman, R. C. Liu, D. M. Adams. *Journal of the American Chemical Society* **2003**, *125*, 12649-12654.

[48] F. Wurthner. *Chemical Communications* **2004**, 1564-1579.

[49] K. Balakrishnan, A. Datar, T. Naddo, J. L. Huang, R. Oitker, M. Yen, J. C. Zhao, L. Zang. *Journal of the American Chemical Society* **2006**, *128*, 7390-7398.

[50] J. van Herrikhuyzen, A. Syamakumari, A. Schenning, E. W. Meijer. *Journal of the American Chemical Society* **2004**, *126*, 10021-10027.

[51] F. Wurthner, C. Thalacker, S. Diele, C. Tschierske. *Chemistry-a European Journal* **2001**, *7*, 2245-2253.

[52] L. L. Chua, J. Zaumseil, J. F. Chang, E. C. W. Ou, P. K. H. Ho, H. Sirringhaus, R. H. Friend. *Nature* **2005**, *434*, 194-199.

[53] J. J. Dittmer, E. A. Marseglia, R. H. Friend. *Advanced Materials* **2000**, *12*, 1270-1274.

[54] K. Balakrishnan, A. Datar, R. Oitker, H. Chen, J. M. Zuo, L. Zang. *Journal of the American Chemical Society* **2005**, *127*, 10496-10497.

[55] J. S. Trent, J. I. Scheinbeim, P. R. Couchman. *Macromolecules* **1983**, *16*, 589-598.

[56] G. Klebe, F. Graser, E. Hadicke, J. Berndt. *Acta Crystallographica Section B* **1989**, *45*, 69-77.

[57] W. S. Shin, H. H. Jeong, M. K. Kim, S. H. Jin, M. R. Kim, J. K. Lee, J. W. Lee, Y. S. Gal. *Journal of Materials Chemistry* **2006**, *16*(4), 384-390.

4: THESIS SUMMARY AND FUTURE WORK

4.1 Summary

π-conjugated polymers have attracted considerable attention over the past three decades on account of their special properties, which include electronic conductivity, electroluminescence and light-harvesting. This thesis looks at the synthesis of new post-functionalized conjugated polymer materials and studies their structure, morphology, property relationships, from their fundamental properties to the solar cell device fabrication. Control of phase segregation in donor-acceptor blends of polymer photovoltaic devices by post-functionalization of conjugated polymer is an ideal approach for the application. Blending post-functionalized P3HT with acceptors offers a convenient way to produce desired phase segregation with nano-structures.

Chapter 2 introduced a new strategy that used a π-conjugated polymer bearing graft chains that are compatible with a fullerene, chemically modified with a similar motif so as to promote their intimate mixing at the nanoscopic level. This chapter presents the synthesis of a graft copolymer consisting of a polythiophene backbone bearing polyvinyl triazole moieties. The graft copolymer is obtained by nitroxide-mediated radical polymerization of a vinyl triazole onto a postfunctionalized poly(3-hexylthiophene) (P3HT) backbone. The chemical similarity of the triazole functionality attached to P3HT and the fullerene leads to the formation of films with uniform, stable, nanophase morphologies.

Synthesis of perylene-functionalized P3HT and its solution casting in the presence of perylene (PDI) were investigated in the Chapter 3. The strategy is demonstrated with P3HT, partially post-functionalized with perylenebisimide (PP3HT). Polymer-assisted crystal growth of PDI was accomplished through blending PDI small molecules with PP3HT. The unique film morphology is 1-D assemblies of PDI, which are hundreds of nanometers wide, 10 – 20 nm thick, several microns in length, and run parallel to the surface of the substrate. Nano-sized domains of the polymer and an n-type material are in intimate contact. These domains encapsulate 1-D assemblies of nanocrystallites. This research offers an alternative route for the fabrication of innovative supramolecular structures for optoelectronic applications.

4.2 New Directions

4.2.1 Photovoltaic Devices Based on Perylene-Functionalized P3HT with a Series of Perylene Diimide

Perylene diimide derivatives are promising candidates for applications in molecular electronic devices and organic photovoltaic solar cells. As shown In Chapter 3 of this thesis, the self-assembly behaviour of perylene and resultant film morphology have been dramatically influenced by perylene-functionalized poly(3-hexylthiophene). The unique film morphology is achieved as the 1-D assemblies of PDI run parallel to the surface of the substrate. However, the 1-D assembly of perylene vertical to the surface of the substrate, rather than parallel to the surface of the substrate, is desired for organic photovoltaic devices application, as it can facilitate electron transport to the electrode. A systematic

study on various perylenes, which have different functional groups, is needed to find the most suitable acceptor structure for the future bulk heterojunction photovoltaic devices. The perylene diimide structures may include molecules shown in **Figure 4.1**.

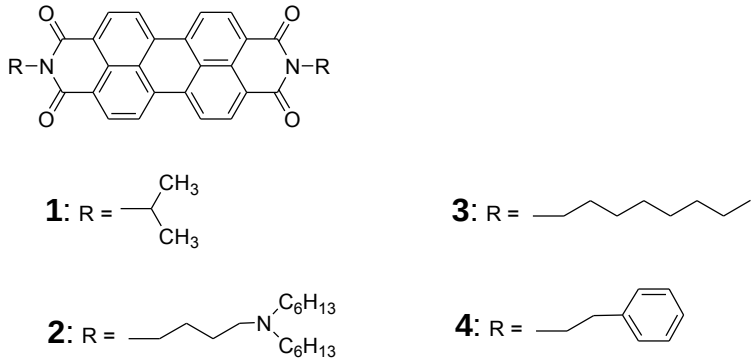

Figure 4.1: Structures of different perylene molecules.

Differences in properties of devices can be expected from the different structural and physical properties of perylene molecules. For example, swallow-tailed perylene diimide with longer alkyl chains are more soluble in solution and will show better miscibility with conjugated polymers. While perylene diimide with small functional groups possess reduced steric hindrance and gives better stacking properties.[1] So, different film morphologies with assembly of perylenes, which may facilitate electron transport to the electrodes and influence the devices properties, can be achieved.

4.2.2 Thin Film Transistors (TFTs) Based on Perylene-functionalized P3HT

In the past decades, there has been tremendous progress in the performance of organic thin film transistors (TFTs). Photo-sensitive TFTs such as

optoelectronic switches and memory devices based on conjugated polymers blending with carbon nanotube transistors have been previously reported.[2, 3] The mechanism proposed was based on the trapping of photogenerated electrons at the nanotube/gate dielectric interface. These trapped electrons act as an “optical gate” for the polymer/nanotube transistor.

N-type organic and p-type thin-film transistors based on a perylene diimide and polythiophene have been reported respectively.[4, 5] In Chapter 3 of this thesis, it has been shown that polymer-assisted crystal growth of perylene was accomplished through blending perylene small molecules with perylene-functionalized poly(3-hexylthiophene). Connected and continuous network of 1-D perylene was formed in the film. The 1-D assemblies of perylene run parallel to the surface of the substrate. Nano-sized domains of polymer and perylene material encapsulate 1-D assemblies of nanocrystallites. This unique morphology could be ideal for photo-sensitive thin film transistors, as the network of 1-D perylene assemblies may provide good conductivity traverse though the film. The film combining polythiophene as an electron donor and perylene as an electron acceptor can produce photogenerated electrons and could act as an “optical gate” in TFTs.

4.2.3 Synthesis of a Graft Copolymer Consisting of a Polythiophene Backbone Bearing Polyvinyl Perylene Moieties

In the design of bulk heterojunction photovoltaic devices, an electron acceptor is combined with an electron donor to form bicontinuous morphology.

Upon photoexcitation, the generated excitons diffuse to the donor/acceptor interface and dissociate, whereupon charges diffuse to their respective electrodes. Considering an exciton diffusion length of ~10 nm, the donor and acceptor phases should be within the length scale of this order to minimize recombination. As shown in Chapter 3 of this thesis, blends of the pristine P3HT (electron donor) and the perylene diimide (electron acceptor) are initially phase separated on the micron scale domains. High photoluminescence intensity indicated the quenching was not efficient for these blends. More efficient morphologies for charge separation and transport would be those associated with nanophase-separated copolymers. Copolymers microphase can separate into a variety of nanoscale morphologies depending on the molecular weight and chemical nature of the blocks. The sizes of the microdomains are comparable to the exciton diffusion length.

P3HT is the most widely used electron-donating and hole-conducting conjugated polymer and shows superior performance in solar cells. PCBM is the most successful fullerene derivative as the electron acceptor of bulk heterojunction polymer solar cells. However, it has a number of drawbacks for application in polymer solar cells, including a weak absorption in the visible region, the possibility of phase separation from the donor polymer and difficulty to tune the energy levels. Therefore, considerable effort has been devoted to developing other types of electron acceptor materials to replace PCBM. Perylene diimide is a promising electron acceptor material, and is attracting increasing interest due to advantageous properties, such as thermal stability, low cost and

strong absorption in the visible region, as well as good electron accepting properties. Perylene diimides have been used as the electron acceptor in photovoltaic devices, however, the PCEs are relatively low at present, which is probably due to the difficulty of forming the interpenetrating networks necessary for efficient transport of both electrons and holes to the electrodes.

So as mentioned above, novel graft copolymers are specifically designed for an optimal PV response. They possess a donor (polythiophene blocks) that are incompatible with the acceptor (polyvinyl perylene blocks), leading to nanoscale phase separation and interpenetrating networks.

The synthesis steps for the monomer and polymer are shown in Scheme 4.1 **and Scheme 4.2**, respectively. The synthesis step from compound **2** to **3** is a Steglich condensation, which has been used in Chapter 3. The synthesis procedure for the graft copolymer **4** is the same as shown in the Chapter 2 of this thesis. It uses a combination of post-functionalization of polythiophenes followed by TEMPO-assisted free radical polymerization. With control of both the molecular weights of each block and the compositional ratio of each block, bicontinous morphologies can be obtained. These would seem ideal structures for designing bulk heterojunction polymeric devices. The graft copolymer obtained may also be used as a compatibilizer blended with donor and acceptor to control the morphology. Once the polymer has been synthesized and characterized, they can be used in the context of cast films in order to fabricate photovoltaic devices.

Post-functionalization of conjugated polymers is a facile approach towards tailored structures and properties of polymers. It should be a useful method to control phase segregation in donor-acceptor blends by post-functionalization of conjugated polymers for electro-optical applications.

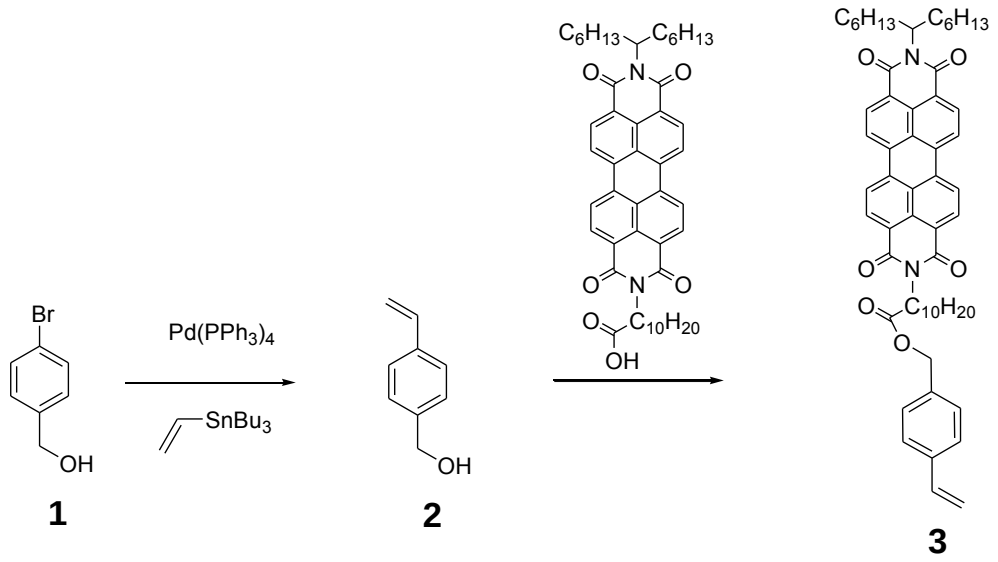

1 **2** **3**

Scheme 4.1: Synthetic route for the vinyl perylene monomer.

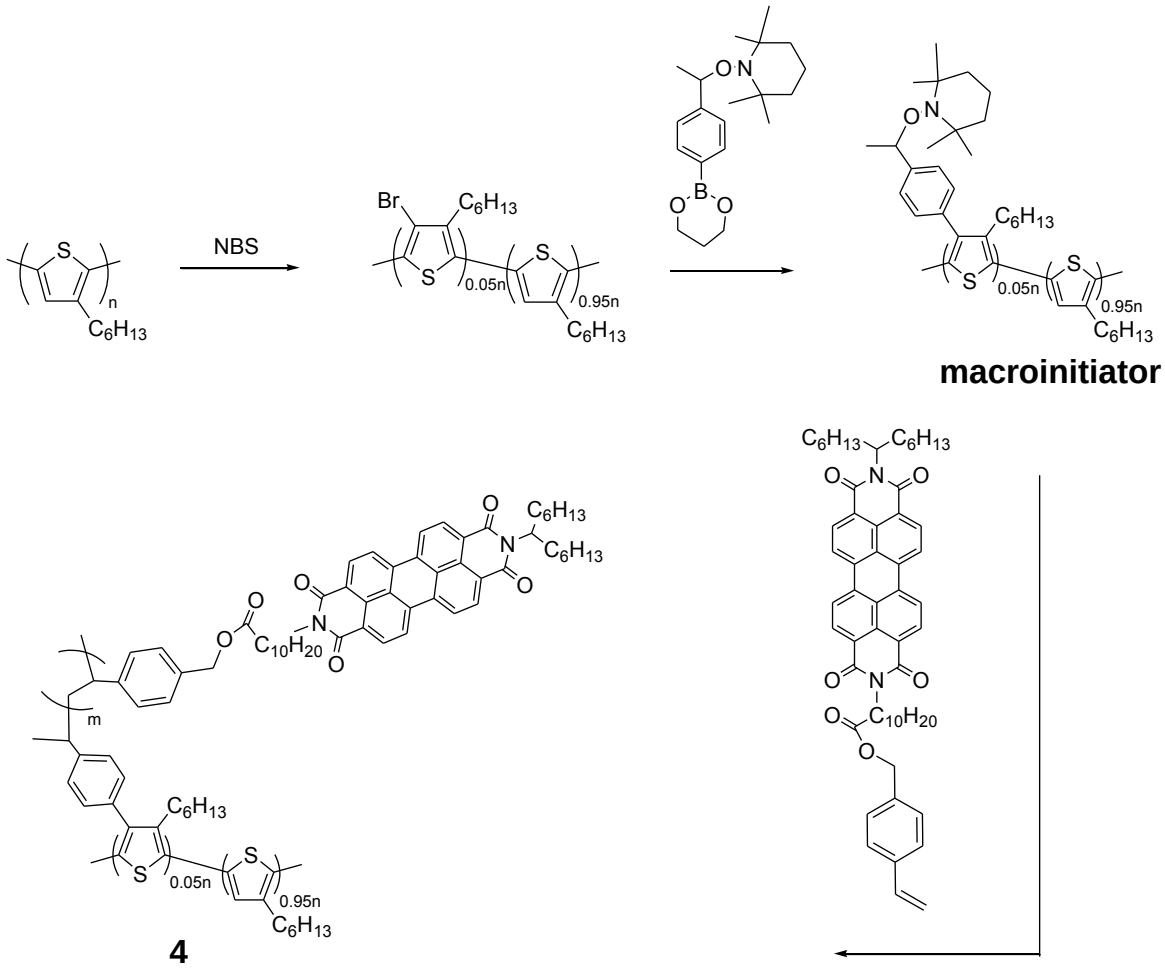

Scheme 4.2: Synthetic route for the polythiophene-graft-polyvinylperylene.

4.3 Reference

[1] S. G. Liu, G. D. Sui, R. A. Cormier, R. M. Leblanc, B. A. Gregg. *Journal of Physical Chemistry B* **2002**, *106*(6), 1307-1315.

[2] J. Borghetti, V. Derycke, S. Lenfant, P. Chenevier, A. Filoramo, M. Goffman, D. Vuillaume, J. P. Bourgoin. *Advanced Materials* **2006**, *18*(19), 2535-2541.

[3] A. Star, Y. Lu, K. Bradley, G. Gruner. *Nano Letters* **2004**, *4*(9), 1587-1591.

[4] A. Tsumura, H. Koezuka, T. Ando. *Applied Physics Letters* **1986**, *49*(18), 1210-1212.

[5] P. R. L. Malenfant, C. D. Dimitrakopoulos, J. D. Gelorme, L. L. Kosbar, T. O. Graham, A. Curioni, W. Andreoni. *Applied Physics Letters* **2002**, *80*(14), 2517-2519.

APPENDIX

A1 Synthesis of the Perylene Diimides in Chapter 3

N,N'-bis(1-hexylheptyl)perylene-3,4,9,10-tetracarboxylbisimide (7) In a 500 mL round bottom flask, 3.7 g (9.4 mmol) perylene-3,4,9,10-tetracarboxylicdianhydride, 4.5 g (23 mmol) of 1-hexylheptylamine and 1g zinc acetate in 15 g imidazole were stirred 4h at 180° C. The mixture was then cooled, dissolved in $CHCl_3$, and directly purified by column chromatography on silica gel ($CHCl_3$) to give 6.1 g (86% yield) of a deep red solid. ^1H NMR (δ/ppm, $CDCl_3$): 0.79 (t, 12H), 1.18-1.30 (m, 32 H), 1.84 (m, 4H), 2.23 (m, 4H), 5.16 (m, 2H), 8.62-8.75 (m, 8H).

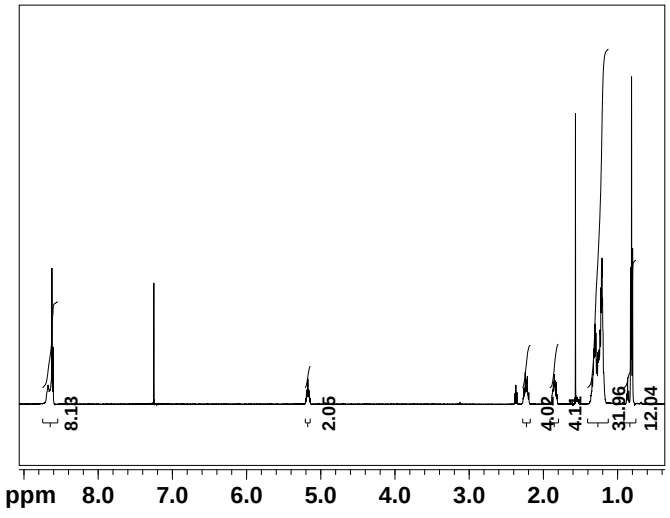

Figure A 1: NMR spectrum of N,N'-bis(1-hexylheptyl)perylene-3,4,9,10-tetracarboxylbisimide in $CDCl_3$.

N-(1-hexylheptyl)-N'-(12-carboxylicdodecyl)perylene-3,4,9,10 tetracarboxylbisimide (8) In a 250 mL RBF, 400 mg (0.70 mmol) N-(1-hexylheptyl)perylene-3,4,9,10-tetracarboxyl-3,4-anhydride-9,10-imide and 196 mg (0.97 mmol, 1.4 eq), 11-aminododecanoic acid were dissolved in 2.5 g imidazole and stirred 4h at 160º C. The reaction mixture was cooled to r.t., suspended in 50 mL EtOH, then treated with 400 mL 2N HCl and stirred overnight. The dark red precipitate was filtered and dried at 130º C to give 370 mg (70%) of dark red solid. ^{1}H NMR (δ/ppm, $CDCl_3$): 0.82 (t, 6H), 1.29 (m, 32H), 1.64 (quint, 2H), 1.77 (quint, 2H), 1.88 (m, 2H), 2.27 (m, 2H), 2.36 (t, 2H), 4.20 (t, 2H), 5.18 (m, 1H), 8.68 (dd, 8H).

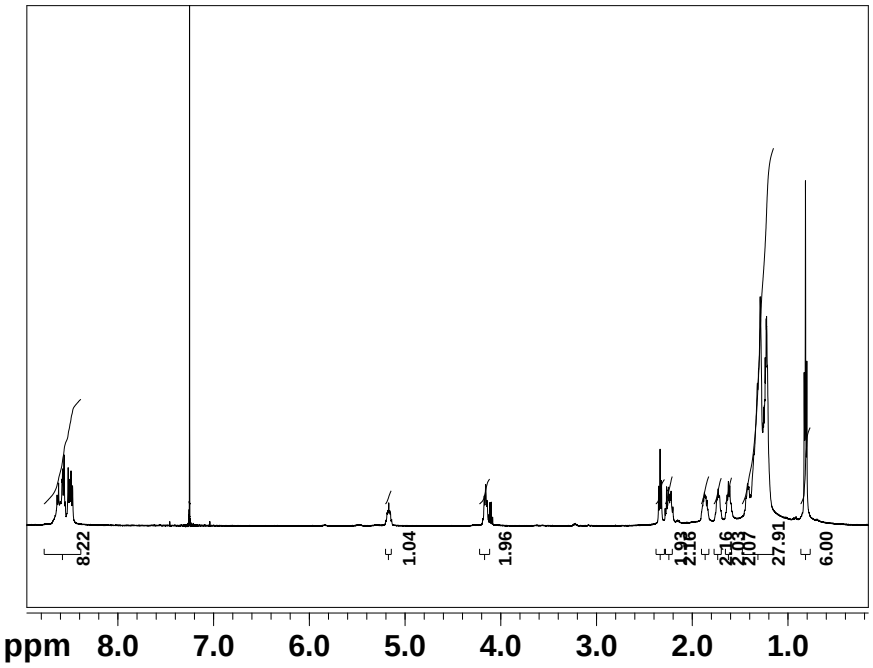

Figure A 2: NMR spectrum of N-(1-hexylheptyl)-N'-(12-carboxylicdodecyl)perylene-3,4,9,10 tetracarboxylbisimide in $CDCl_3$.

A2 Additional TEM Images for Thin Films of PP3HT:PDI in Chapter 3

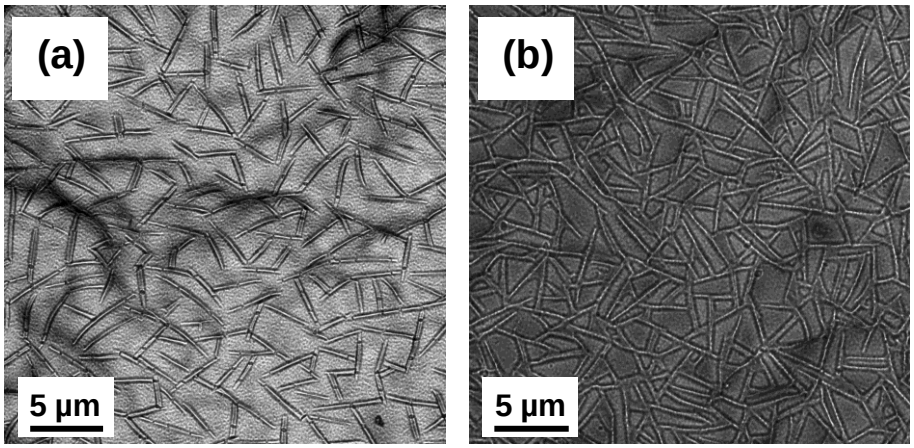

Figure A 3: Transmission electron micrographs for thin films of PP3HT:PDI for 1:1 (a) and 1:2 (b) wt ratios.